NUREG-1824 EPRI 1011999
Final Report

Verification and Validation of Selected Fire Models for Nuclear Power Plant Applications

Volume 3:
Fire Dynamics Tools (FDT^S)

U.S. Nuclear Regulatory Commission
Office of Nuclear Regulatory Research
Washington, DC 20555-0001

Electric Power Research Institute
3420 Hillview Avenue
Palo Alto, CA 94303

U.S.NRC
UNITED STATES NUCLEAR REGULATORY COMMISSION
Protecting People and the Environment

EPRI | ELECTRIC POWER RESEARCH INSTITUTE

Verification & Validation of Selected Fire Models for Nuclear Power Plant Applications

Volume 3: Fire Dynamics Tools (FDT^S)

NUREG-1824 **EPRI 1011999**

Final Report

May 2007

U.S. Nuclear Regulatory Commission
Office of Nuclear Regulatory Research (RES)
Two White Flint North, 11545 Rockville Pike
Rockville, MD 20852-2738

U.S. NRC-RES Project Manager
M. H. Salley

Electric Power Research Institute (EPRI)
3420 Hillview Avenue
Palo Alto, CA 94303

EPRI Project Manager
R.P. Kassawara

DISCLAIMER OF WARRANTIES AND LIMITATION OF LIABILITIES

ORGANIZATION(S) THAT PREPARED THIS DOCUMENT:

U.S. Nuclear Regulatory Commission, Office of Nuclear Regulatory Research

Science Applications International Corporation

National Institute of Standards and Technology

NOTE

CITATIONS

This report was prepared by

U.S. Nuclear Regulatory Commission,
Office of Nuclear Regulatory Research (RES)
Two White Flint North, 11545 Rockville Pike
Rockville, MD 20852-2738

Principal Investigators:
K. Hill
J. Dreisbach

Electric Power Research Institute (EPRI)
3420 Hillview Avenue
Palo Alto, CA 94303

Science Applications International Corp (SAIC)
4920 El Camino Real
Los Altos, CA 94022

Principal Investigators:
F. Joglar
B. Najafi

National Institute of Standards and Technology
Building Fire Research Laboratory (BFRL)
100 Bureau Drive, Stop 8600
Gaithersburg, MD 20899-8600

Principal Investigators:
K McGrattan
R. Peacock
A. Hamins

Volume 1, Main Report: B. Najafi, F. Joglar, J. Dreisbach
Volume 2, Experimental Uncertainty: A. Hamins, K. McGrattan
Volume 3, FDT^S: J. Dreisbach, K. Hill
Volume 4, FIVE-Rev1: F. Joglar
Volume 5, CFAST: R. Peacock, P. Reneke (NIST)
Volume 6, MAGIC: F. Joglar, B. Guatier (EdF), L. Gay (EdF), J. Texeraud (EdF)
Volume 7, FDS: K. McGrattan

This report describes research sponsored jointly by U.S. Nuclear Regulatory Commission, Office of Nuclear Regulatory Research (RES) and Electric Power Research Institute (EPRI).

The report is a corporate document that should be cited in the literature in the following manner:

Verification and Validation of Selected Fire Models for Nuclear Power Plant Applications, Volume 3: Fire Dynamics Tools (FDT^S), U.S. Nuclear Regulatory Commission, Office of Nuclear Regulatory Research (RES), Rockville, MD, 2007, and Electric Power Research Institute (EPRI), Palo Alto, CA, NUREG-1824 and EPRI 1011999.

ABSTRACT

There is a movement to introduce risk-informed and performance-based analyses into fire protection engineering practice, both domestically and worldwide. This movement exists in the general fire protection community, as well as the nuclear power plant (NPP) fire protection community. The U.S. Nuclear Regulatory Commission (NRC) has used risk-informed insights as part of its regulatory decision making since the 1990s.

In 2002, the National Fire Protection Association (NFPA) developed NFPA 805, *Performance-Based Standard for Fire Protection for Light-Water Reactor Electric Generating Plants, 2001 Edition.* In July 2004, the NRC amended its fire protection requirements in Title 10, Section 50.48, of the *Code of Federal Regulations* (10 CFR 50.48) to permit existing reactor licensees to voluntarily adopt fire protection requirements contained in NFPA 805 as an alternative to the existing deterministic fire protection requirements. In addition, the NPP fire protection community has been using risk-informed, performance-based (RI/PB) approaches and insights to support fire protection decision-making in general.

One key tool needed to further the use of RI/PB fire protection is the availability of verified and validated fire models that can reliably predict the consequences of fires. Section 2.4.1.2 of NFPA 805 requires that only fire models acceptable to the Authority Having Jurisdiction (AHJ) shall be used in fire modeling calculations. Furthermore, Sections 2.4.1.2.2 and 2.4.1.2.3 of NFPA 805 state that fire models shall only be applied within the limitations of the given model, and shall be verified and validated.

This report is the first effort to document the verification and validation (V&V) of five fire models that are commonly used in NPP applications. The project was performed in accordance with the guidelines that the American Society for Testing and Materials (ASTM) set forth in ASTM E 1355, *Standard Guide for Evaluating the Predictive Capability of Deterministic Fire Models*. The results of this V&V are reported in the form of ranges of accuracies for the fire model predictions.

FOREWORD

Fire modeling and fire dynamics calculations are used in a number of fire hazards analysis (FHA) studies and documents, including fire risk analysis (FRA) calculations; compliance with, and exemptions to the regulatory requirements for fire protection in 10 CFR Part 50; the Significance Determination Process (SDP) used in the inspection program conducted by the U.S. Nuclear Regulatory Commission (NRC); and, most recently, the risk-informed performance-based (RI/PB) voluntary fire protection licensing basis established under 10 CFR 50.48(c). The RI/PB method is based on the National Fire Protection Association (NFPA) Standard 805, *Performance-Based Standard for Fire Protection for Light-Water Reactor Generating Plants*.

The seven volumes of this NUREG-series report provide technical documentation concerning the predictive capabilities of a specific set of fire dynamics calculation tools and fire models for the analysis of fire hazards in postulated nuclear power plant (NPP) scenarios. Under a joint memorandum of understanding (MOU), the NRC Office of Nuclear Regulatory Research (RES) and the Electric Power Research Institute (EPRI) agreed to develop this technical document for NPP application of these fire modeling tools. The objectives of this agreement include creating a library of typical NPP fire scenarios and providing information on the ability of specific fire models to predict the consequences of those typical NPP fire scenarios. To meet these objectives, RES and EPRI initiated this collaborative project to provide an evaluation, in the form of verification and validation (V&V), for a set of five commonly available fire modeling tools.

The road map for this project was derived from NFPA 805 and the American Society for Testing and Materials (ASTM) Standard E 1355, *Standard Guide for Evaluating the Predictive Capability of Deterministic Fire Models*. These industry standards form the methodology and process used to perform this study. Technical review of fire models is also necessary to ensure that those using the models can accurately assess the adequacy of the scientific and technical bases for the models, select models that are appropriate for a desired use, and understand the levels of confidence that can be attributed to the results predicted by the models. This work was performed using state-of-the-art fire dynamics calculation methods/models and the most applicable fire test data. Future improvements in the fire dynamics calculation methods/models and additional fire test data may impact the results presented in the seven volumes of this report.

This document does not constitute regulatory requirements, and NRC participation in this study neither constitutes nor implies regulatory approval of applications based on the analysis contained in this text. The analyses documented in this report represent the combined efforts of individuals from RES and EPRI. Both organizations provided specialists in the use of fire models and other FHA tools to support this work. The results from this combined effort do not constitute either a regulatory position or regulatory guidance. Rather, these results are intended to provide technical analysis of the predictive capabilities of five fire dynamic calculation tools, and they may also help to identify areas where further research and analysis are needed.

Brian W. Sheron, Director
Office of Nuclear Regulatory Research
U.S. Nuclear Regulatory Commission

CONTENTS

FIGURES

TABLES

REPORT SUMMARY

This report documents the verification and validation (V&V) of five selected fire models commonly used in support of risk-informed and performance-based (RI/PB) fire protection at nuclear power plants (NPPs).

Background

Since the 1990s, when it became the policy of the NRC to use risk-informed methods to make regulatory decisions where possible, the nuclear power industry has been moving from prescriptive rules and practices toward the use of risk information to supplement decision-making. Several initiatives have furthered this transition in the area of fire protection. In 2001, the National Fire Protection Association (NFPA) completed the development of NFPA Standard 805, *Performance-Based Standard for Fire Protection for Light-Water Reactor Electric Generating Plants*, 2001 Edition. Effective July 16, 2004, the NRC amended its fire protection requirements in Title 10, Section 50.48(c), of the *Code of Federal Regulations* [10 CFR 50.48(c)] to permit existing reactor licensees to voluntarily adopt fire protection requirements contained in NFPA 805 as an alternative to the existing deterministic fire protection requirements. RI/PB fire protection often relies on fire modeling for determining the consequence of fires. NFPA 805 requires that the "fire models shall be verified and validated," and "only fire models that are acceptable to the Authority Having Jurisdiction (AHJ) shall be used in fire modeling calculations."

Objectives

- To perform V&V studies of selected fire models using a consistent methodology (ASTM I 1335)
- To investigate the specific fire modeling issue of interest to NPP fire protection applications
- To quantify fire model predictive capabilities to the extent that can be supported by comparison with selected and available experimental data.

Approach

This project team performed V&V studies on five selected models: (1) NRC's NUREG-1805 Fire Dynamics Tools (FDTS), (2) EPRI's Fire-Induced Vulnerability Evaluation Revision 1 (FIVE-Rev1), (3) National Institute of Standards and Technology's (NIST) Consolidated Model of Fire Growth and Smoke Transport (CFAST), (4) Electricité de France's (EdF) MAGIC, and (5) NIST's Fire Dynamics Simulator (FDS). The team based these studies on the guidelines of the ASTM E 1355, *Standard Guide for Evaluating the Predictive Capability of Deterministic Fire Models*. The scope of these V&V studies was limited to the capabilities of the selected fire models and did not cover certain potential fire scenarios that fall outside the capabilities of these fire models.

Results

The results of this study are presented in the form of relative differences between fire model predictions and experimental data for fire modeling attributes such as plume temperature that are important to NPP fire modeling applications. While the relative differences sometimes show agreement, they also show both under-prediction and over-prediction in some circumstances. These relative differences are affected by the capabilities of the models, the availability of accurate applicable experimental data, and the experimental uncertainty of these data. The project team used the relative differences, in combination with some engineering judgment as to the appropriateness of the model and the agreement between model and experiment, to produce a graded characterization of each fire model's capability to predict attributes important to NPP fire modeling applications.

This report does not provide relative differences for all known fire scenarios in NPP applications. This incompleteness is attributable to a combination of model capability and lack of relevant experimental data. The first problem can be addressed by improving the fire models, while the second problem calls for more applicable fire experiments.

EPRI Perspective

The use of fire models to support fire protection decision-making requires a good understanding of their limitations and predictive capabilities. While this report makes considerable progress toward this goal, it also points to ranges of accuracies in the predictive capability of these fire models that could limit their use in fire modeling applications. Use of these fire models presents challenges that should be addressed if the fire protection community is to realize the full benefit of fire modeling and performance-based fire protection. Persisting problems require both short-term and long-term solutions. In the short-term, users need to be educated on how the results of this work may affect known applications of fire modeling, perhaps through pilot application of the findings of this report and documentation of the resulting lessons learned. In the long-term, additional work on improving the models and performing additional experiments should be considered.

Keywords

Fire
Fire Modeling
Verification and Validation (V&V)
Performance-Based
Risk-Informed Regulation
Fire Hazard Analysis (FHA)
Fire Safety
Fire Protection
Nuclear Power Plant
Fire Probabilistic Risk Assessment (PRA)
Fire Probabilistic Safety Assessment (PSA)

PREFACE

This report is presented in seven volumes. Volume 1, the Main Report, provides general background information, programmatic and technical overviews, and project insights and conclusions. Volume 2 quantifies the uncertainty of the experiments used in the V&V study of the five fire models considered in this study. Volumes 3 through 7 provide detailed discussions of the verification and validation (V&V) of the fire models:

Volume 3 Fire Dynamics Tools (FDT^S)

Volume 4 Fire-Induced Vulnerability Evaluation, Revision 1 (FIVE-Rev1)

Volume 5 Consolidated Model of Fire Growth and Smoke Transport (CFAST)

Volume 6 MAGIC

Volume 7 Fire Dynamics Simulator (FDS)

ACKNOWLEDGMENTS

The work documented in this report benefited from contributions and considerable technical support from several organizations.

The verification and validation (V&V) studies for FDT^s (Volume 3), CFAST (Volume 5), and FDS (Volume 7) were conducted in collaboration with the U.S. Department of Commerce, National Institute of Standards and Technology (NIST), Building and Fire Research Laboratory (BFRL). Since the inception of this project in 1999, the NRC has collaborated with NIST through an interagency memorandum of understanding (MOU) and conducted research to provide the necessary technical data and tools to support the use of fire models in nuclear power plant fire hazard analysis (FHA).

We appreciate the efforts of Doug Carpenter and Rob Schmidt of Combustion Science Engineers, Inc. for their comments and contributions to Volume 3.

In addition, we acknowledge and appreciate the extensive contributions of Electricité de France (EdF) in preparing Volume 6 for MAGIC.

We thank Drs. Charles Hagwood and Matthew Bundy of NIST for the many helpful discussions regarding Volume 2.

We also appreciate the efforts of organizations participating in the International Collaborative Fire Model Project (ICFMP) to Evaluate Fire Models for Nuclear Power Plant Applications, which provided experimental data, problem specifications, and insights and peer comment for the international fire model benchmarking and validation exercises, and jointly prepared the panel reports used and referred to in this study. We specifically appreciate the efforts of the Building Research Establishment (BRE) and the Nuclear Installations Inspectorate in the United Kingdom, which provided leadership for ICFMP Benchmark Exercise (BE) #2, as well as Gesellschaft für Anlagen-und Reaktorsicherheit (GRS) and Institut für Baustoffe, Massivbau und Brandschutz (iBMB) in Germany, which provided leadership and valuable experimental data for ICFMP BE #4 and BE #5. In particular, ICFMP BE #2 was led by Stewart Miles at BRE; ICFMP BE #4 was led by Walter Klein-Hessling and Marina Rowekamp at GRS, and R. Dobbernack and Olaf Riese at iBMB; and ICFMP BE #5 was led by Olaf Riese and D. Hosser at iBMB, and Marina Rowekamp at GRS. Simo Hostikka of VTT, Finland also assisted with ICFMP BE#2 by providing pictures, tests reports, and answered various technical questions of those experiments. We acknowledge and sincerely appreciate all of their efforts.

We greatly appreciate Paula Garrity, Technical Editor for the Office of Nuclear Regulatory Research, and Linda Stevenson, agency Publications Specialist, for providing editorial and publishing support for this report. Lionel Watkins and Felix Gonzalez developed the graphics

for Volume 1. We also greatly appreciate Dariusz Szwarc and Alan Kouchinsky for their assistance finalizing this report.

We wish to acknowledge the team of peer reviewers who reviewed the initial draft of this report and provided valuable comments. The peer reviewers were Dr. Craig Beyler and Mr. Phil DiNenno of Hughes Associates, Inc., and Dr. James Quintiere of the University of Maryland.

Finally, we would like to thank the internal and external stakeholders who took the time to provide comments and suggestions on the initial draft of this report when it was published in the *Federal Register* (71 FR 5088) on January 31, 2006. Those stakeholders who commented are listed and acknowledged below.

Janice Bardi, ASTM International

Moonhak Jee, Korea Electric Power Research Institute

U.S. Nuclear Regulatory Commission, Office of Nuclear Reactor Regulation Fire Protection Branch

J. Greg Sanchez, New York City Transit

David Showalter, Fluent, Inc.

Douglas Carpenter, Combustion Science & Engineering, Inc.

Nathan Siu, U.S. Nuclear Regulatory Commission, Office of Nuclear Regulatory Research

Clarence Worrell, Pacific Gas & Electric

LIST OF ACRONYMS

AGA	American Gas Association
AHJ	Authority Having Jurisdiction
ASME	American Society of Mechanical Engineers
ASTM	American Society for Testing and Materials
BE	Benchmark Exercise
BFRL	Building and Fire Research Laboratory
BRE	Building Research Establishment
BWR	Boiling-Water Reactor
CDF	Core Damage Frequency
CFAST	Consolidated Fire Growth and Smoke Transport Model
CFD	Computational Fluid Dynamics
CFR	*Code of Federal Regulations*
CSR	Cable Spreading Room
EdF	Electricité de France
EPRI	Electric Power Research Institute
FDS	Fire Dynamics Simulator
FDT^S	Fire Dynamics Tools (NUREG-1805)
FHA	Fire Hazard Analysis
FIVE-Rev1	Fire-Induced Vulnerability Evaluation, Revision 1
FMRC	Factory Mutual Research Corporation
FM/SNL	Factory Mutual & Sandia National Laboratories
FPA	Foote, Pagni, and Alvares
FRA	Fire Risk Analysis
GRS	Gesellschaft für Anlagen-und Reaktorsicherheit (Germany)
HGL	Hot Gas Layer
HRR	Heat Release Rate

IAFSS	International Association of Fire Safety Science
iBMB	Institut für Baustoffe, Massivbau und Brandschutz
ICFMP	International Collaborative Fire Model Project
IEEE	Institute of Electrical and Electronics Engineers
IPEEE	Individual Plant Examination of External Events
LIFT	Lateral Flame Ignition Test
LLNL	Lawrence Livermore National Laboratory
LNG	Liquified Natural Gas
MCC	Motor Control Center
MCR	Main Control Room
MQH	McCaffrey, Quintiere, and Harkleroad
MOU	Memorandum of Understanding
NBS	National Bureau of Standards (now NIST)
NFPA	National Fire Protection Association
NIST	National Institute of Standards and Technology
NPP	Nuclear Power Plant
NRC	U.S. Nuclear Regulatory Commission
NRR	Office of Nuclear Reactor Regulation (NRC)
PMMA	Polymethyl-methacrylate
PRA	Probabilistic Risk Assessment
PWR	Pressurized Water Reactor
RCP	Reactor Coolant Pump
RES	Office of Nuclear Regulatory Research (NRC)
RI/PB	Risk-Informed, Performance-Based
SBDG	Stand-By Diesel Generator
SDP	Significance Determination Process
SFPE	Society of Fire Protection Engineers
SNL	Sandia National Laboratory
SWGR	Switchgear Room
V&V	Verification & Validation

1
INTRODUCTION

As the use of fire modeling tools increases in support of day-to-day nuclear power plant (NPP) applications including fire risk studies, the importance of verification and validation (V&V) studies of these tools also increases. V&V studies give fire modeling analysts confidence in applying analytical tools by quantifying and discussing the performance of the given model in predicting the fire conditions measured in a particular experiment. The underlying assumptions, capabilities, and limitations of the model are discussed and evaluated as part of the V&V study.

This volume documents the V&V study of the library of quantitative fire hazards analysis (FHA) models known as Fire Dynamics Tools (FDT^S). Quantitative FHA tools can be useful in predicting the risks of fire hazards in various settings within an NPP. Consequently, a number of quantitative FHA tools (including the FDT^S library) have been developed — with varying capabilities and levels of complexity — to serve this purpose.

The U.S. Nuclear Regulatory Commission (NRC), Office of Nuclear Reactor Regulation (NRR), developed the FDT^S library [1] using state-of-the-art principles of fire dynamics to assist fire protection inspectors in performing risk-informed evaluations of credible fires that may cause critical damage to essential safe-shutdown equipment. Toward that end, the FDT^S library comprises a series of Microsoft® Excel® spreadsheets, which are pre-programmed with fire dynamics equations and correlations to assist inspectors in performing quick, first-order calculations for potential fire scenarios. The technical bases for the models included in the FDT^S library were primarily derived from the *National Fire Protection Association (NFPA) Fire Protection Handbook* [2], the *Society of Fire Protection Engineers (SFPE) Handbook of Fire Protection Engineering* [3], and other fire science literature. This report describes the equations included in the spreadsheets that have been subjected to V&V, the technical bases of those equations, and evaluation of the sensitivities and predictive capabilities of the component spreadsheets.

The V&V methodology employed in this report generally follows the guidelines outlined in ASTM E 1355, *Standard Guide for Evaluating the Predictive Capability of Deterministic Fire Models* [4]. These guidelines were published by the American Society for Testing and Materials (ASTM). As such, this report presents the fire model evaluation methodology in terms of the following basic focuses of evaluation:

- Define the model and scenarios for which the evaluation is to be conducted.
- Assess the appropriateness of the theoretical basis and assumptions used in the model.
- Assess the mathematical and numerical robustness of the model.
- Quantify the uncertainty and accuracy of the model results in predicting the course of events in similar fire scenarios.

In accordance with ASTM E 1355, it is critical to evaluate fire models to establish their acceptable uses and limitations. Evaluation is also necessary to ensure that those using the models can assess the adequacy of their scientific and technical bases, select appropriate models for a desired use, and understand the levels of confidence that can be placed on the results predicted by the models. Adequate evaluation will also help to prevent unintended misuse of fire models.

Evaluation of a fire model includes model verification and validation. Verification is the process to determine that a model correctly represents the developer's conceptual description. It is used to decide whether the model was "built" correctly. Validation is the process to determine that a model is a suitable representation of the real world and is capable of reproducing phenomena of interest. As such, validation is used to decide whether the right model was "built."

It is not possible to evaluate a fire model in its entirety. Thus, guidance such as that provided in ASTM E 1355 is intended to define a methodology for evaluating the predictive capabilities for a specific use. Validation for one application does not indicate validation for a different scenario.

In accordance with ASTM E 1355, this report is structured as follows:

- Chapter 2 provides qualitative background information about FDT^S and the V&V process.
- Chapter 3 describes the technical and theoretical bases of the FDT^S correlations that were included in this V&V study. This chapter also discusses the assumptions and limitations associated with each of the evaluated correlations.
- Chapter 4 discusses the mathematical and numerical robustness of the FDT^S correlations.
- Chapter 5 presents a sensitivity analysis, for which the researchers defined a "base case" scenario and varied selected input parameters in order to test each correlation's response to changes in the input parameters.
- Chapter 6 presents the results of the V&V study in the form of relative differences classified according to relevant attributes of enclosure fires in NPPs.
- Appendix A presents the technical details supporting the calculated accuracies discussed in Chapter 6.

2
MODEL DEFINITION

This chapter provides qualitative background information about FDT^S and the V&V process, as suggested by ASTM E 1355. Sufficient documentation of calculation methods is necessary to assess the adequacy of their scientific and technical bases, as well as the accuracy of the computational procedures for the scenarios of interest. In addition, adequate documentation helps to prevent the unintentional misuse of the models.

This chapter briefly describes the FDT^S library, following the framework suggested by ASTM E 1355 [4]. As such, this chapter identifies the version of the library that was evaluated in this study; identifies its type, developers, and relevant publications; discusses its governing equations and assumptions, as well as the required input data, property data, and results; and outlines the uses and limitations of the library. Chapter 3 presents more detailed information concerning the equations and correlations that comprise each of the library's component spreadsheets.

2.1 Name and Version of the Model

The majority of this study evaluated Version 1805.0 of the Fire Dynamics Tools (FDT^S), which the NRC released in December 2004. However, certain spreadsheets have been corrected and were released in June and August 2005 as Version 1805.1. When the analysts used these spreadsheets, they used Version 1805.1. The versions of the specific spreadsheets are identified in Chapter 3.

2.2 Type of Model

The FDT^S library contains a series of Microsoft® Excel® spreadsheets, which are pre-programmed with fire dynamics equations and correlations to assist users in performing quick, first-order calculations for potential fire scenarios. Each spreadsheet also contains a list of the physical and thermal properties of the materials commonly encountered in NPPs.

2.3 Model Developers

The FDT^S library was developed by the staff of the NRC's Office of Nuclear Reactor Regulation (NRR).

2.4 Relevant Publications

The FDT^S library is documented in NUREG-1805, "Fire Dynamics Tools (FDT^S): Quantitative Fire Hazard Analysis Methods for the U.S. Nuclear Regulatory Commission Fire Protection Inspection Program" [1]. NUREG-1805 contains the FDT^S Excel® worksheets and a detailed discussion of the technical and theoretical bases for each of the fire dynamics tools included in the package. The document also describes the uses and limitations of the spreadsheets and includes sample applications for each.

Other relevant texts include the *NFPA Fire Protection Handbook* [2] and the *SFPE Handbook of Fire Protection Engineering* [3], as well as other references in NUREG-1805.

2.5 Governing Equations and Assumptions

The governing equations and assumptions used in the FDT^S spreadsheets come primarily from the principles described in the *NFPA Fire Protection Handbook* [2] , the *SFPE Handbook of Fire Protection Engineering* [3], and other fire science literature. Those governing equations and assumptions are generally accepted within the fire science community as the state-of-the-art in calculation methods for fire phenomena. Chapter 3 provides detailed descriptions of the equations programmed into the spreadsheets included in this V&V study.

2.6 Input Data Required to Run the Model

Each FDT^S spreadsheet requires the user to input certain fire parameters that are necessary for the equations to compute the output of interest. For example, a spreadsheet may require information about the dimensions of the fire enclosure, the fire size, the ambient room conditions, material properties and so forth. To reduce the chance of user error, the spreadsheets include drop-down selection menus for pre-programmed properties of various materials that are commonly found in NPPs.

2.7 Property Data

Some of the models in the FDT^S library require the following property data:

- thermal properties of enclosure surfaces:
  - thermal inertia
  - thermal conductivity
  - specific heat
  - density
- fuel properties:
  - mass burning rate
  - effective heat of combustion
  - density
  - fuel vapor mass
  - fuel vapor density
- target properties:
  - material thermal inertia
  - material ignition temperature
  - material critical heat flux for ignition

2.8 Model Results

The FDT^S spreadsheets use simple algebraic calculations that require little or no computation time to produce first-order results. The output generated by each FDT^S spreadsheet is presented as either a single point value numerical result or a series of point values accompanied by a plot showing the trend in the results within the Excel® spreadsheet.

2.9 Uses and Limitations of the Model

Chapter 3 discusses the limitations and assumptions associated with each of the fire dynamics tools, within the context of its technical basis.

The primary objective of the FDT^S library and the accompanying documentation (NUREG-1805) is to provide a methodology for NRC fire protection inspectors to use in assessing potential fire hazards in NRC-licensed NPPs. The methodology uses simplified, quantitative FHA techniques to evaluate the potential hazard associated with credible fire scenarios. One purpose of these evaluations is to determine whether a potential fire can cause critical damage to safe-shutdown components. Its intent is to provide insights into fire dynamics, without using the sophisticated mathematics that are normally associated with the study of fire dynamics. Inspectors using these tools need a working knowledge of algebra, graphical interpretation, scientific notation, formulas, and use of some simple mathematics functions to understand the quantitative aspects of fire phenomena.

3
THEORETICAL BASIS FOR FDT^S

This chapter presents a technical description of the FDT^S library, including theoretical background and the underlying physics and chemistry inherent in the component models. The discussion includes assumptions and approximations, an assessment of whether the open literature provides sufficient scientific evidence to justify the approaches and assumptions used, and an assessment of empirical or reference data used for constant or default values in the context of the model. In so doing, this chapter addresses the ASTM E 1355 guidance to "verify the appropriateness of the theoretical basis and assumptions used in the model."

FDT^S is a set of algebraic hand calculations pre-programmed into Microsoft® Excel® spreadsheets. The FDT^S library includes 23 distinct spreadsheets that can be used to calculate various fire parameters under varying conditions. Documentation of the theoretical bases underlying the equations used in the FDT^S spreadsheets will help to ensure that users understand the significance of the inputs that each spreadsheet requires, and why a particular spreadsheet should (or should not) be selected for a particular analysis. This chapter explains the predictive equations used in the FDT^S spreadsheets that were subjected to V&V in this study, as listed in Table 3-1. Note that some spreadsheets in the FDT^S library have not been subjected to V&V in this study because of a lack of applicable and useable experimental data for comparison. NUREG-1805 provides complete documentation of the equations and theoretical bases for the FDT^S library.

Table 3-1: Spreadsheets Included in the V&V Study

Spreadsheet Name	Excel File Name	V&V
Predicting Hot Gas Layer Temperature and Smoke Layer Height in a Room Fire With Natural Ventilation Compartment	02.1_Temperature_NV.xls (v. 1805.0)	Yes
Predicting Hot Gas Layer Temperature in a Room Fire With Forced Ventilation Compartment	02.2_Temperature_FV.xls (v. 1805.0)	Yes
Predicting Hot Gas Layer Temperature in a Fire Room With Door Closed	02.3_Temperature_CC.xls (v. 1805.1)	Yes
Estimating Burning Characteristics of Liquid Pool Fire, Heat Release Rate, Burning Duration and Flame Height	03_HRR_Flame_Height_Burning _Duration_Calculation.xls (v. 1805.0)	Yes (flame height only)
Estimating Wall Fire Flame Height, Line Fire Flame Height Against the Wall, and Corner Fire Flame Height	04_Flame_Height_Calculations.xls	No
Estimating Radiant Heat Flux From Fire to a Target Fuel at Ground Level Under Wind-Free Condition	05.1_Heat_Flux_Calculations_ Wind_Free.xls (v. 1805.0)	Yes (Point Source Radiation, and Solid Flame 2 Models)
Estimating Radiant Heat Flux From Fire to a Target Fuel above Ground Level Under Wind-Free Condition	05.1_Heat_Flux_Calculations_ Wind_Free.xls	No
Estimating Radiant Heat Flux From Fire to a Target Fuel Under Presence of Wind	05.2_Heat_Flux_Calculations_ Wind.xls	No
Estimating Thermal Radiation from Hydrocarbon Fireball	05.3_Thermal_Radiation_From_ Hydrocarbon_Fireballs.xls	No
Estimating the Ignition Time of a Target Fuel Exposed to a Constant Radioactive Heat Flux	06_Ignition_Time_Calculations.xls	No
Estimating Full-Scale Heat Release Rate of a Cable Tray Fire	07_Cable_HRR_Calculations.xls	No
Estimating Burning Duration of Solid Combustibles	08_Burning_Duration_Soild.xls	No
Estimating Centerline Temperature of a Buoyant Fire Plume	09_Plume_Temperature_ Calculations.xls (v. 1805.0)	Yes
Estimating Detector Response Time	10_Detector_Activation_Time.xls	No
Predicting Compartment Flashover	13_Compartment_ Flashover_ Calculations.xls	No

Spreadsheet Name	Excel File Name	V&V
Estimating Pressure Rise Attributable to a Fire in a Closed Compartment	14_Compartment_Over_Pressure_ Calculations.xls	No
Estimating the Pressure Increase and Explosive Energy Release Associated with Explosions	15_Explosion_Claculations.xls	No
Calculating the Rate of Hydrogen Gas Generation in Battery Rooms	16_Battery_Room_Flammable_Gas _Conc.xls	No
Calculating the Fire Resistance of Structural Steel Members-Empirical Correlations	17.1_FR_Beams_Columns_ Substitution_Correlation.xls	No
Calculating the Fire Resistance of Structural Steel Members- Beam and Column Substitution Correlations and Heat Transfer Analysis using Numerical Methods (Spray Applied)	17.2_FR_Beams_Columns_Quasi_ Steady_State_Spray_Insulated.xls	No
Calculating the Fire Resistance of Structural Steel Members- Beam and Column Heat Transfer Analysis using Numerical Methods (Board Materials)	17.3_FR_Beams_Columns_Quasi_ Steady_State_Board_Insulated.xls	No
Calculating the Fire Resistance of Structural Steel Members- Unprotected Beam and Column Heat Transfer Analysis using Numerical Methods	17.4_FR_Beams_Columns_Quasi_ Steady_State_Uninsulated.xls	No
Estimating Visibility Through Smoke	18_Visibility_Through_Smoke.xls	No

3.1 Estimating Hot Gas Layer Temperature

The various FDT^S spreadsheets include a number of correlations for estimating the average hot gas layer (HGL) temperature under varying conditions. The correlations assume a homogenous upper layer in a compartment; thus, the output is an average. The spreadsheet for calculating HGL temperature in a compartment with natural ventilation also includes a calculation for HGL or smoke layer height. This section discusses the predictive equations for each of the correlations used to estimate HGL temperature; while Section 3.2 discusses the correlations for smoke layer height. Section 3.3 summarizes the assumptions and limitations inherent to these spreadsheets. Chapter 2 of NUREG-1805 [1] is the reference for the following discussion on estimating HGL temperature and smoke layer height.

3.1.1 Natural Ventilation: Method of McCaffrey, Quintiere, and Harkleroad (MQH)

A compartment with a single rectangular wall opening (such as a door or window) is commonly used for room fire experiments. Such compartments are also commonly involved in real fire scenarios, in which a single door or vent opening serves as the only path for fire-induced natural ventilation to the compartment. The hot gas layer that forms in compartment fires descends within the opening

until a quasi-steady balance is struck between the rate of mass inflow to the layer and the rate of mass outflow from the layer.

The temperatures throughout a compartment in which a fire is burning are affected by the amount of air supplied to the fire and the location at which the air enters the compartment. Ventilation-limited fires produce different temperature profiles in a compartment than well-ventilated fires. As the flow of air into the fire affects the temperature, as does the flow out of the compartment. In this effect, the energy transferred from the fire to the air and hot gases can be exhausted as fresh air comes into the compartment. In addition, heat from the fire is lost to and through the compartment boundaries. The losses of heat and energy out through openings, as well as to and through the walls, balance the energy in the compartment attributable to the fire itself.

McCaffrey, Quintiere, and Harkleroad (MQH) [5] have developed a simple best fit dimensionless correlation for evaluating HGL temperature in a compartment with natural ventilation. This MQH correlation is based on 100 experimental fires (from 8 test series involving several types of fuel) in conventional-sized rooms with a variety of wall lining materials and openings. The temperature differences varied from ΔT = 20 °C to 600 °C (68 to 1,112 °F). The fire source was away from walls (i.e., data were obtained from fires located in the center of the compartment). The larger the heat release rate (HRR) and the smaller the vent, the higher we expect the upper-layer gas temperature to increase.

The approximate formula for the HGL temperature increase, ΔT_g, above ambient (T_g - T_a) is as follows:

$$\Delta T_g = 6.85\left[\frac{\dot{Q}^2}{\left(A_v\sqrt{h_v}\right)\left(A_T h_k\right)}\right]^{\frac{1}{3}} \qquad (3\text{-}1)$$

Where:
ΔT_g = upper-layer gas temperature rise above ambient (T_g - T_a) (K)
$\dot{Q}$ = heat release rate of the fire (kW)
A_v = area of ventilation opening(s) (m^2)
h_v = height of ventilation opening (m)
h_k = heat transfer coefficient (kW/m^2-K)
A_T = total area of the compartment enclosing surfaces (m^2), excluding area of vent opening(s)

This method assumes that heat loss occurs as a result of mass flowing out through openings.

The compartment interior surface area, A_T, is calculated as follows:

$$A_T = [2\ (w_c \times l_c) + 2\ (h_c \times w_c) + 2\ (h_c \times l_c)] - A_v \qquad (3\text{-}2)$$

Where:
A_T = total compartment interior surface area (m^2), excluding area of vent opening(s)
w_c = compartment width (m)

l_c = compartment length (m)
h_c = compartment height (m)
A_v = total area of ventilation opening(s) (m^2)

To determine the heat transfer coefficient, h_k, in Eq. 3-1, we have to consider the time when conduction through the boundary walls reaches steady-state. This time is referred to as the thermal penetration time, t_p, which can be calculated as follows:

$$t_p = \left(\frac{\rho c_p}{k}\right)\left(\frac{\delta}{2}\right)^2 \qquad (3\text{-}3)$$

Where:
ρ = density of the interior lining (kg/m^3)
c_p = thermal capacity of the interior lining (kJ/kg-K)
k = thermal conductivity of the interior lining (kW/m-K)
δ = thickness of the interior lining (m)

For very thin solids, or for conduction through a solid that continues for a long time, the process of conduction becomes steady-state. These solids are said to be "thermally thin." The thermal penetration time (t_p) is greater than or equal to the time of interest ($t \geq t_p$). The heat transfer coefficient, h_k, after long heating times, can be written as follows:

$$h_k = \frac{k}{\delta} \qquad (3\text{-}4)$$

Where:
k = thermal conductivity (kW/m-K) of the interior lining

δ = thickness of the interior lining (m)

However, if the burning time is less than the thermal penetration time, t_p, the boundary material retains most of the energy transferred to it and little will be lost out the non-fire (cold) side. The solid is referred to as "thermally thick." The thermal penetration time (t_p) is less than the time of interest ($t < t_p$). In this case, the heat transfer coefficient, h_k, can be estimated using the following equation:

$$h_k = \sqrt{\frac{k\rho c}{t}} \qquad (3\text{-}5)$$

Where:
$k\rho c$ = interior construction thermal inertia [$(kW/m^2\text{-}K)^2$-sec]

t = time after ignition in seconds (characteristic burning time)

As previously indicated, the kρc parameter is a thermal property of the material responsible for the rate of temperature increase. This is the product of the material thermal conductivity (k), material density (ρ), and heat capacity (c). Collectively, kρc is known as the thermal inertia of a solid material. For most materials, c does not vary significantly, and the thermal conductivity is largely a function of material density. This means that density tends to be the most important material property.

Thermal inertias (kρc), for a variety of generic materials have been reported in the literature. These values have been derived from measurements in the small-scale lateral ignition and flame spread test (LIFT) apparatus [6].

3.1.2 Natural Ventilation (Compartment Closed): Method of Beyler

Beyler [7] developed a correlation based on a non-steady energy balance to the closed compartment, by assuming that the compartment has sufficient leaks to prevent pressure buildup (also reported by Walton and Thomas [8]). For constant HRR, the compartment HGL temperature increase, ΔT_g, above ambient (T_g - T_a) is given by the following equation:

$$\Delta T_g = T_g - T_a = \frac{2K_2}{K_1^2}\left(K_1\sqrt{t} - 1 + e^{-K_1\sqrt{t}}\right) \qquad (3\text{-}6)$$

Where:

$$K_1 = \frac{2\left(0.4\sqrt{k\rho c}\right)A_T}{mc_p} \ , \ K_2 = \frac{\dot{Q}}{mc_p}$$

And:

ΔT_g = upper-layer gas temperature rise above ambient (T_g - T_a) (K)
A_T = total area of internal compartment boundaries (m^2)
k = thermal conductivity of the interior lining (kW/m-K)
ρ = density of the interior lining (kg/m^3)
c = thermal capacity of the interior lining (kJ/kg-K)
$\dot{Q}$ = heat release rate of the fire (kW)
m = mass of the gas in the compartment (kg)
c_p = specific heat of air (kJ/kg-k)
t = exposure time (sec)

This correlation has been favorably compared against data from experiments that ranged from 50kW to 400kW ($0.2 > Q_d^* > 1.5$). These tests were ventilation-controlled.

3.1.3 Forced Ventilation: Method of Foote, Pagni, and Alvares (FPA)

Foote, Pagni, and Alvares [10] developed another method that follows the basic correlations of the MQH method, but adds components for forced-ventilation fires (also reported in references 8 and 9). This method is based on temperature data that were obtained from a series of tests conducted at Lawrence Livermore National Laboratory (LLNL), in which fresh air was introduced at the floor and pulled out the ceiling by an axial fan. Test fires from 150 to 490 kW ($0.5 > Q_d^* > 1.9$) were used, producing ceiling jet temperatures of 100 to 300 °C (212 to 572 °F). The approximate constant ventilation rates were roughly 200 to 575 cfm, and were chosen to be representative of possible fires in rooms with seven room air changes per hour. These tests were well-ventilated.

The upper-layer gas temperature increase above ambient is given as a function of the fire HRR, compartment ventilation flow rate, gas-specific heat capacity, compartment surface area, and effective heat transfer coefficient. The non-dimensional form of the resulting temperature correlation is as follows:

$$\frac{\Delta T_g}{T_a} = 0.63\left(\frac{\dot{Q}}{\dot{m}c_p T_a}\right)^{0.72}\left(\frac{h_k A_T}{\dot{m}c_p}\right)^{-0.36} \qquad (3\text{-}7)$$

Where:
ΔT_g = hot gas layer temperature rise above ambient ($T_g - T_a$) (K)
T_a = ambient air temperature (K)
$\dot{Q}$ = HRR of the fire (kW)
$\dot{m}$ = compartment mass ventilation flow rate (kg/sec)
c_p = specific heat of air (kJ/kg-K)
h_k = heat transfer coefficient (kW/m^2-K)
A_T = total area of compartment enclosing surfaces (m^2)

3.1.4 Forced Ventilation: Method of Deal and Beyler

Deal and Beyler [11] developed a simple model of forced-ventilation compartment fires (also reported in reference 9). The model is based on a quasi-steady simplified energy equation with a simple wall heat loss model. The model is based on data up to 2,000 seconds into fire tests. At longer times, the heat loss model breaks down as a result of the simple formulation of the steady-state heat loss model [12]. The approximate compartment HGL temperature increase, ΔT_g, above ambient ($T_g - T_a$) is given by the following equation:

$$\Delta T_g = T_g - T_a = \frac{\dot{Q}}{\dot{m}c_p + h_k A_T} \qquad (3\text{-}8)$$

Where:

ΔT_g = hot gas layer temperature rise above ambient (T_g - T_a) (K)
T_a = ambient air temperature (K)
$\dot{Q}$ = HRR of the fire (kW)
$\dot{m}$ = compartment mass ventilation flow rate (kg/sec)
c_p = specific heat of air (kJ/kg-K)
h_k = convective heat transfer coefficient (kW/m^2-K)
A_T = total area of compartment enclosing surfaces (m^2)

The convective heat transfer coefficient is given by the following expression:

$$h_k = 0.4 \max\left(\sqrt{\frac{k\rho c}{t}}, \frac{k}{\delta}\right) \qquad (3\text{-}9)$$

Where:
k = thermal conductivity of the interior lining (kW/m-K)
ρ = density of the interior lining (kg/m^3)
c = thermal capacity of the interior lining (kJ/kg-K)
t = exposure time (sec)
δ = thickness of the interior lining (m)

This correlation has been compared against an expansive database of experiments with favorable results [9].

3.2 Estimating Smoke Layer Height

The smoke layer can be described as the accumulated thickness of smoke below a physical or thermal barrier (e.g., ceiling). The smoke layer is not necessarily a homogeneous mixture, and it does not typically have a uniform temperature. However, for first-order approximations, the calculation methods presented below assume homogeneous conditions. The smoke layer includes a transition zone that is non-homogeneous and separates the hot upper layer from the smoke-free air (i.e., two zones).

3.2.1 Natural Ventilation (Smoke Filling): The Non-Steady-State Yamana and Tanaka Method

In a compartment with larger openings (windows or doors), there will be little or no buildup of pressure attributed to the volumetric expansion of hot gases, with the exception of rapid accumulation of mass or energy. Thus, for first-order approximations, pressure is assumed to remain at the ambient pressure. The opening flows are thus determined by the hydrostatic pressure differences across the openings, and mass flows out of and into the compartment. We also assume that the upper-layer density (ρ_g) is some average constant value at all times throughout the smoke-filling process.

Assuming a constant average density in the upper hot gas layer allows one to form an analytical solution of the smoke-filling rate, and we can use the conservation of mass to get an expression for the smoke-filling rate. This expression allows one to calculate the height of the smoke layer as a function of time, and we can use the conservation of energy to check the stipulated value of ρ_g.

Yamana and Tanaka [13] developed a general expression for the height of the smoke layer interface, z, as a function of time. The general expression can be simplified as follows for a constant HRR (also reported in reference 14):

$$z = \left(\frac{2k\dot{Q}^{\frac{1}{3}}t}{3A_c} + \frac{1}{h_c^{\frac{2}{3}}} \right)^{-\frac{3}{2}} \qquad (3\text{-}10)$$

Where:
z = height (m) of the smoke layer interface above the floor
$\dot{Q}$ = heat release rate of the fire (kW)
t = time after ignition (sec)
A_c = compartment floor area (m^2)
h_c = compartment height (m)

And:
k = a constant given by the following equation:

$$k = \frac{0.21}{\rho_g}\left(\frac{\rho_a^2 g}{c_p T_a} \right)^{\frac{1}{3}} \qquad (3\text{-}11)$$

Where:
ρ_g = hot gas density kg/m^3
ρ_a = ambient density = 1.20 kg/m^3
g = acceleration of gravity = 9.81 m/sec^2
c_p = specific heat of air = 1.0 kJ/kg-K
T_a = ambient air temperature = 298 K

Substituting the above numerical values in Equation 3-11, we obtain the following expression:

$$k = \frac{0.076}{\rho_g} \qquad (3\text{-}12)$$

Where density of the hot gas layer (ρ_g) is given by the following equation:

$$\rho_g = \frac{353}{T_g} \qquad (3\text{-}13)$$

Where:
T_g = hot gas layer temperature (K) calculated from Equation 3-1

3.3 Assumptions and Limitations for Hot Gas Layer Calculations

The methods discussed in this chapter have several underlying assumptions and limitations.

*The following assumptions and limitations apply to **all** forced and natural ventilation situations:*

(1) These methods best apply to conventional-sized compartments; they have not been validated as extensively for large compartments.

(2) These methods apply to both transient and steady-state fire growth, subject to the limitations of each individual method for the scenario being examined.

(3) The HRR must be known; it does not need to be constant, and can be allowed to change with time.

(4) Compartment geometry assumes that a given space can be analyzed as a rectangular space with no beam pockets. This assumption affects the smoke filling rate within a space if the space has beam pockets. For irregularly shaped compartments, equivalent compartment dimensions (length, width, and height) must be calculated and should yield slightly higher layer temperatures than would actually be expected from a fire in the given compartment.

(5) These methods predict average temperatures and do not apply to cases in which prediction of local temperature is desired. For example, this method should not be used to predict detector or sprinkler actuation or the material temperatures resulting from direct flame impingement.

(6) Caution should be exercised when the compartment overhead are highly congested with obstructions such as cable trays, conduits, ducts, and so forth.

(7) A single heat transfer coefficient may be used for the entire inner surface of the compartment.

(8) The heat flow to and through the compartment boundaries is unidimensional (i.e., corners and edges are ignored, and thermally thick boundaries are assumed to be semi-infinite slabs).

*The following assumptions and limitations apply only to **natural ventilation** situations:*

(1) The correlations hold for compartment upper-layer gas temperatures up to approximately 600 °C (1,112 °F) only for naturally ventilated spaces in which a quasi-steady balance develops between the rates of mass inflow and outflow from the hot gas layer.

(2) These correlations assume that the fire is located in the center of the compartment or away from the walls. If the fire is flush with a wall or in a corner of the compartment, the MQH correlation is not valid with coefficient 6.85. The smoke layer height correlation assumes an average constant value of upper-layer density throughout the smoke-filling process.

*The following assumptions and limitations apply only to **forced ventilation** situations:*

(1) These correlations assume that the test compartment is open to the outside at the inlet, and its pressure is fixed near 1 atmosphere.

(2) These correlations do not explicitly account for evaluation of the fire source, and they assume that the fire is located in the center of the compartment or away from the walls. If the fire is flush with a wall or in a corner of the compartment, the FPA correlation is not valid with coefficient 0.63.

3.4 Flame Height

As documented in Chapter 3 of NUREG-1805 [1], the height of a flame is a significant indicator of the hazard posed by the flame. Flame height directly relates to flame heat transfer and the propensity of the flame to impact surrounding objects. The height and temperature of the flame are important in estimating the ignition of adjacent combustibles. Figure 3-1 shows a characteristic sketch of the flame height fluctuations associated with the highly intermittent pulsing structure of a flame, particularly along its perimeter and near its top. This intermittence is driven largely by the turbulent mixing of air and subsequent combustion. The pulsing behavior, in turn, affects the temperature of the flame. Thus, the temperature at a fixed position fluctuates widely, particularly around the edges and near the top of the flame. This is why flame temperature is usually reported in terms of the centerline temperature or average flame temperature.

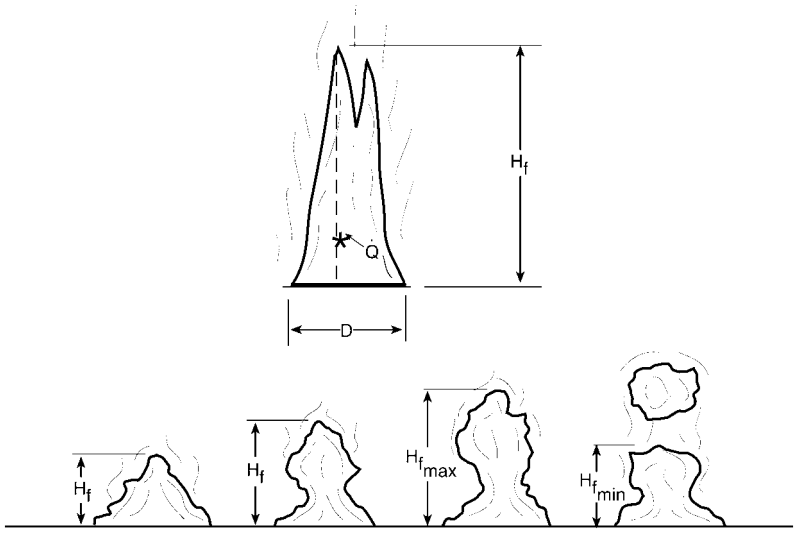

Figure 3-1: Characteristics of Flame Height Fluctuations

Above the fuel source, the flaming region is characterized by high temperature and is generally luminous. Flames from pool fires fluctuate periodically so that the tip of the flame is significantly different from the length of the continuous combustion (or luminous) region. Consequently, flame height has been defined by various criteria in order to correlate data. Researchers define flame height as the height at which the flame is observed at least 50% of the time.

The flame height is an important quantitative characteristic of a fire and may affect fire detection and suppression system design, fire heating of building structures, smoke filling rates, and fire ventilation. The Heskestad correlation is widely used to determine the flame height of pool fires [15]:

$$H_f = 0.235\dot{Q}^{\frac{2}{5}} - 1.02D \qquad (3\text{-}14)$$

Where:

H_f = flame height (m)

$\dot{Q}$ = heat release rate of the fire (kW)

D = diameter of the fire (m)

The HRR of the fire can be determined by laboratory or field testing. In the absence of experimental data, the maximum HRR for the fire is given by the following equation [16]:

$$\dot{Q} = \dot{m}''\Delta H_{c,eff} A_f (1 - e^{-k\beta D}) \qquad (3\text{-}15)$$

Where:

$\dot{Q}$ = heat release rate of the fire (kW)

$\dot{m}''$ = burning or mass loss rate per unit area (kg/m^2-sec)

$\Delta H_{c,eff}$ = effective heat of combustion (kJ/kg)

A_f = burning area of the fuel (m^2)

$k\beta$ = empirical constant (m^{-1})

D = diameter of burning area (m)

For non-circular pools, the effective diameter is defined as the diameter of a circular pool with an area equal to the actual pool area given by the following equation:

$$D = \sqrt{\frac{4A_f}{\pi}} \qquad (3\text{-}16)$$

Where:

A_f is the surface area of the non-circular pool

3.4.1 Assumptions and Limitations

(1) The flame height correlation described in this chapter was developed for horizontal pool fire sources in the center or away from the center of the compartment. The pool fires were assumed to be circular or nearly circular.

(2) The size of the fire (flame height) depends on the diameter of the fuel and the HRR.

(3) There is no fire growth period. (As previously stated, real liquid pool fires grow very quickly, and it is realistic to assume that the pool fire instantaneously reaches its maximum HRR.)

3.5 Estimating Radiant Heat Flux from Fire to a Target

Chapter 5 of NUREG-1805 [1] provides a complete discussion on the methods FDT^S uses to estimate radiant heat flux from fire to a target. The two methods used in this V&V study are summarized below.

3.5.1 Point Source Radiation Model

A point source estimate of radiant flux is conceptually the simplest model of a radiant source used in calculating the heat flux from a flame to target located outside the flame. The point source model assumes that radiation emanates from a single point located in the middle of the flame to predict the thermal radiation field of the flame.[1] The point source model provides a simple relationship that varies as the inverse square of the distance, R. Figure 3-2 illustrates the point source model. For an actual point source of radiation or a spherical source of radiation, the distance, R, is simply the distance from the point or from the center of the sphere to the target.

The thermal radiation hazard from a fire depends on a number of parameters, including the composition of the fuel, size and shape of the fire, its duration, proximity to the object at risk, and thermal characteristics of the object exposed to the fire. The point source method may be used for either fixed or transient combustibles.

The radiant heat flux at any distance from the source fire is inversely related to the horizontal separation distance (R), by the following equation [17]:

$$\dot{q}'' = \frac{\chi_r \dot{Q}}{4\pi R^2} \qquad (3\text{-}17)$$

Where:

$\dot{q}''$ = radiant heat flux (kW/m$^{2)}$

$\dot{Q}$ = heat release rate of the fire (kW)

R = radial distance from the center of the flame to the edge of the target (m)

χ_r = fraction of total energy radiated

In general, χ_r depends on the fuel, flame size, and flame configuration, and can vary from approximately 0.15 for low-sooting fuels (e.g., alcohol) to 0.60 for high sooting fuels (e.g., higher-order hydrocarbons). For large fires (several meters in diameter), cold soot enveloping the luminous flames can considerably reduce χ_r.

[1] More realistic radiator shapes give rise to very complex configuration factor equations.

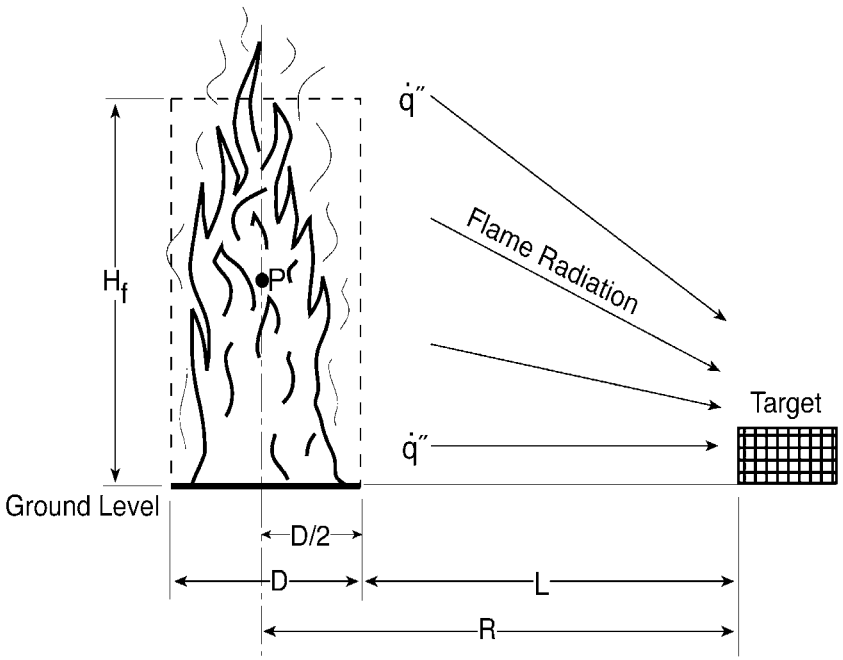

Figure 3-2: Radiant Heat Flux from a Pool Fire to a Floor-Based Target Fuel (Point Source Model)

The HRR of a fire can be determined by laboratory or field testing. In the absence of experimental data, the maximum HRR for the fire, is given by Equation 3-15.

For non-circular pools, the effective diameter is defined as the diameter of a circular pool with an area equal to the actual pool area, given by Equation 3-16.

3.5.2 Solid Flame Radiation Model with Target at and Above Ground Level

The solid flame radiation model is a more detailed method for assessing the impact of radiation from pool fires to potential targets using configuration factor algebra. This method covers a range of detailed calculations, some of which are most appropriate for first-order initial hazard assessments, while others are capable of more accurate predictions.

The solid flame model assumes that (1) the fire can be represented by a solid body of a simple geometrical shape, (2) thermal radiation is emitted from its surface, and, (3) non-visible gases do not emit much radiation. Figure 3-3 and Figure 3-4 illustrate the solid flame model. To ensure that the fire volume is not neglected, the model must account for the volume, because a portion of the fire may be obscured as seen from the target. The intensity of thermal radiation from the pool fire to an element outside the flame envelope for no-wind conditions and for windblown flames is given by the following equation [18]:

$$\dot{q}'' = EF_{1\rightarrow 2} \qquad (3\text{-}18)$$

Where:

$\dot{q}''$ = incident radiative heat flux (kW/m^2)

E = average emissive power at flame surface (kW/m^2)

$F_{1\rightarrow 2}$ = configuration factor

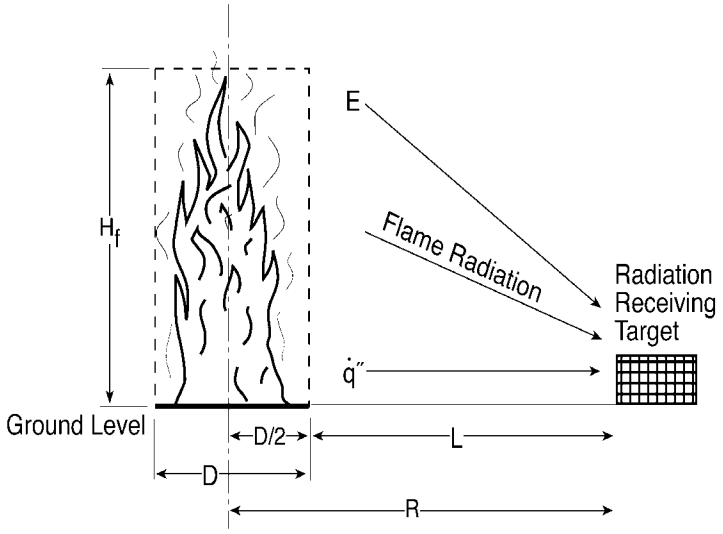

Figure 3-3: Solid Flame Radiation Model with No Wind and Target at Ground Level

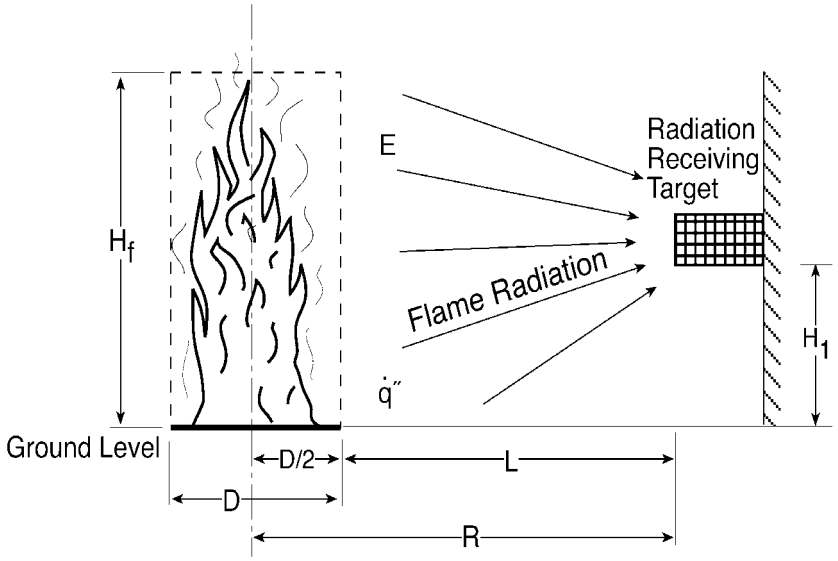

Figure 3-4: Solid Flame Radiation Model with No Wind and Target Above Ground

Emissive power is the total radiative power leaving the surface of the fire per unit area per unit time. Emissive power can be calculated using Stefan's law, which gives the radiation of a black body in relation to its temperature (black body is defined as a perfect radiator; a surface with an emissivity of unity and, therefore, a reflectivity of zero). Because a fire is not a perfect black body, the emissive power is a fraction (ε) of the black body radiation [18]:

$$E = \varepsilon\sigma T^4 \qquad (3\text{-}19)$$

Where:

E = flame emissive power (kW/m^2)
ε = flame emissivity
σ = Stefan-Boltzmann constant = 5.67 x 10-11 (kW/m^2-K^4)
T = temperature of the fire (K)

The use of the Stefan-Boltzmann constant to calculate radiation heat transfer requires knowledge of the temperature and emissivity of the fire; however, turbulent mixing causes the fire temperature to vary. Consequently, Shokri and Beyler [19] correlated experimental data of flame radiation to external targets in terms of an average emissive power of the flame. For that correlation, the flame is assumed to be a cylindrical, black body, homogeneous radiator with an average emissive power. Thus, effective emissive power of the pool fire in terms of effective diameter is given by the following equation:

$$E = 58\left(10^{-0.00823D}\right) \qquad (3\text{-}20)$$

Where:

E = flame emissive power (kW/m^2)
D = diameter of pool fire (m)

This represents the average emissive power over the entire the flame and is significantly less than the emissive power that can be attained locally. The emissive power is further reduced with increasing pool diameter as a result of the increasing prominence of black smoke outside the flame, which obscures the radiation from the luminous flame.

For non-circular pools, the effective diameter is defined as the diameter of a circular pool with an area equal to the actual pool area, given by Equation 3-16.

The configuration factor is a purely geometric quantity, which provides the fraction of the radiation leaving one surface that strikes another surface directly. In other words, the configuration factor gives the fraction of hemispherical surface area seen by one differential element when looking at another differential element on the hemisphere.

The configuration factor is a function of target location, flame size (height), and fire diameter, and is a value between 0 and 1. When the target is very close to the flame, the configuration factor approaches 1, because everything viewed by the target is the flame. The flame is idealized with a diameter equal to the pool diameter, D, and a height equal to the flame height, H_f. If the pool has a length-to-width ratio near 1, an equivalent area circular source can be used in determining the flame length, H_f, for non-circular pools. Figure 3-5 and Figure 3-6 illustrate the cylindrical flame model under wind-free conditions.

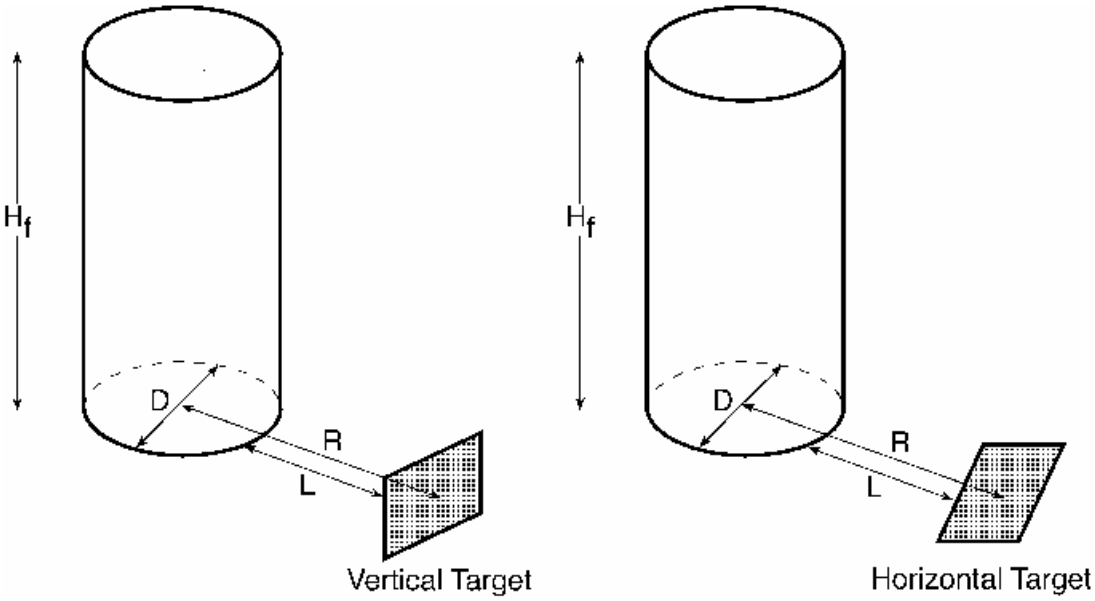

Figure 3-5: Cylindrical Flame Shape Configuration Factor Geometry for Vertical and Horizontal Targets at Ground Level with No Wind

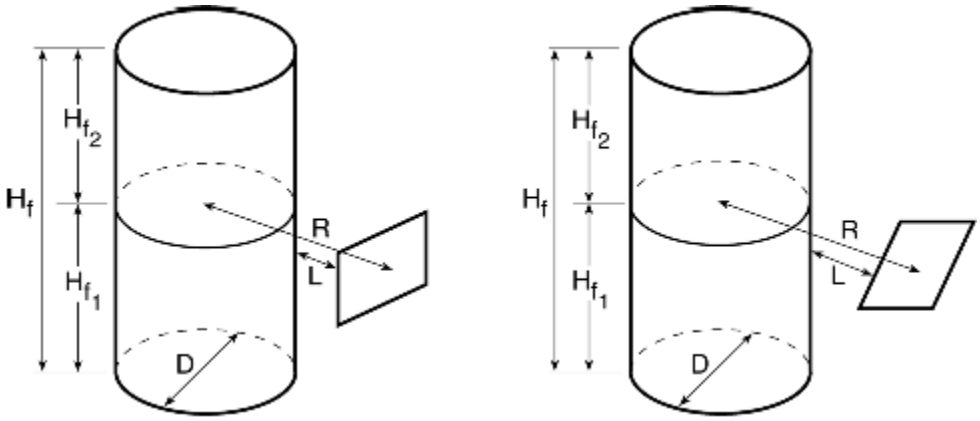

Figure 3-6: Cylindrical Flame Shape Configuration Factor Geometry for Vertical and Horizontal Targets Above Ground with No Wind

The flame height of the pool can be determined by Equation 3-14.

The radiation exchange factor between a fire and an element outside the fire depends on the shape of the flame, the relative distance between the fire and the receiving element, and the relative orientation of the element. The turbulent diffusion flame can be approximated by a cylinder. Under wind-free conditions, the cylinder is vertical, as shown by Figure 3-5. If the target is either at ground level or at the flame height, a single cylinder can represent the flame. However, if the target is above the ground, two cylinders should be used to represent the flame.

For horizontal and vertical target orientations at ground level with no-wind conditions, given the diameter and height of the flame, the configuration (or view factor) $F_{1\rightarrow 2}$ is determined using the following equations related to cylindrical radiation sources [18]:

$$F_{1\to 2,H} = \left(\begin{array}{l} \dfrac{\left(B-\dfrac{1}{S}\right)}{\pi\sqrt{B^2-1}}\tan^{-1}\sqrt{\dfrac{(B+1)(S-1)}{(B-1)(S+1)}} - \\ \dfrac{\left(A-\dfrac{1}{S}\right)}{\pi\sqrt{A^2-1}}\tan^{-1}\sqrt{\dfrac{(A+1)(S-1)}{(A-1)(S+1)}} \end{array} \right) \qquad (3\text{-}21)$$

$$F_{1\to 2,V} = \left(\begin{array}{l} \dfrac{1}{\pi S}\tan^{-1}\left(\dfrac{h}{\sqrt{S^2-1}}\right) - \dfrac{h}{\pi S}\tan^{-1}\sqrt{\dfrac{(S-1)}{(S+1)}} + \\ \dfrac{Ah}{\pi S\sqrt{A^2-1}}\tan^{-1}\sqrt{\dfrac{(A+1)(S-1)}{(A-1)(S+1)}} \end{array} \right) \qquad (3\text{-}22)$$

Where:

$$A = \frac{h^2+S^2+1}{2S}, \quad B = \frac{1+S^2}{2S}$$

$$S = \frac{2R}{D}, \quad h = \frac{2H_f}{D}$$

And:
R = the distance between the center of the cylinder (flame) to the target (m)
H_f = the height of the cylinder (flame) (m)
D = the cylinder (flame) diameter (m)

The maximum configuration factor (or view factor) at a point is given by the vectorial sum of the horizontal and vertical configuration factors:

$$F_{1\to 2,\max(\text{no-wind})} = \sqrt{F_{1\to 2,H}^2 + F_{1\to 2,V}^2} \qquad (3\text{-}23)$$

As previously stated, for targets above the ground, two cylinders should be used to represent the flame. In such instances, one cylinder represents the flame below the height of the target, while the other represents the flame above the height of the target, as shown by Figure 3-6. Thus, the following expressions are used to estimate the configuration factor (or view factor) under wind-free conditions for targets above ground level:

$$F_{1\to 2,V_1} = \left(\begin{array}{l} \dfrac{1}{\pi S}.\tan^{-1}\left(\dfrac{h_1}{\sqrt{S^2-1}}\right) - \dfrac{h_1}{\pi S}\tan^{-1}\sqrt{\dfrac{(S-1)}{(S+1)}} + \\ \dfrac{A_1h_1}{\pi S\sqrt{A_1^{\,2}-1}}\tan^{-1}\sqrt{\dfrac{(A_1+1)(S-1)}{(A_1-1)(S+1)}} \end{array} \right) \qquad (3\text{-}24)$$

Where:

$$S = \frac{2R}{D}$$

$$h_1 = \frac{2H_{f_1}}{D}$$

$$A_1 = \frac{h_1^2 + S^2 + 1}{2S}$$

$$F_{1\to 2,V_2} = \left(\begin{array}{l} \frac{1}{\pi S}.\tan^{-1}\left(\frac{h_2}{\sqrt{S^2-1}}\right) - \frac{h_2}{\pi S}\tan^{-1}\sqrt{\frac{(S-1)}{(S+1)}} + \\ \frac{A_2 h_2}{\pi S\sqrt{A_2{}^2-1}}\tan^{-1}\sqrt{\frac{(A_2+1)(S-1)}{(A_2-1)(S+1)}} \end{array} \right) \qquad (3\text{-}25)$$

Where:

$$S = \frac{2R}{D}$$

$$h_2 = \frac{2H_{f_2}}{D}$$

$$A_2 = \frac{h_2^2 + S^2 + 1}{2S}$$

And:

R = the distance between the center of the cylinder (flame) to the target (m)

H_f = the height of the cylinder (flame) (m)

D = the cylinder (flame) diameter (m)

The total configuration factor or (view factor) at a point is given by the sum of two configuration factors, as follows:

$$F_{1\to 2,V(no-wind)} = F_{1\to 2,V1} + F_{1\to 2,V2} \qquad (3\text{-}26)$$

3.5.3 Assumptions and Limitations

The methods discussed in this chapter are subject to several assumptions and limitations. For all radiation models, we assume that the pool is circular or nearly circular.

The following assumptions and limitations apply to point source radiation models:

(1) Except near the base of pool fires, radiation to the surroundings can be approximated as being isotropic or emanating from a point source.

(2) The point source model overestimates the intensity of thermal radiation at the observer's (target) locations close to the fire. This is primarily because the near-field radiation is greatly influenced by the flame size, shape, and tilt, as well as the relative orientation of the observer (target).

(3) A theoretical analysis of radiation from small pool fire by Modak [20] indicated that the point source model is within 5% of the correct incident heat flux when L/D > 2.5.

(4) The energy radiated from the flame is a specified fraction of the energy released during combustion.

The following limitation applies to solid flame radiation models at and above ground level:

(1) The correlation of emissive power was developed on the basis of data from experiments that included kerosene, fuel oil, gasoline, JP-4, JP-5, and liquified natural gas (LNG). With the exception of the LNG, these are quite luminous flames, so the correlation should be suitable for most fuels. The pool diameters ranged from 1 to 50 m (3.3 to 164 ft).

3.6 Estimating the Centerline Temperature of a Buoyant Plume

As discussed in Chapter 9 of NUREG-1805 [1], the peak temperature is found in the plume centerline, and decreases toward the edge of the plume where more ambient air is entrained to cool the plume. The centerline temperature, denoted as $T_{p(centerline)}$, varies with height. In the continuous flame region, for example, the centerline temperature is roughly constant and represents the mean flame temperature. By contrast, the temperature decreases sharply above the flames as an increasing amount of ambient air is entrained into the plume. $\Delta T_{p(centerline)}$ describes the increase in centerline plume temperature above the ambient temperature, T_a, as shown in the following equation:

$$\Delta T_{p(centerline)} = T_{p(centerline)} - T_a \qquad (3\text{-}27)$$

Numerous correlations are available to estimate the plume centerline temperature. These correlations relate the temperature as a function of HRR and of height above the source.

Heskestad [15] provided a simple correlation for estimating the maximum centerline temperature of a fire plume as a function of ceiling height and HRR:

$$T_{p(centerline)} - T_a = \frac{9.1\left(\frac{T_a}{g c_p^2 \rho_a^2}\right)^{\frac{1}{3}} \dot{Q}_c^{\frac{2}{3}}}{\left(z - z_0\right)^{\frac{5}{3}}} \qquad (3\text{-}28)$$

Where:
$T_{p(centerline)}$ = plume centerline temperature (K)
T_a = ambient air temperature (K)
$\dot{Q}_c$ = convective HRR (kW)
g = acceleration of gravity (m/sec^2)
c_p = specific heat of air (kJ/Kg-K)
ρ_a = ambient air density (kg/m^3)
z = elevation above the fire source (m)
z_0 = vertical distance of the virtual origin relative to the fire source (m)

The virtual origin is the equivalent point source height of a finite area fire (Figure 3-7). The location of the virtual origin is needed to calculate the thermal plume temperature for fires that originate in an area heat source. The thermal plume calculations are based on the assumption that the plume originates in a point heat source. Area heat sources include pool fires and burning three-dimensional objects such as cabinets and cable trays. The use of a point heat source model for area sources is accomplished by calculating the thermal plume parameters at the virtual point source elevation, rather than the actual area source elevation.

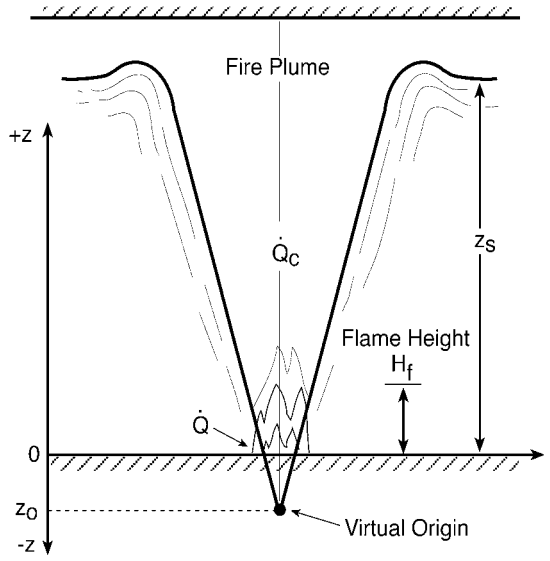

Figure 3-7: Point Source Fire Plume

The virtual origin, z_0, depends on the diameter of the fire source and the total energy released, as follows:

$$\frac{z_0}{D} = -1.02 + 0.083\frac{\dot{Q}^{\frac{2}{5}}}{D} \qquad (3\text{-}29)$$

Where:
z_0 = virtual origin (m)
D = diameter of fire source (m)
$\dot{Q}$ = total HRR (kW)

For non-circular pools, the effective diameter is defined as the diameter of a circular pool with an area equal to the actual area given by Equation 3-16.

Total HRR ($\dot{Q}$) is used when calculating the mean flame height and position of the virtual origin. However, the convective HRR ($\dot{Q}_c$) is used when estimating other plume properties, because this is the part of the energy release rate that causes buoyancy. The energy losses attributable to radiation from the flame are typically on the order of 20–40% of $\dot{Q}$. The higher of these values is valid for the sootier and more luminous flames, often from fuels that burn with a low combustion efficiency. $\dot{Q}_c$ is, therefore, often in the range of 60–80% of $\dot{Q}$.

3.6.1 Assumptions and Limitations

The methods discussed in this chapter are subject to several assumptions and limitations:

(1) All heat energy is released at a point.

(2) The correlation was developed for two-dimensional area sources.

(3) If the surrounding air is at an elevated temperature, the temperature difference between the plume and the surrounding environment is small. In this situation, the thermal plume cools less effectively, so Equation 3-28 will underestimate the temperature.

(4) The thermal plume equation is not valid when the momentum forces in a plume dominate the buoyant forces, as in a jet fire. If this type of situation is encountered, specialized calculation approaches should be used.

(5) Equation 3-28 is only valid above the flame.

4
MATHEMATICAL AND NUMERICAL ROBUSTNESS

This chapter documents the mathematical and numerical robustness of the FDT^S library, which involves verifying that the implementation of the model matches the stated documentation. A model's mathematical and numerical robustness refers to its stability and ability to reliably produce the results that the model developers intended it to produce. Specifically, ASTM E 1355 suggests the following analyses to address the mathematical and numerical robustness of models:

- Analytical tests involve testing the correct functioning of the model. In other words, these tests use the code to solve a problem with a known mathematical solution. However, there are relatively few situations for which analytical solutions are known. The models in the FDT^S library used in this study do not solve problems with known mathematical solutions. Therefore, the model results cannot be compared with known solutions to assess the correct functioning of the models.
- The correlations pre-programmed in the spreadsheets of FDT^S have been compared against hand calculations using the same equations. This comparison verified the correctness of the spreadsheet algorithms, as well as the handling of data. These comparisons have been documented by the NRC [21].
- Code checking refers to verifying the computer code on a structural basis. This verification can be achieved manually or by using a code-checking program to detect irregularities and inconsistencies within the computer code. Code checking can increase the level of confidence in the program's ability to correctly process the data to the program; however, it does not give any indication of the likely adequacy or accuracy of the program in use. The FDT^S library comprises relatively simple closed-form equations that are pre-programmed into Excel® spreadsheets. Each function requires a set of inputs and returns either a single point value or a series of values showing a trend. Problems related to irregularities and inconsistencies within the computer code are not expected; therefore, code checking in this sense is not necessary for the FDT^S library.
- Numerical tests investigate the magnitude of the residuals from the solution of a numerically solved system of equations employed in the model (as an indicator of numerical accuracy) and the reduction in residuals (as an indicator of numerical convergence). The models in the FDT^S library are closed-form mathematical expressions that are not solved using numerical methods. As a result, there are no numerical instabilities or convergence issues associated with the solutions to the models.

The spreadsheets used in this study of the FDT^S library have been verified against hand calculations. The equations and data within the tables used in the FDT^S spreadsheets are primarily described in the *SFPE Handbook of Fire Protection Engineering* [3], the *NFPA Fire Protection Handbook* [2], and other fire science literature. They are generally reliable and accepted within the fire science community as the state-of-the-art in calculation methods for fire phenomena.

In FDT^S version 1805.0, an error was identified in the algorithm for estimating the HGL temperature in a closed compartment. This error was identified because it was found that the output for this algorithm was not consistent with the conceptual basis for this calculation. The algorithm was subsequently corrected and re-released in version 1805.1 on the NRC's Web page [http://www.nrc.gov/reading-rm/doc-collections/nuregs/staff/sr1805/final-report/index.html].

5
MODEL SENSITIVITY

This chapter discusses sensitivity analysis, which ASTM E 1355 defines as a study of how changes in model parameters affect the results. In other words, sensitivity refers to the rate of change of the model output with respect to input variations. The standard also indicates that model predictions may be sensitive to (1) uncertainties in input data, (2) the level of rigor employed in modeling the relevant physics and chemistry, and (3) the accuracy of numerical treatments. Thus, the purpose of a sensitivity analysis is to assess the extent to which uncertainty in the model inputs is manifested as uncertainty in the model results of interest. The information obtained can be used to determine the dominant variables in the models, define the acceptable range of values for each input variable, quantify the sensitivity of output variables to variations in input data, and inform and caution any potential users about the degree and level of care that should be taken in selecting inputs and running the model.

When an input parameter is changed, there is also a relative magnitude change in the output. A sensitivity analysis has been conducted to determine and examine this relative magnitude change, which varies with each input. Some might have a greater effect on the output than others.

When examining the results obtained from the sensitivity analysis, the goal is to determine which inputs cause the greatest changes in the final output. In order to stay consistent, a base case must be established. The inputs for each base case are set at a value, and then each input is varied over a defined percentage change. If the percentage change in the output is greater than the percentage change in the input, the model is more sensitive to the input parameter. Conversely, if the relative change in output is less than the relative change in input, the model is less sensitive to the parameter that was changed.

5.1 Definition of Base Case Scenario for Sensitivity Analysis

A sensitivity analysis involves defining a base case scenario, and varying selected input parameters. The resultant variations in the model output are then measured with respect to the base case scenario, in order to consider the extent to which uncertainty in model inputs influences model output. The base case scenario used in this study is Benchmark Exercise (BE) #3, Test 3 (Cable F), conducted as part of the International Collaborative Fire Model Project (ICFMP).

Of all the physical input parameters, the simulation results are most sensitive to the heat release rate. In this section, one of the validation experiments (ICFMP BE #3, Test 3) is used to demonstrate the result of increasing and decreasing the specified HRR by 15%. Figure 5-1 shows plots of various output quantities, demonstrating their sensitivity to the change in HRR. Gas and surface temperatures, oxygen concentration, and compartment pressures show roughly 10% diversions from baseline, whereas the heat fluxes show roughly 20% diversions. The height of the hot gas layer is relatively insensitive to changes in the HRR. The results are not unexpected and consistent with the analysis described in Volume 2.

5.2 Sensitivity Analysis for FDT^S

FDT^S contains a number of algorithms; however, for this study, only the HGL temperature and two heat flux radiation models included in the validation were analyzed. Most of the correlations are linear; therefore, it is expected that a small change in input will not result in a large change in output. For this study, each input was varied by +15% and -15% from the base case. Figures 5-1 through 5-4 show the inputs changed along with corresponding sensitivity ratio, the maximum, minimum, and average values for each ratio.

5.3 Sensitivity to Heat Release Rate

Of all the physical input parameters, the simulation results are most sensitive to the heat release rate. In this section, one of the validation experiments (ICFMP BE #3, Test 3) is used to demonstrate the results of increasing and decreasing the specified HRR by 15%. Figure 5-1 displays plots of various output quantities demonstrating their sensitivity to changes in HRR. The hot gas layer temperature shows roughly 10% differences from baseline, whereas the heat fluxes show roughly 15% diversions for the point source model and 6–30% diversions for the solid flame model. These results for the point source model are not unexpected and consistent with the analysis described in Volume 2 to assess the sensitivity of the quantities of interest to the uncertainty in the measured HRR. The large range from baseline for the solid flame model is primarily attributable to the effect of the configuration factor. As the fire changes in height and power output, the configuration factor will change as a result of more or less exposure to the flame. The results for the solid flame model show that sensitivity to heat release rate can be significant.

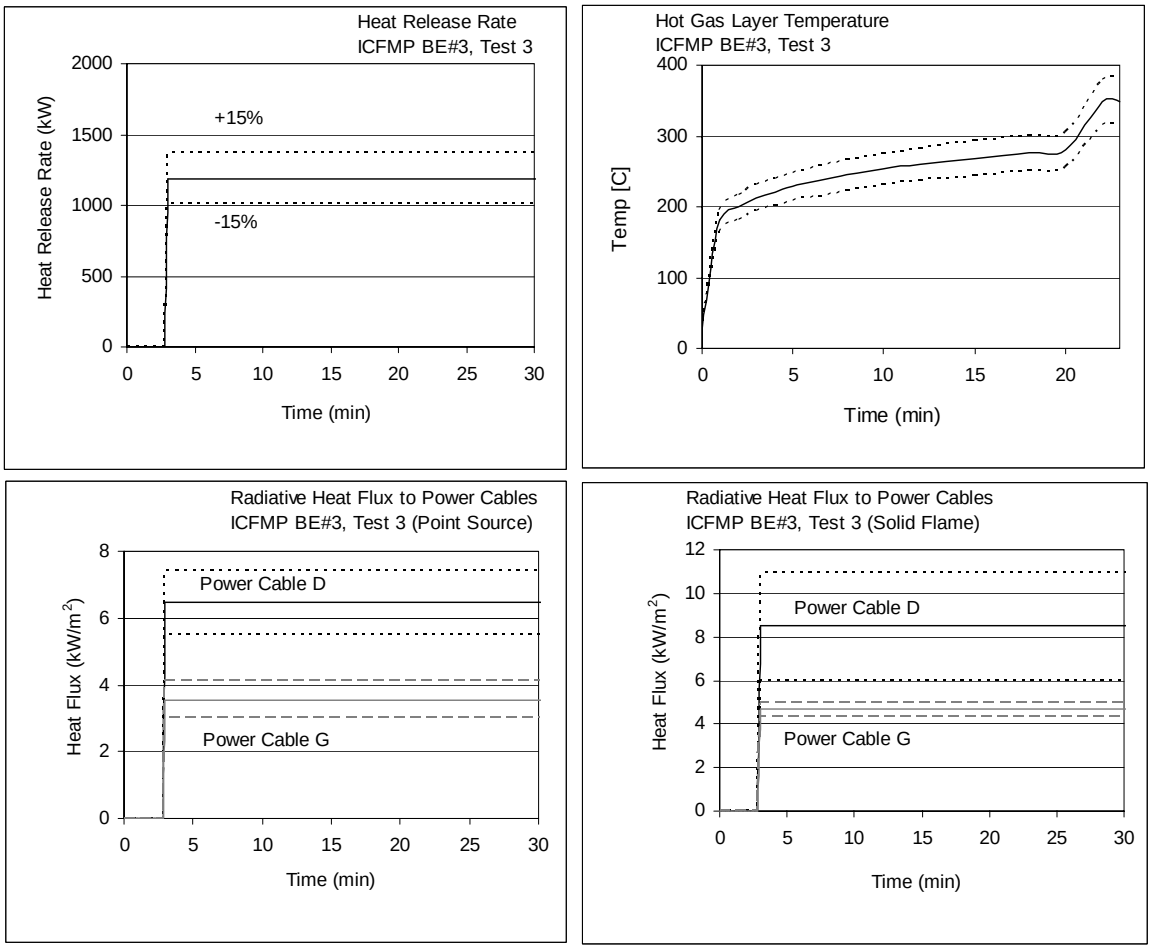

Figure 5-1: Sensitivity of Various Output Quantities to Changes in HRR

5.4 Sensitivity to Radial Distance

In this section, one of the validation experiments (ICFMP BE #3, Test 3) is used to demonstrate the results of increasing and decreasing the specified radial distance to the target by 15%. Figure 5-2 displays plots of various output quantities demonstrating their sensitivity to the change in radial distance. Both the point source radiation and solid flame radiation models were analyzed. The heat fluxes show roughly 25–39% differences for the point source model and 22–32% differences for the solid flame model. The results for the point source model are expected because the heat flux has an inverse squared relationship with the radial term. The large range from baseline for the solid flame model is primarily attributable to the effect of the configuration factor. As the target changes its distance to the fire, the configuration factor changes respectively as a result of more or less exposure to the flame. As the radial distance from the target to the fire gets smaller, the configuration factor approaches 1, which implies that the target receives all radiation released from the fire. The results for both the point source and solid flame models show that sensitivity to radial distance is relatively significant.

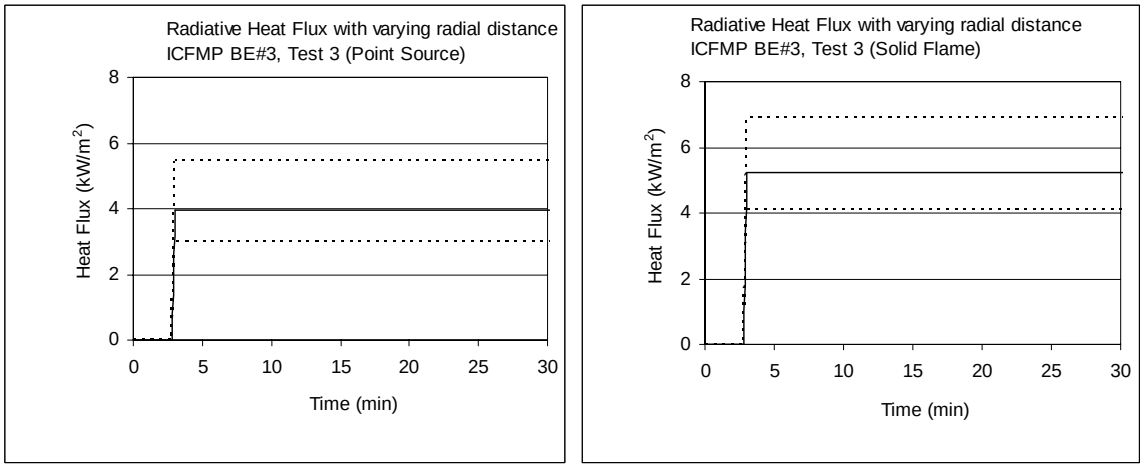

Figure 5-2: Sensitivity of Various Output Quantities to Changes in Radial Distance

5.5 Sensitivity to Radiation Fraction

In this section, one of the validation experiments (ICFMP BE #3, Test 3) is used to demonstrate the results of increasing and decreasing the specified radiation fraction of the fuel by 15%. Figure 5-3 displays a plot demonstrating the sensitivity of the point source radiation model to a varying radiation fraction. Only the point source radiation model was analyzed. The heat flux shows roughly 15% difference for the point source model. The results for the point source model are expected because the effective heat flux has a direct dependence on radiation fraction.

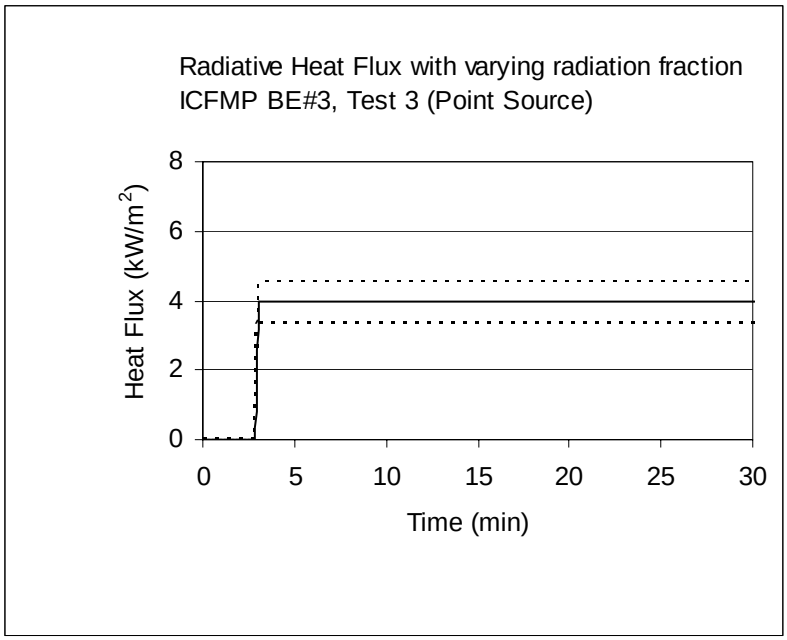

Figure 5-3: Sensitivity of Various Output Quantities to Changes in Radiation Fraction

5.6 Sensitivity to Diameter

In this section, one of the validation experiments (ICFMP BE #3, Test 3) is used to demonstrate the results of increasing and decreasing the diameter of the fire by 15%. Figure 5-4 displays a plot demonstrating the sensitivity of the solid flame radiation model to a varying diameter fire. The solid flame radiation model was analyzed, and the resulting heat flux showed roughly a 6% difference for the solid flame model. The "effective" emissive power is very insensitive to changes in diameter (0.28%), so the overall heat flux sensitivity to diameter depends on the configuration factor. However, this sensitivity is very low, as shown by the results.

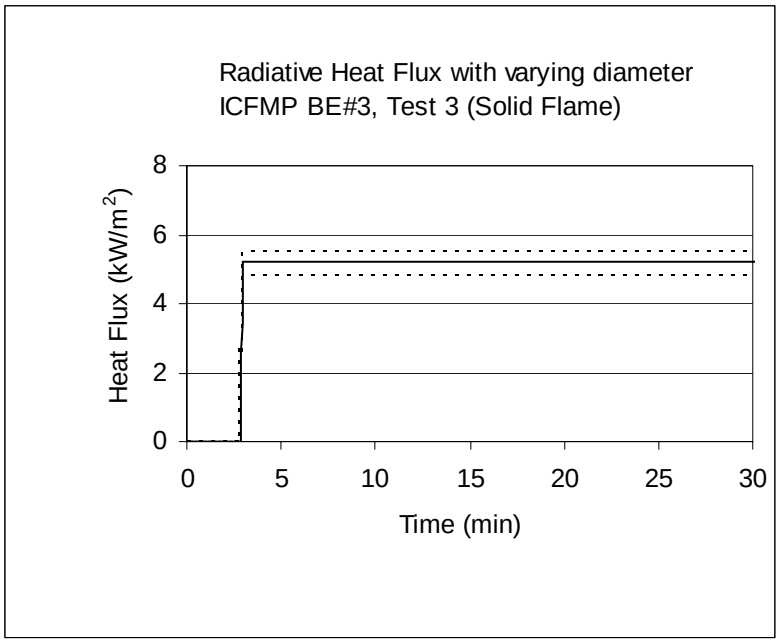

Figure 5-4: Sensitivity of Various Output Quantities to Changes in Diameter

5.7 Conclusions

This chapter describes the sensitivity of FDT^S results to changes of numerical and physical input parameters for the point source and solid flame radiation models, as well as HGL temperature. Chapter 6 (Model Validation) and Appendix A of this volume, as well as Chapter 5 of Volume 2, provide additional examples that demonstrate how changes in various input parameters affect the FDT^S predictions.

6
MODEL VALIDATION

Consistent with Section 11 of ASTM E 1355, "Model Evaluation," this chapter summarizes the results of the validation study conducted for the FDT^S library. Appendix A to this volume presents the technical details supporting the validation, including model output and comparison with experimental data.

Six experimental test series were used in the V&V study. A brief description of each is given here. Further details can be found in Volume 7 and in the individual test reports.

ICFMP BE #2: Benchmark Exercise #2 consisted of eight experiments, representing three sets of conditions, to study the movement of smoke in a large hall with a sloped ceiling. The results of the experiments were contributed to the International Collaborative Fire Model Project (ICFMP) for use in evaluating model predictions of fires in larger volumes representative of turbine halls in NPPs. The tests were conducted inside the VTT Fire Test Hall, which has dimensions of 19 m high x 27 m long x 14 m wide (62 ft x 89 ft x 46 ft). Each case involved a single heptane pool fire, ranging from 2 MW to 4 MW.

ICFMP BE #3: Benchmark Exercise #3, conducted as part of the ICFMP and sponsored by the NRC, consists of 15 large-scale tests performed at NIST in June, 2003. The fire sizes range from 350 kW to 2.2 MW in a compartment with dimensions 21.7 m high x 7.1 m long x 3.8 m wide (71.2 ft x 23.3 ft x 2.5 ft), designed to represent a variety of spaces in a NPP containing power and control cables. The walls and ceiling are covered with two layers of marinate boards, with each layer 0.0125 m (0.5 in) thick, while the floor was covered with one layer of 0.0125-m (0.5-in) thick gypsum board on top of a 0.0183-m (23/32-in) layer of plywood. The room has one door with dimensions of 2 m x 2 m (6.6 ft x 6.6 ft), and a mechanical air injection and extraction system. Ventilation conditions and fire size and location are varied, and the numerous experimental measurements include gas and surface temperatures, heat fluxes, and gas velocities.

ICFMP BE #4: Benchmark Exercise #4 consists of kerosene pool fire experiments conducted at the Institut für Baustoffe, Massivbau und Brandschutz (iBMB) of the Braunschweig University of Technology in Germany. The results of two experiments were contributed to the ICFMP. These fire experiments involve relatively large fires in a relatively small [3.6 m x 3.6 m x 5.7 m (12 ft x 12 ft x 19 ft)] concrete enclosure. Only one of the two experiments was selected for the present V&V study (Test 1).

ICFMP BE #5: Benchmark Exercise #5 consists of fire experiments conducted with realistically routed cable trays in the same test compartment as BE #4. The compartment was configured slightly differently, and the height was 5.6 m (18.4 ft) in BE #5. Only Test 4 was selected for the present evaluation, and only the first 20 minutes during which an ethanol pool fire pre-heats the compartment.

FM/SNL Series: The Factory Mutual & Sandia National Laboratories (FM/SNL) Test Series is a series of 25 fire tests conducted for the NRC by Factory Mutual Research Corporation (FMRC),

under the direction of Sandia National Laboratories (SNL). The primary purpose of these tests was to provide data with which to validate computer models for various types of NPP compartments. The experiments were conducted in an enclosure measuring 18 m long x 12 m wide x 6 m high (60 ft x 40 ft x 20 ft), constructed at the FMRC fire test facility in Rhode Island. All of the tests involved forced ventilation to simulate typical NPP installation practices. The fires consist of a simple gas burner, a heptane pool, a methanol pool, or a polymethyl-methacrylate (PMMA) solid fire. Four of these tests were conducted with a full-scale control room mockup in place. Parameters varied during testing were fire intensity, enclosure ventilation rate, and fire location. Only three of these tests have been used in the present evaluation (Tests 4, 5 and 21). Test 21 involves the full-scale mock-up. All are gas burner fires.

NBS Multi-Room Series: The National Bureau of Standards (NBS, now the National Institute of Standards and Technology, NIST) Multi-Compartment Test Series consists of 45 fire tests representing 9 different sets of conditions, with multiple replicates of each set, which were conducted in a three-room suite. The suite consists of two relatively small rooms, connected via a relatively long corridor. The fire source, a gas burner, is located against the rear wall of one of the small compartments. Fire tests of 100, 300, and 500 kW were conducted, but only three 100-kW fire experiments were used for the current V&V study (Test 100A, 100O, and 100Z).

The results for FDT^S comparisons are organized by the following quantities:

- hot gas layer temperature and height
- plume temperature
- flame height
- target/radiant heat flux

As previously defined, validation is the process of determining the degree to which a calculation method accurately represents the real world from the perspective of its intended uses. To fulfill the need for validation, the experiments described above were modeled using the appropriate FDT^S spreadsheets, and the results from the FDT^S computations were then compared to the experimental measurements and presented in the form of relative differences. Peak values were compared from both the model predictions and the experimental data. For the comparison, the following equation was used to calculate the relative difference between model and experiment:

$$\varepsilon = \frac{\Delta M - \Delta E}{\Delta E} = \frac{\left(M_p - M_o\right) - \left(E_p - E_o\right)}{\left(E_p - E_o\right)}$$

where ΔM is the difference between the modeled peak value (M_p) of the evaluated parameter and its original value (M_o), and ΔE is the difference between the experimental observation (E_p) and its original value (E_o). For this study, we assumed $M_o = E_o$. Appendix A lists the calculated relative differences for the fire modeling parameters listed above using FDT^S.

The measure of model "accuracy" used throughout this study is related to experimental uncertainty. Volume 2 discusses this issue in detail. In brief, the accuracy of a *measurement* (e.g., gas temperature) is related to the measurement device (e.g., a thermocouple). In addition, the accuracy of the *model prediction* of the gas temperature is related to the simplified physical description of the fire and the accuracy of the input parameters (e.g., the *specified* heat release rate, which is based on experimental measurements). Ideally, the purpose of a validation study is to determine the accuracy of the model in the absence of any errors related to the measurement

of both its inputs and outputs. Because it is impossible to eliminate experimental uncertainty, at the very least a combination of the uncertainty in the measurement of model inputs and output can be used as a yard stick. If the numerical prediction falls within the range of uncertainty attributable to both the measurement of the input parameters and the output quantities, it is not possible to quantify its accuracy further. At this stage, it is said that the prediction is *within experimental uncertainty*.

Each section in this chapter contains a scatter plot that summarizes the relative difference results for all of the predictions and measurements of the quantity under consideration. Details of the calculations, the input assumptions, and the time histories of the predicted and measured output are included in Appendix A. Only a brief discussion of the results for each test series is included in this chapter. Included in the scatter plots are an estimate of the combined uncertainty for the experimental measurements and uncertainty in the model inputs. It is important to understand that these are simply estimates of the lower bounds of uncertainty and do not include systematic uncertainty in the experimental measurements or model predictions. Along with expert engineering judgment of the project team, these uncertainty bounds serve as guidelines to judge the predictive capability of the model.

At the end of each section, a color rating is assigned to each of the output categories, indicating, in a very broad sense, how well the model treats that particular quantity. A detailed discussion of this rating system is included in Volume 1. For FDT^S, the Green, Yellow+, and Yellow ratings have been assigned to 4 of the 13 quantities of interest because these quantities fall within the capability of the FDT^S library. The Green rating indicates that the research team concluded the physics of the model accurately represent the experimental conditions and the calculated relative differences comparing the model and the experimental are consistent with the combined experimental and input uncertainty. The Yellow+ rating indicates that the research team concluded the physics of the model accurately represent the experimental conditions and the model consistently over predicted the experimental measurements outside the combined experimental and input uncertainty. The user should take care and use caution when interpreting the results of the model for these parameters. The Yellow rating suggests that one exercise caution when using the model to evaluate this quantity; consider carefully the assumptions made by the model, how the model has been applied, and the accuracy of its results. There is specific discussion of model limitations for the quantities assigned a Yellow rating. Parameters that are not given a color rating indicate that the model does not include output to be able to evaluate that parameter in its as-tested version.

6.1 Hot Gas Layer Temperature and Height

The single most important prediction a fire model can make is the temperature of the hot gas layer (HGL). After all, the impact of the fire is not so much a function of the heat release rate, but rather the temperature of the compartment. Following is a summary of the accuracy assessment for the HGL temperature predictions of the six test series. Relative differences for HGL Height calculations were not evaluated because FDT^S does not contain a method applicable to any of the test series. Figure 6-1 illustrates the relative differences in the form of a scatterplot.

ICFMP BE #2: FDT^S, using the method of Beyler, over-predicted the HGL temperature for Cases 1 and 2 of BE #2. The method of Foote, Pagni, and Alvarez also over-predicted for Case 3. For Cases 1 and 2, the doors were closed; for Case 3, a fan was extracting smoke throughout

the test. None of the predictions fell within the combined uncertainty bands. The relative differences may stem from an imprecise accounting of leakage in the model. The model calculations were performed using mineral wool as the wall material because it is much less conductive than steel and results in more realistic model results. In the actual experiment, the walls were made up of a 1-mm (0.04-in) thick layer of sheet metal covering a 0.5-cm (2-in) layer of mineral wool. Figure A-1 illustrates both the experimental and predicted temperature profiles.

HGL height calculations were not possible for this test series because the Yamana and Tanaka method is not applicable.

ICFMP BE #3: FDT^S over-predicted the HGL temperature for all 15 tests. The method of McCaffrey, Quintiere, and Harkleroad (MQH) was used for the open door tests (Tests 3, 9, 14, 15, and 18). Beyler's method was used for the closed door tests (Tests 1, 2, 7, 8, 13, 17). The FPA method was used for the tests that included forced ventilation (Tests 4, 5, 10, 16). The predictions for the open door tests are closer to experimental data than the closed door tests, with the exception of Test 5. In this test, the combination of open doors and mechanical ventilation led to experimental temperatures that were lower than similar tests without mechanical ventilation. None of the predictions fell within the combined uncertainty bands. For the closed compartment predictions, the relative differences may be the result of actual leakage. Beyler's correlation for closed compartments assumes a small leakage rate that will prevent a pressure buildup in the compartment, but energy lost through this leakage is ignored. If significant leakage did exist during the actual tests it could have contributed to lower temperatures by allowing the hot gases inside the compartment to escape. Beyler's method does not account for this. Another possible explanation for large relative differences for closed compartment tests may be the sensitivity of the Beyler correlation to the thermal inertia of the wall materials. The wall materials used in BE #3 had a thermal inertia about 7 times lower than the wall materials in the tests Beyler used validate his correlation. A relatively small variation between the actual thermal inertia of the materials used in the test and the properties we assumed in modeling may cause a higher relative difference. Figures A–2, A–3, and A–4 illustrate both the experimental and predicted temperature profiles.

The algorithm used to deduce HGL height from compartment temperatures is not appropriate for the closed compartment tests [22]. HGL height calculations were possible for the open door tests, but not useful for this study. The algorithm used to determine layer height from compartment temperatures showed the layer descending to the top of the door within 1–2 minutes, and spilling out of the compartment. This means the Yamana and Tanaka method would only be applicable for these 1–2 minutes, before the smoke layer spills out of the room. Plots of the experimental data and FDT^S predictions for these 1–2 minutes can be found in Section A.1.2 of Appendix A. Relative differences for layer height were not calculated for these tests.

ICFMP BE #4: Using the MQH method, FDT^S predicted the HGL temperature for this test within the combined uncertainty bands. However, the experimental temperatures reached levels outside the recognized bounds where this correlation is applicable. Figure A-6 illustrates both the experimental and predicted temperature profiles.

HGL height comparisons were not made for this test series. The algorithm used to deduce HGL height from compartment temperatures is not appropriate for this test [22]. The test included a relatively large fire in a relatively small room, which resulted in a rapidly descending HGL, creating one zone in the compartment very quickly.

ICFMP BE #5: Test ICFMP BE #5 was conducted in the same compartment as test ICFMP BE #4, but the compartment had a smaller doorway and a lower HRR fire. As a result, FDT^S, using the MQH method for a naturally ventilated compartment, over-predicted by a small margin the combined experimental uncertainty. Figure A-7 illustrates both the experimental and predicted temperature profiles.

HGL height calculation was possible for this test, but not useful for this study. The algorithm used to determine layer height from compartment temperatures showed the layer height lower than the top of the opening before 1 minute. This means the Yamana and Tanaka method would only be applicable for a limited amount of time. The relative difference for layer height was not calculated for this test.

FM/SNL: The Foote, Pagni, and Alvares (FPA) method was used to predict the HGL temperatures in the FM/SNL tests. FDT^S over-predicted the HGL temperature for the three tests, outside of the combined experimental uncertainty. Tests 4 and 21 had a ventilation rate of approximately 0.38 m^3/s (800 cfm), while Test 5 had a ventilation rate of approximately 3.78 m^3/s (8,000 cfm). The likely reason the FPA method over-predicts the temperature in these tests is the location of the inlet ports for the ventilation system. The compartment had six inlet ports located 1.2 m (3.9 ft) below the ceiling, injecting downward. This configuration means the air was injected toward the lower layer of the compartment, most likely promoting more mixing between the relatively hot upper layer and the relatively cooler lower layer. This mixing reduces the applicability of the two-layer assumption used in the FPA method. Figure A-8 illustrates both the experimental and predicted temperature profiles.

HGL height calculations using the Yamana and Tanaka method were not possible for this test series because of the forced ventilation in the compartment.

NBS Multi-Room: Using the MQH method FDT^S predicted the HGL temperature to within the experimental uncertainty for the three NBS tests. The model calculations were performed with a ceramic fiber as the wall material because it is less conductive than fire brick and results in more realistic model results. It is also important to note that the standard reduction method was not used to compute the experimental HGL temperature or height for this test series. Rather, the test director reduced the layer information individually for the eight thermocouple arrays using an alternative method [23]. Figure A-9 illustrates both the experimental and predicted temperature profiles.

HGL height calculations were not possible for these tests. The algorithm used to determine layer height from compartment temperatures showed the layer height less than the height of the doorway before the test began. This is non-physical and precludes the calculation of relative differences using the Yamana and Tanaka method to calculate layer heights.

The scatter plot shown in Figure 6-1 depicts the relative differences between the peak HGL temperature recorded in the experiments and the predictions made by the FDT^S correlations. The lines shown at -14% and 14% represent the approximate combined uncertainty of the input values and the measurement of the experimental outputs as determined in Volume 2. In these cases, it appears that the maximum HGL temperature estimates for the given conditions were always either over predicted or were predicted within experimental uncertainty. Figure 6-2 presents the same results in a different format, emphasizing the actual values of the HGL temperature.

Summary: **HGL Temperature — YELLOW+**

- The FDT^S models for HGL temperature capture the appropriate physics and are based on appropriate empirical data.
- FDT^S generally over-predicts HGL temperature, outside of uncertainty.

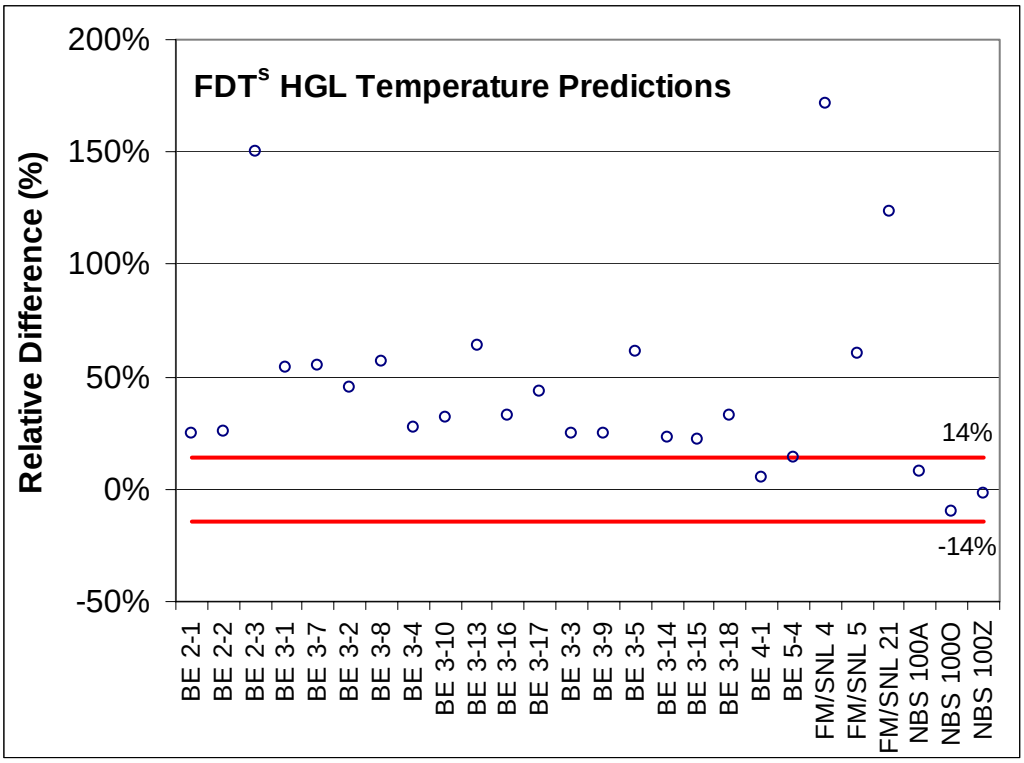

Figure 6-1: Relative Differences for HGL Temperature

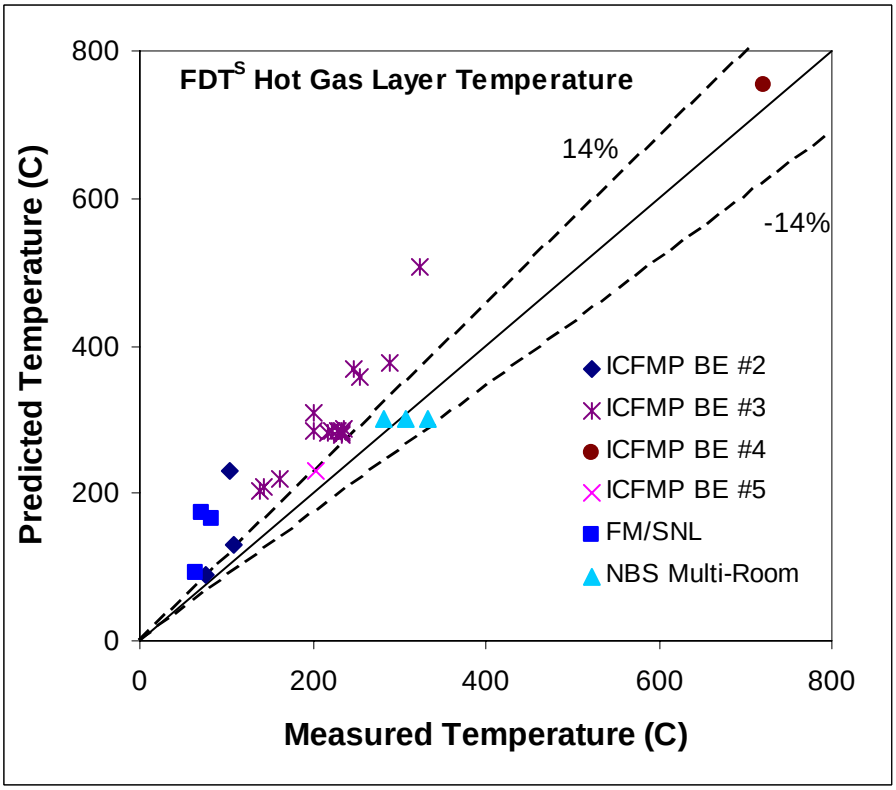

Figure 6-2: Measured vs. Predicted HGL Temperatures

6.2 Plume Temperature

Plume temperature data used to assess the accuracy of FDT^S predictions were taken from ICFMP BE #2 at 6 and 12 m (20 and 40 ft) above the fire source and in the FM/SNL test at 5.66 m (18.57 ft) above the fire source. A total of nine plume temperature data points were included in this study. The spreadsheet in the FDT^S library used to estimate the centerline temperature of a buoyant plume is 09_Plume_Temperature_Calculations.xls.

The primary user inputs to the plume temperature algorithm in FDT^S are HRR, the ambient air temperature of the enclosure, the elevation above the fuel source, and the area of combustible fuel. The inputs and assumptions required for the spreadsheet in FDT^S used to estimate the plume temperature are discussed in detail in Section 3.7. The correlation used for plume temperature in FDT^S was developed from data where the plume was unobstructed, and no hot gas layer developed. This study compares data from tests where a hot gas layer did develop. Figure 6-3 illustrates the relative differences in the form of a scatterplot.

ICFMP BE #2: Heskestad's correlation in FDT^S under-predicts the plume temperature in four of the six cases in this test series. At 12 m above the fire source FDT^S under-predicts by around 40% in all three cases. This is likely attributable to the thermocouple being enveloped by the hot gas layer in the upper part of the compartment in the tests. The correlation used in FDT^S does not account for the effect of the hot gas layer on the plume centerline temperature. At 6 m (20 ft) above the fire source, FDT^S is more accurate, predicting within experimental uncertainty in Cases 1 and 3 and under-predicting in Case 2. At 6 m (20 ft) above the fire, the hot gas layer has less of an effect on the centerline plume temperature, except for Case 2, which had a very large fire. Figure A-10 illustrates the experimental and predicted plume temperatures for this test series.

FM/SNL: In this test series, FDT^S under-predicts the plume temperature in Tests 4 and 5 and predicts within experimental uncertainty in Test 21. In Tests 4 and 5, we again see the hot gas layer affecting the plume centerline thermocouple temperature. The correlation does not account for this effect, and so FDT^S under-predicts. In Test 21, the fire was located inside an electrical cabinet, so the comparison for this test is somewhat suspect as the FDT^S correlation has no way of taking this effect into account. Figure A-11 illustrates the experimental and predicted plume temperatures for this test series.

The scatter plot shown in Figure 6-3 below depicts the relative differences between the peak plume temperature recorded in the experiments and the predictions made by the FDT^S algorithm. The lines shown at -14% and 14% represent the approximate combined uncertainty of the input values and the measurement of the experimental outputs as determined in Volume 2. In these cases, it appears that the maximum plume temperature estimates for the given conditions were always either under predicted or were predicted within experimental uncertainty. Figure 6-4 presents the same results in a different format, emphasizing the actual values of the HGL temperature.

Summary: Plume Temperature – YELLOW

- The FDT^S model for plume temperature is based on appropriate empirical data and is physically appropriate.
- FDT^S generally under-predicts plume temperature, outside of uncertainty, because of the effects of the hot gas layer on test measurements of plume temperature.

- The FDT^S model is not appropriate for predicting the plume temperatures at elevations within a hot gas layer.

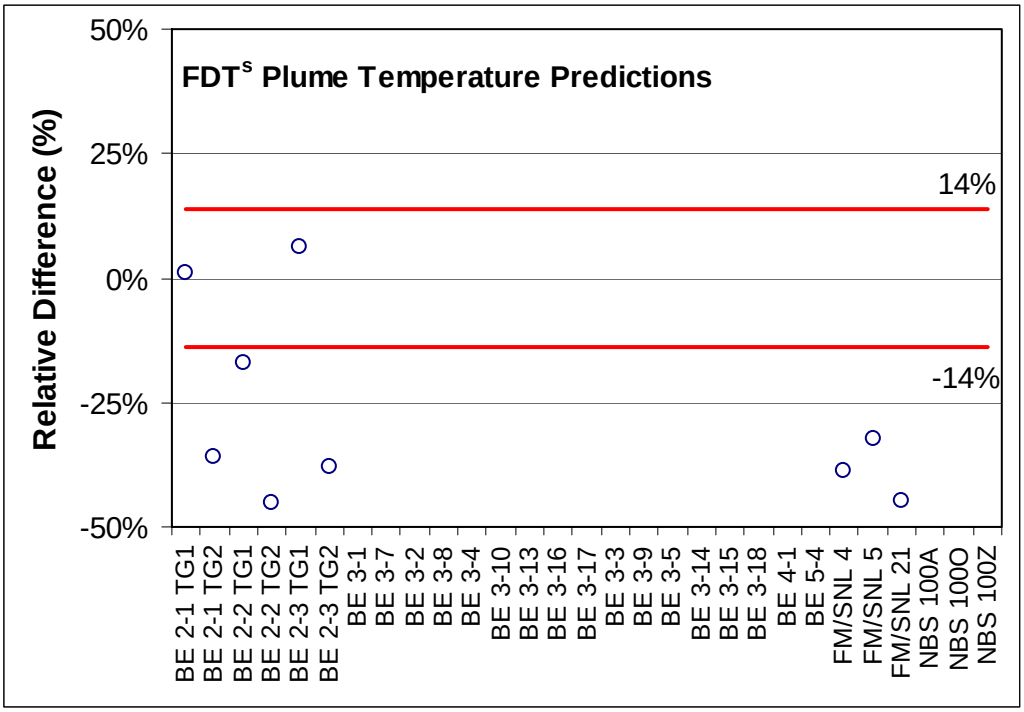

Figure 6-3: Relative Differences for Plume Temperature

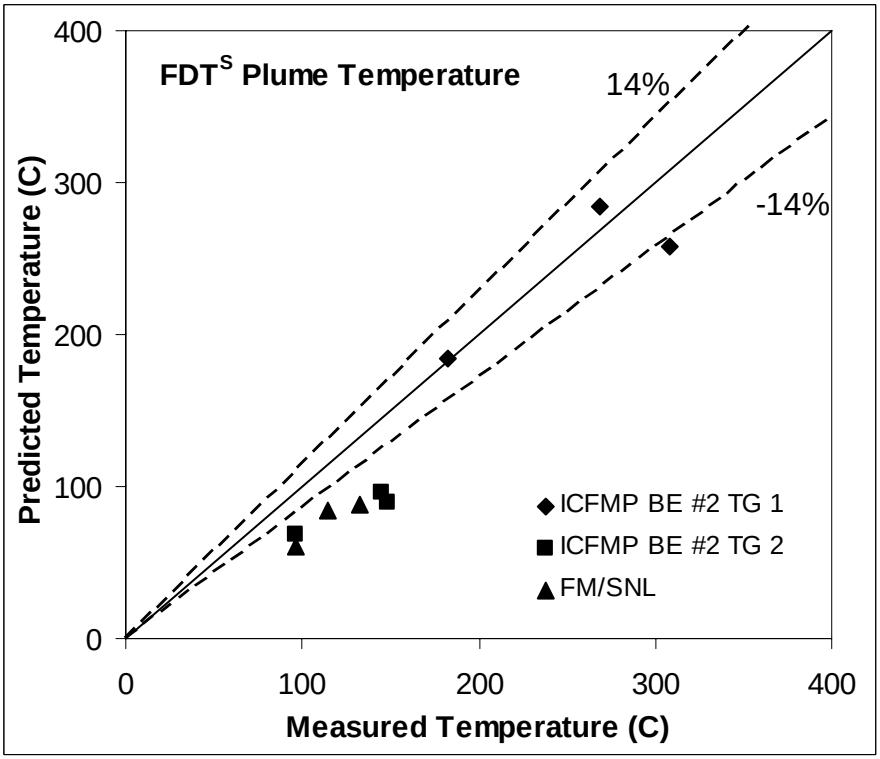

Figure 6-4: Measured vs. Predicted Plume Temperatures

6.3 Flame Height

Flame height is recorded by visual observations, photographs or video footage. Photographs from the ICFMP BE #2 test series and video from BE #3 test series are available. It is difficult to precisely measure the flame height, but the photos and videos allow one to make estimates accurate to within a pan diameter. Such observations can be compared with outputs from Heskestad's flame height correlation.

Heskestad's correlation was developed using more extensive data than the data in these studies, including pool fires and horizontal surface fires.

ICFMP BE #2: The height of the visible flame in these tests has been estimated to be between 2.4 and 3 pan diameters [3.8 to 4.8 m (12.5 to 15.7 ft)]. From Heskestad's flame height correlation in the FDT^S the estimated flame height is 4.3 m (14.1 ft).

ICFMP BE #3: During BE #3, Test 3, the peak flame height is estimated to be 2.8 m (9.2 ft), roughly consistent with the view through the doorway in compartment. FDT^S results in a flame height of 3.0 m (9.8 ft) using Heskestad's flame height prediction.

Summary: Flame Height – GREEN

- The FDT^S model predicted flame heights consistent with visual test observations.

6.4 Target/Radiant Heat Flux

As described in Chapter 3 of this volume, the FDT^S library of correlations includes radiation heat flux models that estimates heat flux at a specific distance away from a fire. Two models were compared to radiant heat flux data from the ICFMP BE #3 experiments. The first was the point source radiation model, and the second was the solid flame radiation model. The FDT^S spreadsheet used to calculate radiant heat flux is 05.1_Heat_Flux_Calculations_Wind_Free.xls. Figure 6-5 and Figure 6-7 illustrate the relative differences in the form of a scatterplot.

ICFMP BE #3: Neither the graphs in Figures A-14 through A-21 in Appendix A nor the scatterplot shown in Figure 6-5 indicates any specific trends about the accuracy of FDT^S in calculating radiant heat flux using the point source model. For a number of tests, the model predicts the peak radiant heat flux at the gauge within the uncertainty of the input parameters and the experimental measurements. For other tests, the model both under-predicts and over-predicts the radiant heat flux at a target, outside uncertainty bands. The reason that the model predictions varied so greatly can be attributed to the fact that the point source radiation model is not meant to be used for locations within a hot gas layer or relatively close to the fire.

As can be seen in Figure 6-5, the majority of the under-predictions occurred at gauge 10, which was located at 1.8 m (5.9 ft) above the floor. This gauge was likely influenced by radiation from the hot gas layer, which is not accounted for in the point source model. Most of the over-predictions occurred at locations higher in the hot gas layer. Gauges 1, 3, and 7 were located at 2, 2.5, and 3 m (6.6, 8, and 9.8 ft), respectively, above the floor. These gauges were immersed in smoke during all the tests by the time that the radiation measurements were selected for comparison. In these cases, the HGL likely prevented the radiation from the fire from reaching the gauge. Again, the correlation does not account for the effects of the HGL.

The scatter plot shown in Figure 6-5 depicts the relative differences between the peak radiant heat flux recorded in the experiments and the predictions made by the FDT^S correlations. The lines shown at -20% and 20% represent the approximate combined uncertainty of the input values and the measurement of the experimental outputs as determined in Volume 2. In these cases, it appears that the maximum radiant heat flux estimates for the given conditions do not indicate a trend of either over- or under-prediction.

Neither the graphs in Figures A-22 through A-29 in Appendix A nor the scatterplot shown in Figure 6-7 indicates any specific trends about the accuracy of FDT^S in calculating radiant heat flux using the solid flame model. For a number of tests, the model predicts the peak radiant heat flux at the gauge within the uncertainty of the input parameters and the experimental measurements. For other tests, the model over-predicts the radiant heat flux at a target for the majority of them, outside uncertainty bands. The model also under-predicts in some situations. The reason that the model predictions varied so greatly can be attributed to the fact that the solid flame radiation model is not meant to be used for locations within a hot gas layer. Another reason may be that all of the experiments used in this study had a diameter of 1 meter whereas the solid flame model was developed using data from pool fires with diameters of 1 to 50 m (3.3 to 164 ft). From the data, a least squares fit was determined for the overall trend of the "effective" emissive power (Equation 3-20). However, for smaller diameter pool fires on the order of 1 m (3.3 ft), the data are sparse for differing fuel types. This would ultimately affect the results of the radiant heat flux, depending on the fuel type.

As can be seen in Figure 6-7, the majority of the under-predictions occurred at gauge 10, which was located at 1.8 m (5.9 ft) above the floor. This gauge was likely influenced by radiation from the hot gas layer, which is not accounted for in the solid flame model. Most of the over-predictions occurred at locations higher in the hot gas layer. Gauges 1, 3, and 7 were located at 2, 2.5, and 3 m (6.6, 8, and 9.8 ft), respectively, above the floor. These gauges were immersed in smoke during all the tests by the time that the radiation measurements were selected for comparison. In these cases, the HGL likely prevented the radiation from the fire from reaching the gauge. Again, the correlation does not account for the effects of the HGL.

The scatter plot shown in Figure 6-8 depicts the relative differences between the peak radiant heat flux recorded in the experiments and the predictions made by the FDT^S correlations. The lines shown at -20% and 20% represent the approximate combined uncertainty of the input values and the measurement of the experimental outputs as determined in Volume 2. In these cases, it appears that the maximum radiant heat flux estimates for the given conditions do not indicate a trend of either over- or under-prediction.

Summary: Radiant Heat Flux – YELLOW

- The FDT^S point source radiation and solid flame radiation model in general are based on appropriate empirical data and is physically appropriate with consideration of the simplifying assumptions.
- The FDT^S point source radiation and solid flame radiation model are not valid for elevations within a hot gas layer.
- FDT^S predictions had no clear trend. The model under- and over-predicted, outside uncertainty.
- The point source radiation model is intended for predicting radiation from flames in an unobstructed and smoke-clear path between flames and targets.

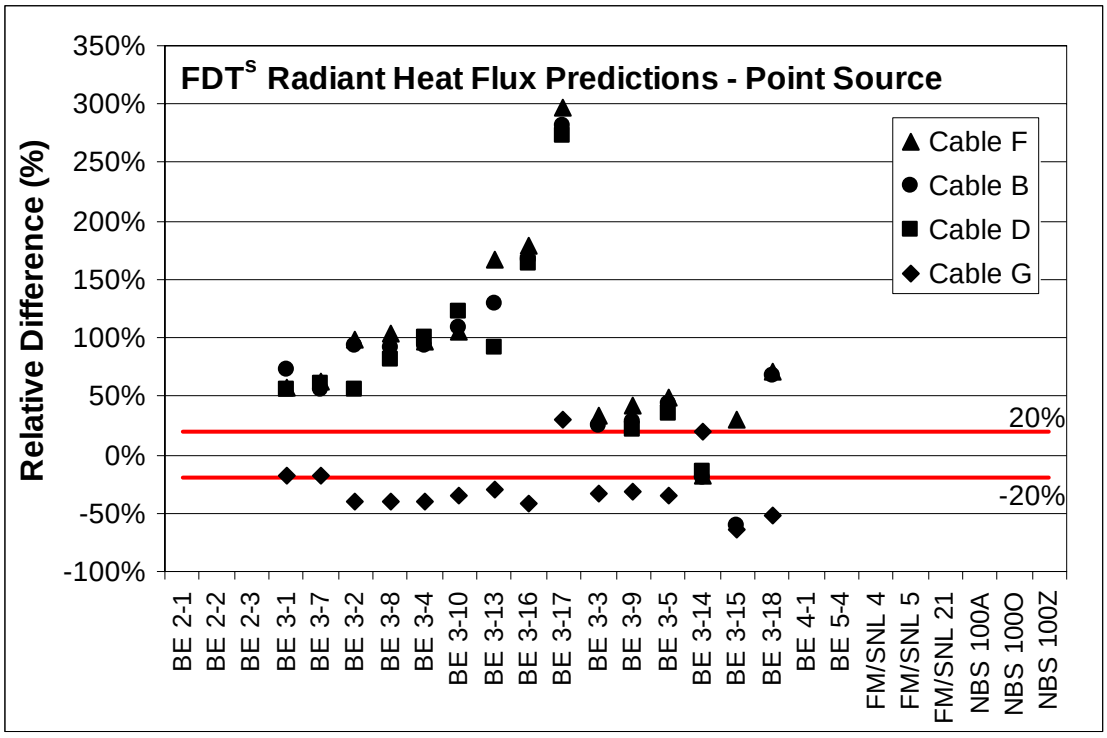

Figure 6-5: Relative Differences for Radiant Heat Flux Using Point Source Radiation Model

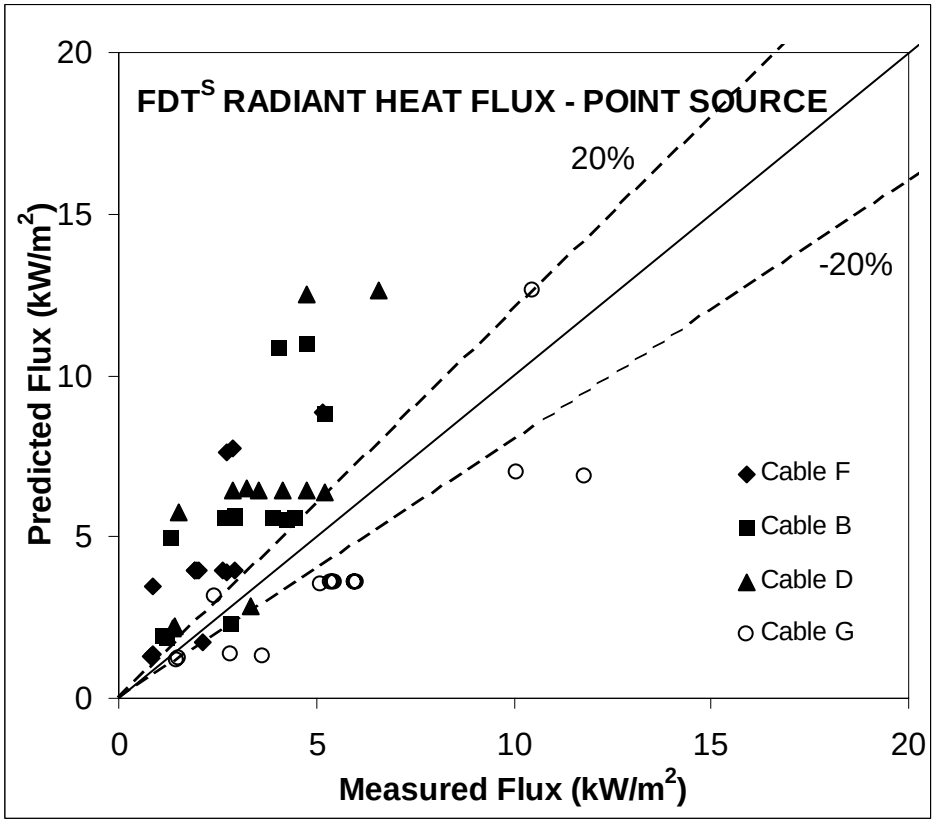

Figure 6-6: Measured vs. Predicted Radiant Heat Flux: Point Source Radiation Model

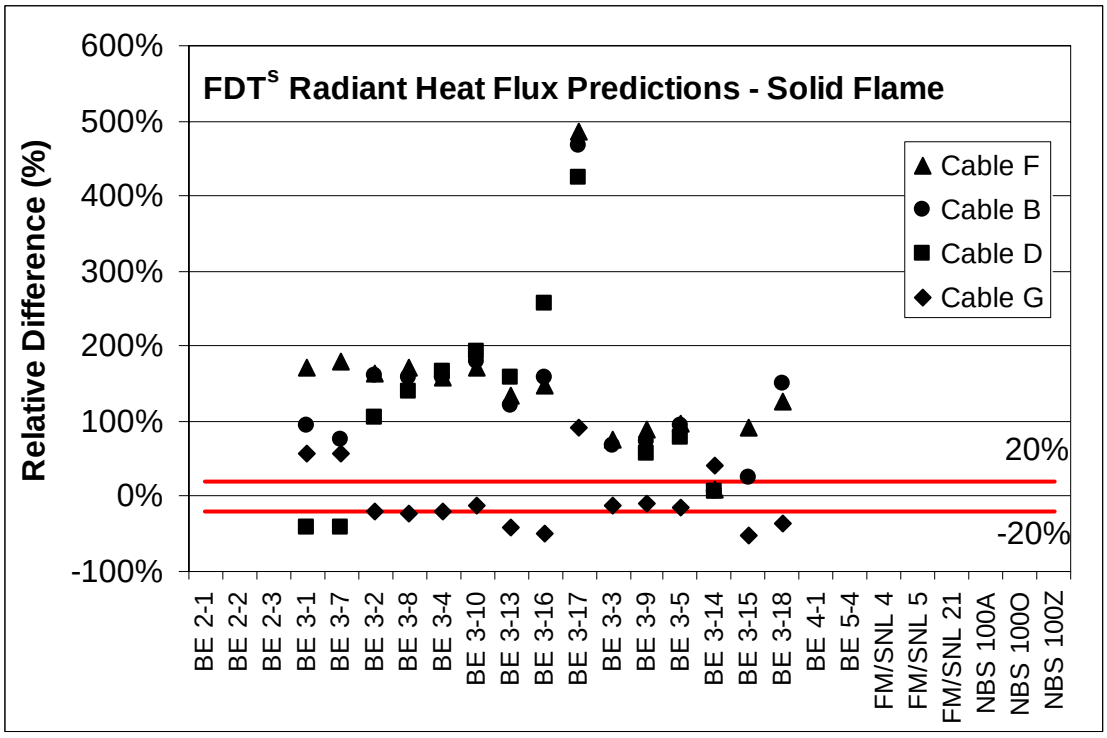

Figure 6-7: Relative Differences for Radiant Heat Flux Using Solid Flame Radiation Model

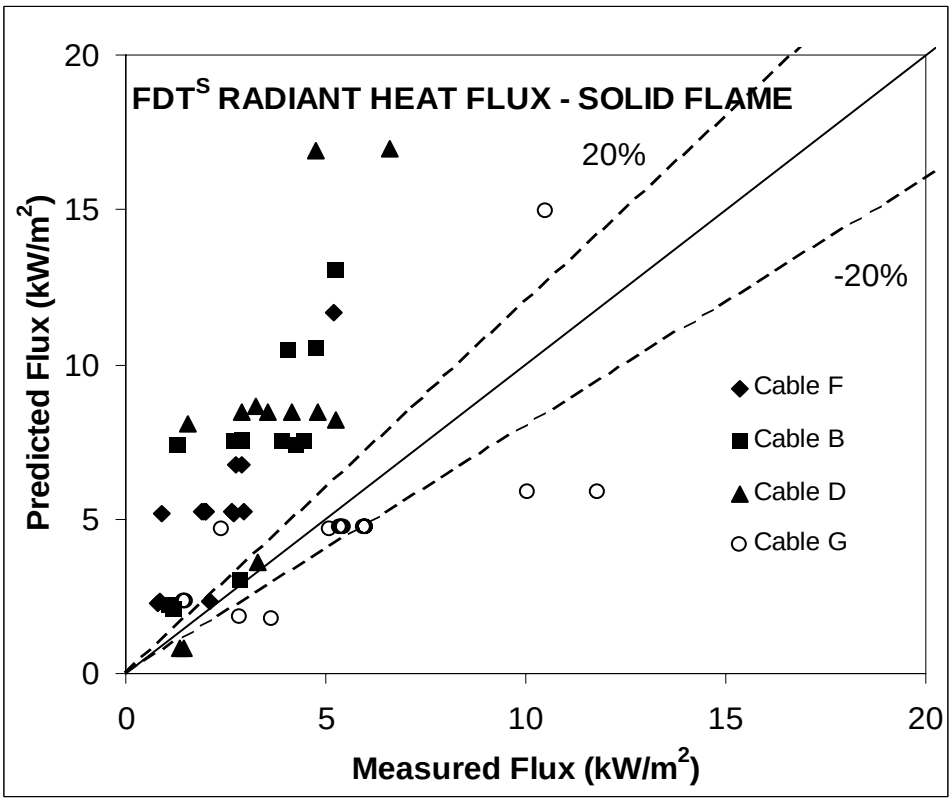

Figure 6-8: Measured vs. Predicted Radiant Heat Flux: Solid Flame Radiation Model

6.5 Summary

This chapter summarizes numerous comparisons of the FDT^S model with a range of experimental results conducted as part of this V&V effort. Four quantities were selected for comparison and a color rating assigned to each of the output categories, indicating, in a very broad sense, how well the model treats that particular quantity:

- Hot Gas Layer (HGL) Temperature: Yellow+
- Plume Temperature: Yellow
- Flame Height: Green
- Radiant Heat Flux: Yellow

One of the quantities (flame height) was assigned a Green rating, indicating that the research team concluded the physics of the model accurately represent the experimental conditions and the calculated relative differences comparing the model and the experimental are consistent with the combined experimental and input uncertainty.

- FDT^S predicts the flame height consistent with visual observations of flame height for the experiments.

One of the quantities (HGL temperature) was assigned a Yellow+ rating, indicating that the research team concluded the physics of the model accurately represent the experimental conditions, but the calculated relative differences comparing the model and the experimental results are not consistent with the combined experimental and input uncertainty. The Yellow+ rating indicates that most of the results outside the relative uncertainty resulted in over-predictions of the HGL temperatures. The user should take caution when using the model to evaluate HGL temperatures and should not automatically assume that the model will always over-predict these values.

Two of the quantities (plume temperature and radiant heat flux) were assigned a Yellow rating, indicating the user should take caution when using the model to evaluate that quantity. This typically indicates limitations in the use of the model. A few notes on the comparisons are appropriate:

- The FDT^S plume temperature, point source radiation, and solid flame radiation models are not valid for elevations within a hot gas layer.
- The point source radiation model is only intended for predicting radiation from flames in an unobstructed and smoke-clear path between flames and targets.
- FDT^S predictions had no clear trend for either parameter. The model under- and over-predicted, outside uncertainty.

The FDT^S predictions in this validation study used physically appropriate models with some limitations, but often resulted in predictions outside of the relative uncertainty. As such, it is important for the user to exercise caution when using the FDT^S spreadsheets to model fire scenarios. Like all predictive models, the best predictions come with a clear understanding of the limitations of the model and of the inputs provided to do the calculations.

7
REFERENCES

1. NUREG-1805, "Fire Dynamics Tools (FDT^s): Quantitative Fire Hazard Analysis Methods for the U.S. Nuclear Regulatory Commission Fire Protection Inspection Program," U.S. Nuclear Regulatory Commission, Washington, DC, December 2004.
2. *NFPA Fire Protection Handbook*, 18th Edition (A.E. Cote, Editor-in-Chief), National Fire Protection Association, Quincy, MA, 1997.
3. *SFPE Handbook of Fire Protection Engineering*, 3rd Edition (P.J. DiNenno, Editor-in-Chief), National Fire Protection Association and The Society of Fire Protection Engineers, Quincy, MA, 2002.
4. *Standard Guide for Evaluating the Predictive Capability of Deterministic Fire Models*, ASTM E 1355-05a, American Society for Testing and Materials, West Conshohocken, PA, 2005.
5. McCaffrey, B.J, J.G. Quintiere, and M.F. Harkleroad, "Estimating Room Temperature and Likelihood of Flashover Using Fire Test Data Correlation," *Fire Technology*, Volume 17, No. 2, pp. 98–119, Quincy, MA, 1981.
6. *Standard Test Method for Determining Material Ignition and Flame Spread Properties*, ASTM E1321-97a, American Society for Testing and Materials, West Conshohocken, PA, 2002.
7. Beyler, C.L., "Analysis of Compartment Fires with Overhead Forced Ventilation," *Proceedings of the 3rd International Symposium, International Association of Fire Safety Science (IAFSS)*, Cox and Langford, Editors, Elsevier Applied Science, New York, NY, pp. 291–300, 1991.
8. Walton, W.D., and P.H. Thomas, Chapter 3, Section 6, "Estimating Temperatures in Compartment Fires," *SFPE Handbook of Fire Protection Engineering*, 2nd Edition (P.J. DiNenno, Editor-in-Chief), National Fire Protection Association and The Society of Fire Protection Engineers, Quincy, MA, 1995.
9. Walton, W.D., and P.H. Thomas, Chapter 3, Section 6, "Estimating Temperatures in Compartment Fires," *SFPE Handbook of Fire Protection Engineering*, 3rd Edition (P.J. DiNenno, Editor-in-Chief), National Fire Protection Association and The Society of Fire Protection Engineers, Quincy, MA, 2002.
10. Foote, K.L, P.J. Pagni, and N.L. Alvares, "Temperature Correlations for Forced-Ventilated Compartment Fires," Fire Safety Science – *Proceedings of the First International Symposium, International Association of Fire Safety Science (IAFSS)*, Grant and Pagni, Editors, Hemisphere Publishing Corporation, New York, NY, pp. 139–148, 1985.

11. Deal, S., and C.L. Beyler, "Correlating Preflashover Room Fire Temperatures," *SFPE Journal of Fire Protection Engineering*, Volume 2, No. 2, pp. 33–48, The Society of Fire Protection Engineers, Quincy, MA, 1990.

12. Thomas, P.H., "The Size of Flames from Natural Fires," *Ninth Symposium (International) on Combustion*, The Combustion Institute, Pittsburgh, Pennsylvania, PA, pp. 844–859, 1962.

13. Yamana, T., and T. Tanaka, "Smoke Control in Large Spaces, Part 1: Analytical Theories for Simple Smoke Control Problems," *Fire Science and Technology*, Volume 5, No. 1, 1985.

14. Karlsson, B., and J.G. Quintiere, *Enclosure Fire Dynamics*, Chapter 8, "Conservation Equations and Smoke Filling," CRC Press LLC, New York, NY, p.206, 1999.

15. Heskestad, G., Chapter 2, Section 2-2, "Fire Plumes," *SFPE Handbook of Fire Protection Engineering*, 2nd Edition (P.J. DiNenno, Editor-in-Chief), National Fire Protection Association and The Society of Fire Protection Engineers, Quincy, MA, 1995.

16. Babrauskas, V., Chapter 3, Section 3-1, "Burning Rates," *SFPE Handbook of Fire Protection Engineering*, 2nd Edition (P.J. DiNenno, Editor-in-Chief), National Fire Protection Association and The Society of Fire Protection Engineers, Quincy, MA, 1995.

17. Drysdale, D.D., *An Introduction to Fire Dynamics*, Chapter 4, "Diffusion Flames and Fire Plumes," 2nd Edition, John Wiley and Sons, New York, NY, pp.109–158, 1998.

18. Beyler, C.L., Chapter 3, Section 1, "Fire Hazard Calculations for Large Open Hydrocarbon Fires," *SFPE Handbook of Fire Protection Engineering*, 3rd Edition (P.J. DiNenno, Editor-in-Chief), National Fire Protection Association and The Society of Fire Protection Engineers, Quincy, MA, 2002.

19. Shokri, M., and C.L. Beyler, "Radiation Hazards from Release of LPG Fires from Pressurized Storage," *Fire Safety Journal*, Volume 4, pp. 197–212, 1982.

20. Modak, A., "Thermal Radiation from Pool Fires," *Combustion and Flames*, Volume 29, pp. 177–192, 1977.

21. "Verification of NUREG-1805 by Hand Calculations," U.S. Nuclear Regulatory Commission, Washington, DC (available in ADAMS under Accession #ML062020082), July 2006.

22. Hamins, A., A. Maranghides, R. Johnsson, M. Donnelly, J. Yang, G. Mulholland, R.L. Anleitner, "Report of Experimental Results for the International Fire Model Benchmarking and Validation Exercise #3," NUREG/CR-6905/NIST SP 1013-1, U.S. Nuclear Regulatory Commission, Washington, DC, May 2006.

23. Peacock, R.D., S. Davis, and B.T. Lee, "An Experimental Data Set for the Accuracy Assessment of Room Fire Models," NBSIR 88-3752, U.S. Department of Commerce, Gaithersburg, MD, April 1988.

A
TECHNICAL DETAILS OF THE FDT^S VALIDATION STUDY

This appendix provides technical basis for the relative difference values listed in Chapter 6 of Volume 2 for the output parameters in the compilation of quantitative fire hazard analysis tools, FDT^S. This appendix is organized into sections for the parameters that have been verified and validated in this study for this specific tool. Not all of the spreadsheets included in FDT^S have been subjected to V&V because of a lack of experimental data for comparison. Each section presents a graph of the experimental data and the model output and a table of relative differences at the peaks between experimental data and the model output. The sections also describe the process and the values selected for input to the model. Within each section, the graphs are grouped by experimental test series. Discussion and analysis of the relative differences can found in Chapter 6 of Volume 2. This appendix is organized into four sections, as follows:

Volume 2 includes detailed discussion of the uncertainties associated with both the experimental data and model predictions presented in this appendix.

A.1 Hot Gas Layer Temperature and Height

Hot gas layer (HGL) temperatures in the experiments were estimated using data from ICFMP benchmark exercises (BE) 2, 3, 4, and 5, the FM/SNL test series, and the NBS multi-compartment fire test series for the room of fire origin. Specifically, thermocouple tree data from those experiments was reduced to an instantaneous average temperature above the estimated layer interface height at a specific time step. The layer interface height is deduced from the continuous vertical profile of temperature indicated by the thermocouple tree data. Relative differences were calculated by comparing the peak HGL temperatures and heights estimated from the experiment to the peak predicted HGL temperatures calculated using FDT^S. Peak or, where available, steady-state heat release rates were used as inputs to the spreadsheets. The heat release rate values for the different experiments are located in tables in this volume.

A.1.1 ICFMP BE #2

This test series consisted of three full-scale experiments with replicates. The experimental data reported here are averages of the replicate tests. In Cases 1 and 2, the test compartment was sealed with the exception of small openings incorporated as "infiltration ventilation," which amounted to approximately 2 m^2 (22 ft^2). Beyler's method for calculating HGL temperature in a closed compartment was used for Cases 1 and 2 (02.3_Temperature_CC.xls). The "infiltration ventilation" was considered small enough compared to the volume of the space so that a natural ventilation condition would not exist and Beyler's method would be appropriate. Also, as a result of a non-natural ventilation condition, the Yamana and Tanaka method for calculating HGL height will not apply.

In Case 3, mechanical extraction [11 m^3/s (388 ft^3/s)] was employed, as well as two doorway openings [3.2 m^2 each (34 ft^3/s)]. Although there is no specific correlation for the scenario with mechanical extraction and open doorways, the method of Foote, Pagni, and Alvares was used (0.2.2_Temperature_FV.xls) to calculate a relative difference for this case. The plot for Case 3 in Figure A-1 also includes a calculation using the Deal and Beyler method, which is also found in the FDT^S spreadsheet, for comparison purposes. When compared with the experimental temperatures from Cases 1 and 2, the experimental data shows that the ventilation rate had relatively minimal effect on the temperatures in the compartment.

Because the Yamana and Tanaka correlation for HGL height is not applicable to any of the experiments in BE #2, we did not make relative difference calculations for HGL height.

For Cases 1 and 2, experimental HRR data at specific times was used as input to the spreadsheet. The interior wall material for these cases was assumed to be a 0.05 m layer of mineral wool. The experimental HRRs can be found in Volume 2 and Table A-3. Tables A-1 and A-2 provide the rest of the input data. Figure A-1 illustrates the experimental and calculated HGL temperature for these tests.

Table A-1: Input Values for ICFMP BE #2, Cases 1 and 2

	Case 1	Case 2
Air		
Ambient Air Temperature (C)	20	20
Ambient Air Density (kg/m^3)	1.2	1.2
Room Size		
Compartment Width (m)	27	27
Compartment Length (m)	13.8	13.8
Compartment Height (m)	15.9	15.9
Wall Properties		
Interior Lining Thermal Inertia [$(kW/m^2\text{-}K)^2$-sec]	0.015	0.015
Interior Lining Thermal Conductivity (kW/m-K)	0.0002	0.0002
Interior Lining Specific Heat (kJ/kg-K)	0.15	0.15
Interior Lining Density (kg/m^3)	500	500
Interior Lining Thickness (m)	0.05	0.05

Table A-2: Input Values for ICFMP BE #2, Case 3

Air	
Ambient Air Temperature (C)	20
Ambient Air Density (kg/m^3)	1.2
Room Size	
Compartment Width (m)	27
Compartment Length (m)	13.8
Compartment Height (m)	15.8
Wall Properties	
Interior Lining Thermal Inertia [(kW/m^2-K)^2-sec]	0.015
Interior Lining Thermal Conductivity (kW/m-K)	0.0002
Interior Lining Specific Heat (kJ/kg-K)	0.15
Interior Lining Density (kg/m^3)	500
Interior Lining Thickness (m)	0.05
Ventilation	
Forced Ventilation Flow Rate (cfm)	23500
Heat Release Rate	
Fire Heat Release Rate (kW)	3640

Table A-3: ICFMP BE #2 Heat Release Rates

Case 1		Case 2		Case 3	
Time (sec)	HRR (kW)	Time (sec)	HRR (kW)	Time (sec)	HRR (kW)
0	0	0	0	0	0
13.2	1251	13.8	2161	13.2	2426
90	1706	30	2540	63	3184
288	1858	91.2	3071	166.2	3601
327	1782	193.2	3260	256.2	3639
409.2	1365	282	3146	292.2	3450
438	0	340.2	2729	330	2654
		372	2275	345	0
		394.8	0		

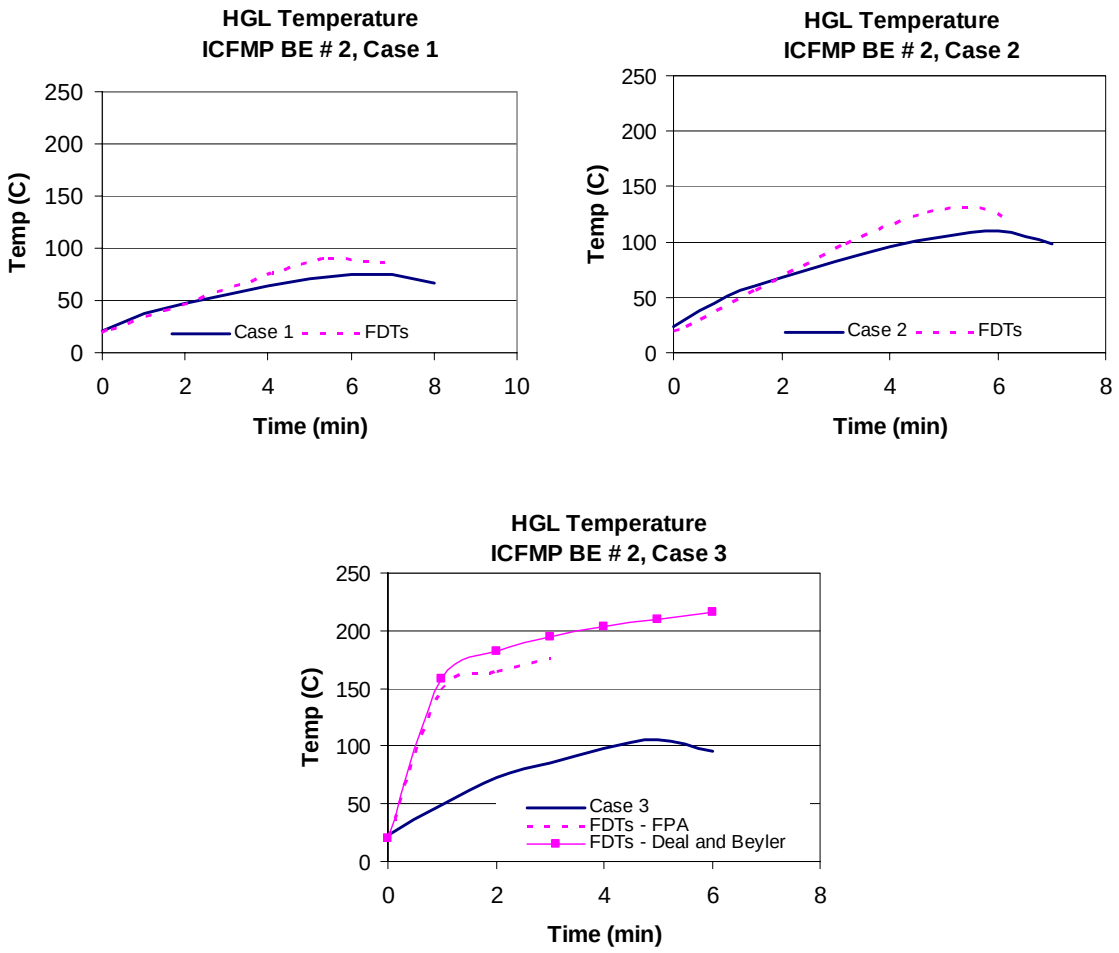

Figure A-1: Hot Gas Layer Temperature, ICFMP BE #2, Cases 1, 2, and 3

A.1.2 ICFMP BE #3

The experiments in this test consisted of heptane and toluene spray fires varying nominally from 350 kW to 2 MW. There were 15 tests conducted with more than 370 channels of data for each test. Six of the 15 tests were conducted with open doors (Tests 3, 5, 9, 14, 15, 18) and 9 with closed doors (Tests 1, 2, 4, 7, 8, 10, 13, 16, 17). One of the open door tests (Test 5) and three of the closed door tests (Tests 4, 10, 16) also had mechanical ventilation of approximately 0.81m^3/s (29 ft^3/s). The MQH model (02.1_Temperature_NV.xls) was used for open door tests without mechanical ventilation. The input values for these tests can be found in Table A-5, and plots are in Figure A-3. Beyler's method for calculating HGL temperature in closed compartments (02.3_Temperature_CC.xls) was used for closed door tests without mechanical ventilation. The input values for these tests can be found in Table A-4, and plots are in Figure A-2. The FPA model was used for all tests with forced ventilation (02.2_Temperature_FV.xls). The input values for these tests can be found in Table A-6, and plots are in Figure A-4. For Test 5, the combination of mechanical ventilation and open doors cannot be directly modeled using FDT^s, so there are two predictions reported — one using the forced ventilation model, and another using the natural ventilation model. The HRRs used for inputs were taken from the experimental

report issued by NIST. For all tests, we assumed a constant HRR that represented the steady-state average HRR of the test data. This does introduce some additional error when the experimental HRR is changing with time. No attempt is made to quantify this error other than to lump it in with general uncertainties in the HRR, as described in Volume 2. The wall material was assumed to be Marinite I and the thermal properties were taken from manufacturer's data.

Table A-4: Input Values for ICFMP BE#3 Closed Compartment Tests

	Test 1	Test 2	Test 7	Test 8	Test 13	Test 17
Air						
Ambient Air Temperature (C)	21.1	23.9	22.2	28.9	32.2	25.6
Ambient Air Density (kg/m^3)	1.2	1.19	1.2	1.17	1.16	1.18
Room Size						
Compartment Width (m)	7.04	7.04	7.04	7.04	7.04	7.04
Compartment Length (m)	21.7	21.7	21.7	21.7	21.7	21.7
Compartment Height (m)	3.82	3.82	3.82	3.82	3.82	3.82
Wall Properties						
Interior Lining Thermal Inertia $[(kW/m^2\text{-}K)^2\text{-}sec]$	0.11	0.111	0.11	0.11	0.11	0.11
Interior Lining Thermal Conductivity (kW/m-K)	0.00012	0.00012	0.00012	0.00012	0.00012	0.00012
Interior Lining Specific Heat (kJ/kg-K)	1.26	1.26	1.26	1.26	1.26	1.26
Interior Lining Density (kg/m^3)	737	737	737	737	737	737
Interior Lining Thickness (m)	0.0254	0.0254	0.0254	0.0254	0.0254	0.0254
Fire Heat Release Rate (kW)						
60 sec	410	1190	400	1190	2330	1160
120 sec	410	1190	400	1190	2330	1160
180 sec	410	1190	400	1190	2330	1160
240 sec	410	1190	400	1190	2330	1160
270 sec						1160
300 sec	410	1190	400	1190	2330	1160
360 sec					2330	
600 sec	410	1190	400	1190	2330	1160
900 sec	410		400		2330	1160
1200 sec	410		400			
1380 sec	410		400			

Table A-5: Input Values for ICFMP BE #3 Open Compartment Tests

	Test 3	Test 9	Test 14	Test 15	Test 18
Air					
Ambient Air Temperature (C)	27.8	28.9	25.6	23.3	24.4
Ambient Air Density (kg/m^3)	1.2	1.2	1.2	1.2	1.2
Room Size					
Compartment Width (m)	7.04	7.04	7.04	7.04	7.04
Compartment Length (m)	21.7	21.7	21.7	21.7	21.7
Compartment Height (m)	3.82	3.82	3.82	3.82	3.82
Wall Properties					
Interior Lining Thermal Inertia [(kW/m^2-K)^2-sec]	0.11	0.11	0.11	0.11	0.11
Interior Lining Thermal Conductivity (kW/m-K)	0.00012	0.00012	0.00012	0.00012	0.00012
Interior Lining Specific Heat (kJ/kg-K)	1.26	1.26	1.26	1.26	1.26
Interior Lining Density (kg/m^3)	737	737	737	737	737
Interior Lining Thickness (m)	0.0254	0.0254	0.0254	0.0254	0.0254
Ventilation					
Vent Width (m)	2	2	2	2	2
Vent Height (m)	2	2	2	2	2
Top of Vent from Floor (m)	2	2	2	2	2
Heat Release Rate					
Fire Heat Release Rate (kW)	1190	1170	1180	1180	1180

Table A-6: Input Values for ICFMP BE #3, Forced Ventilation Tests

	Test 4	Test 5	Test 10	Test 16
Air				
Ambient Air Temperature (C)	26.7	25	24.4	21.1
Ambient Air Density (kg/m^3)	1.2	1.2	1.2	1.2
Room Size				
Compartment Width (m)	7.04	7.04	7.04	7.04
Compartment Length (m)	21.7	21.7	21.7	21.7
Compartment Height (m)	3.82	3.82	3.82	3.82
Wall Properties				
Interior Lining Thermal Inertia [(kW/m^2-K)^2-sec]	0.11	0.11	0.11	0.11
Interior Lining Thermal Conductivity (kW/m-K)	0.00012	0.00012	0.00012	0.00012
Interior Lining Specific Heat (kJ/kg-K)	1.26	1.26	1.26	1.26
Interior Lining Density (kg/m^3)	737	737	737	737
Interior Lining Thickness (m)	0.0254	0.0254	0.0254	0.0254
Ventilation				
Forced Ventilation Flow Rate (cfm)	1907	1907	1907	1907
Heat Release Rate				
Fire Heat Release Rate (kW)	1200	1190	1190	2300

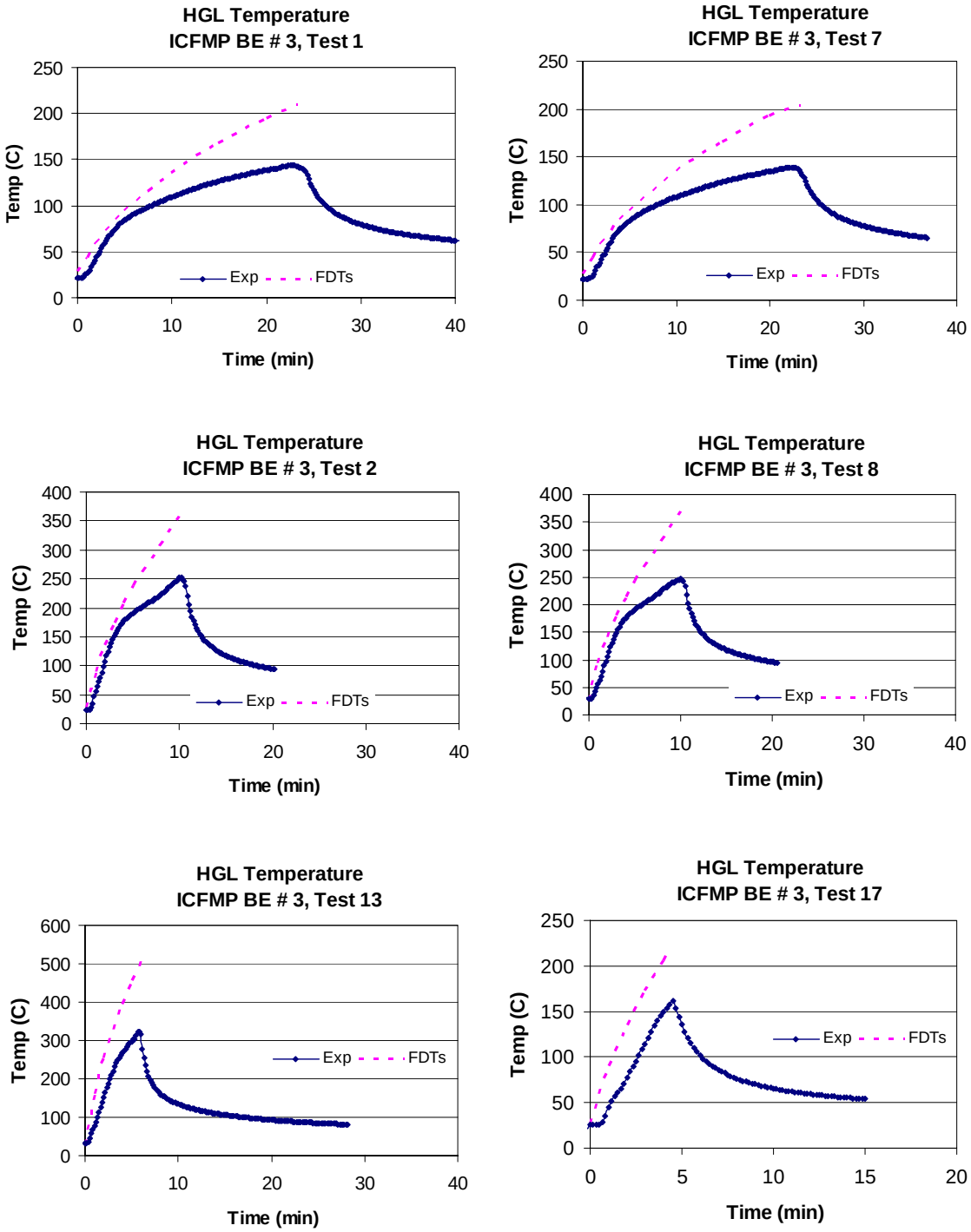

Figure A-2: Hot Gas Layer Temperature, ICFMP BE #3, Closed Compartment Tests

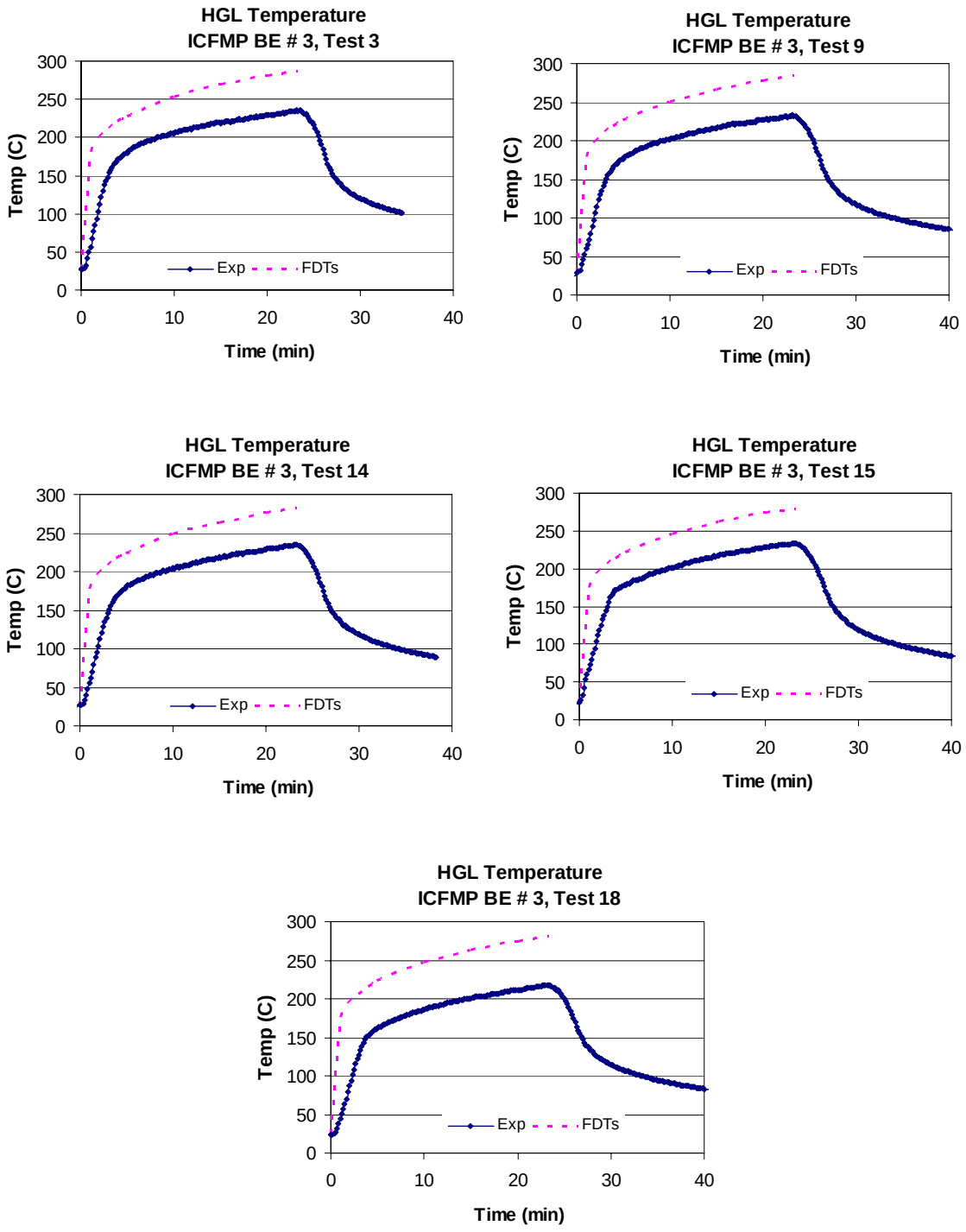

Figure A-3: Hot Gas Layer Temperature, ICFMP BE #3, Open Compartment Tests

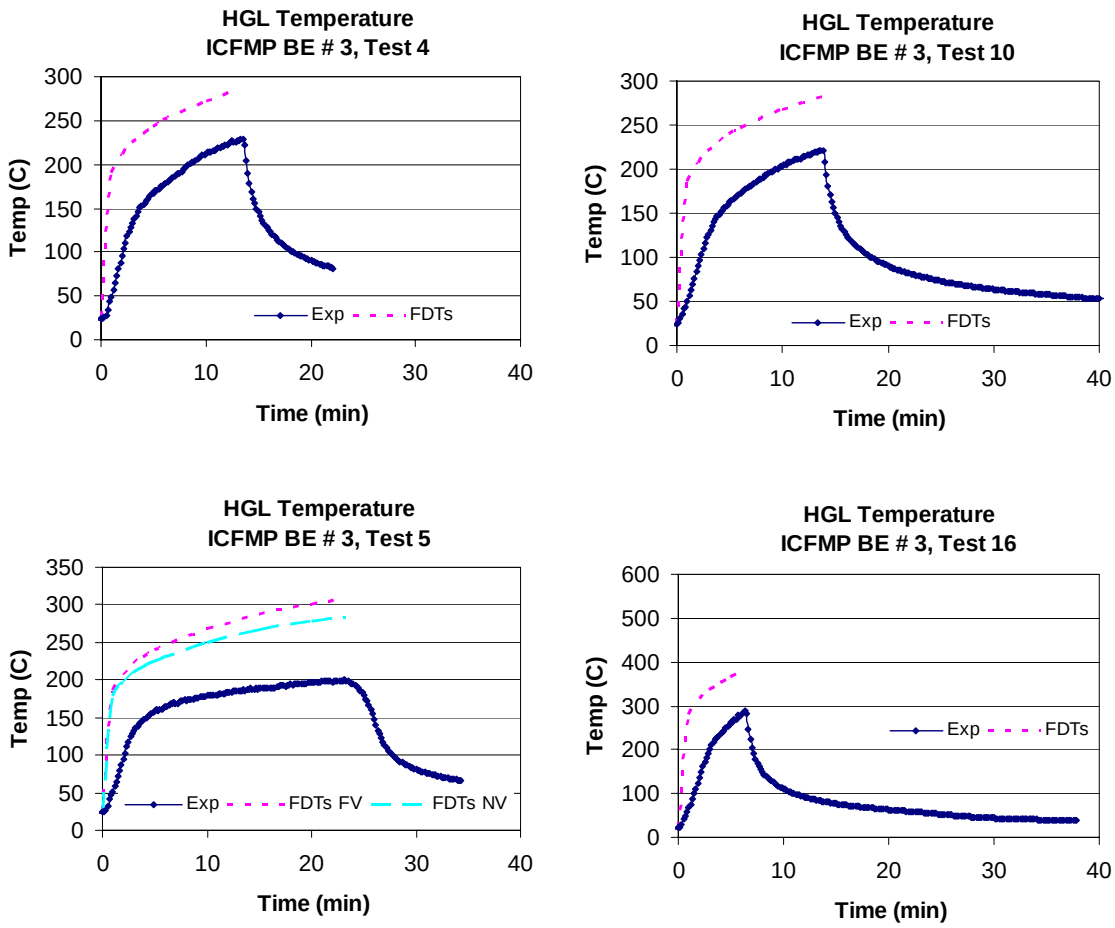

Figure A-4: Hot Gas Layer Temperature, ICFMP BE #3, Forced Ventilation Tests

A calculation method for HGL height is only found on the spreadsheet for open door conditions. However, this calculation method is only valid before the layer descends to an opening and spills out of the fire room. Figure A-5 depicts the HGL height comparisons for open door rooms only during the early times of the test, before the layer spills out of the room. A relative difference comparison is not made because of the restricted application of layer height calculation. The correlation would always over-predict the layer height as it is limited to the top of the doorway, whereas, the experimental results show the layer descending well below the top of the doorway. Other phenomena that are not captured in the correlation are the transport lag of the smoke to the ceiling and the filling time of large ceiling areas before the layer develops and descends. The correlation assumes that the layer is fully formed at the ceiling at time t = 0. The transport lag and filling time is captured in the experimental data and can be seen in Figure A-5 as an early delay in the descent of the layer height.

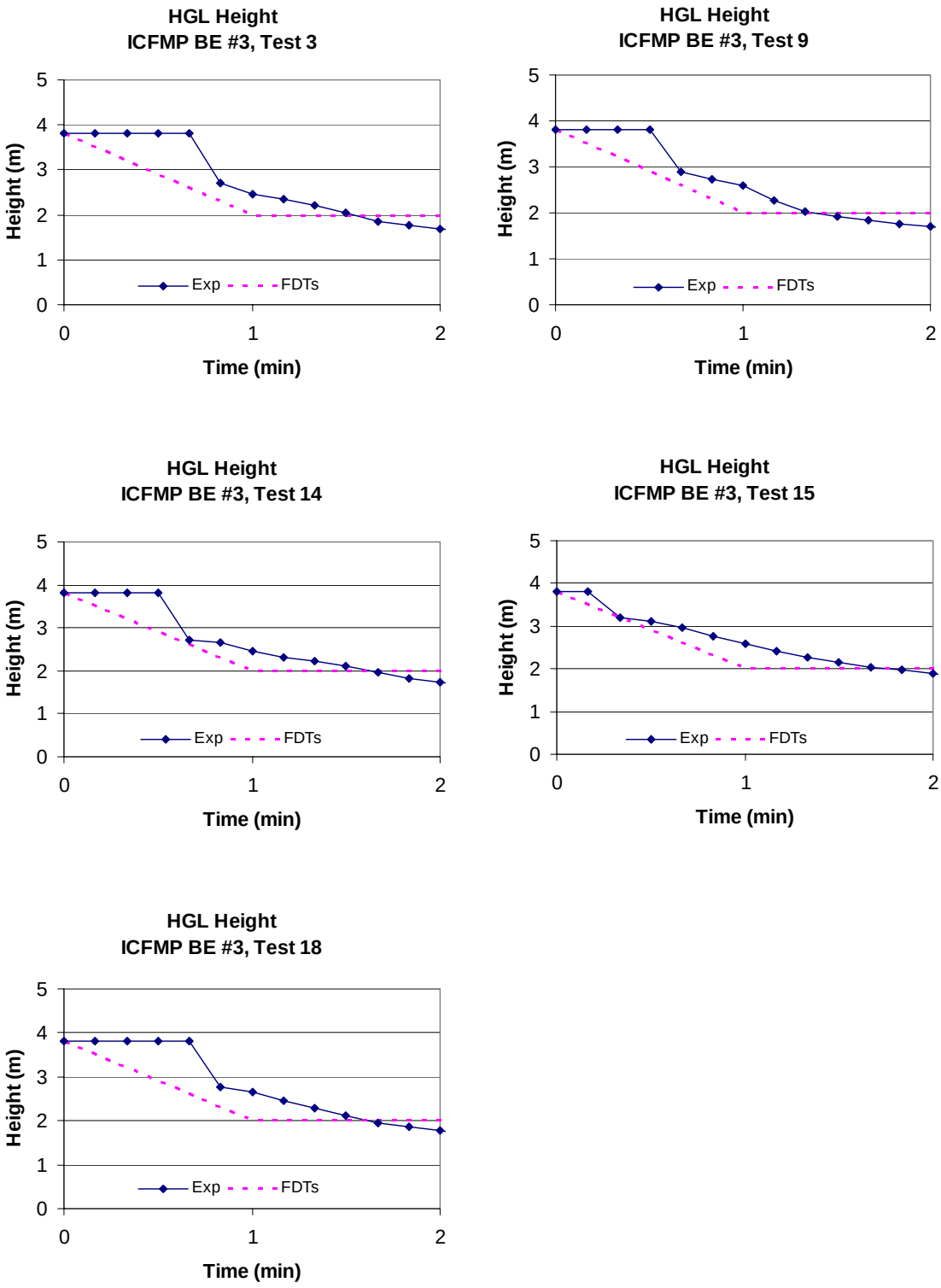

Figure A-5: Hot Gas Layer Height, ICFMP BE #3, Open Compartment Tests

A.1.3 ICFMP BE #4

This experiment included a relatively large fire in a relatively small compartment. The compartment included a doorway of about 2.1 m^2 (23 ft^2) and no mechanical ventilation. The spreadsheet in FDT^S used to estimate the HGL temperature for this exercise was 02.1_Temperature_NV.xls. The maximum experimental HRR was input as a steady-state value for the spreadsheet as a conservative assumption. This does introduce some additional error when the experimental HRR is changing with time. No attempt is made to quantify this error other than to lump it in with general uncertainties in the HRR, as described in Volume 2. The experimental HRR, thermal properties of the wall materials, and other input values can be found in Table A-7. The plot of HGL temperature in this test is Figure A-6. There is some time lag in the data that may be associated with an ambiguous test start, thermocouple lag, or time for fire to spread across the pool surface. These effects are not accounted for in the correlation.

Experimental data for HGL Height during this test is not available for comparison.

Table A-7: Input Values for ICFMP BE #4

Air	
Ambient Air Temperature (C)	20
Ambient Air Density (kg/m^3)	1.2
Room Size	
Compartment Width (m)	3.6
Compartment Length (m)	3.6
Compartment Height (m)	5.7
Wall Properties	
Interior Lining Thermal Inertia [$(kW/m^2\text{-}K)^2$-sec]	9.45
Interior Lining Thermal Conductivity (kW/m-K)	0.00075
Interior Lining Specific Heat (kJ/kg-K)	0.84
Interior Lining Density (kg/m^3)	1500
Interior Lining Thickness (m)	0.3
Ventilation	
Vent Width (m)	0.7
Vent Height (m)	3
Top of Vent from Floor (m)	3.6
Heat Release Rate	
Fire Heat Release Rate (kW)	3518

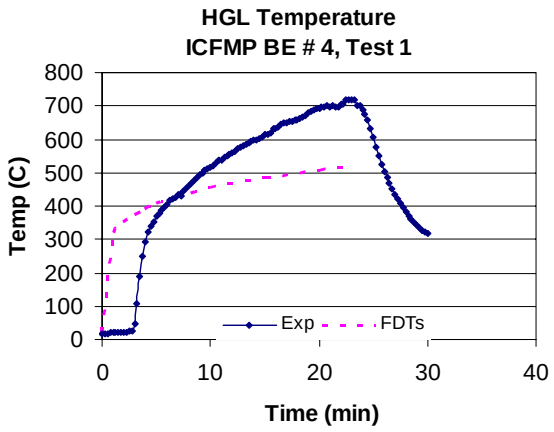

Figure A-6: Hot Gas Layer Temperature, ICFMP BE #4

A.1.4 ICFMP BE #5

This experiment was conducted in the same compartment as ICFMP BE #4, except the doorway was smaller, about 1.5 m^2 (16 ft^2), again with no mechanical ventilation. The HRR of this test was an order of magnitude less than in BE #4. The spreadsheet in FDT^S used to estimate the HGL temperature for this exercise is 02.1_Temperature_NV.xls. The maximum experimental HRR was input as a steady-state value for the spreadsheet as a conservative assumption. This does introduce some additional error, when the experimental HRR is changing with time. No attempt is made to quantify this error other than to lump it in with general uncertainties in the HRR, as described in Volume 2. The HRR and other input values can be found in Table A-8. Figure A-7 illustrates the experimental and calculated HGL temperature for this test.

Table A-8: Input Values for ICFMP BE #5

Air	
Ambient Air Temperature (C)	20
Ambient Air Density (kg/m^3)	1.2
Room Size	
Compartment Width (m)	3.6
Compartment Length (m)	3.6
Compartment Height (m)	5.7
Wall Properties	
Interior Lining Thermal Inertia [(kW/m^2-K)^2-sec]	9.45
Interior Lining Thermal Conductivity (kW/m-K)	0.0075
Interior Lining Specific Heat (kJ/kg-K)	0.84
Interior Lining Density (kg/m^3)	1500
Interior Lining Thickness (m)	0.3
Ventilation	
Vent Width (m)	0.7
Vent Height (m)	2.2
Top of Vent from Floor (m)	3.6
Heat Release Rate	
Fire Heat Release Rate (kW)	716

Experimental data for HGL height during this test are not available for comparison.

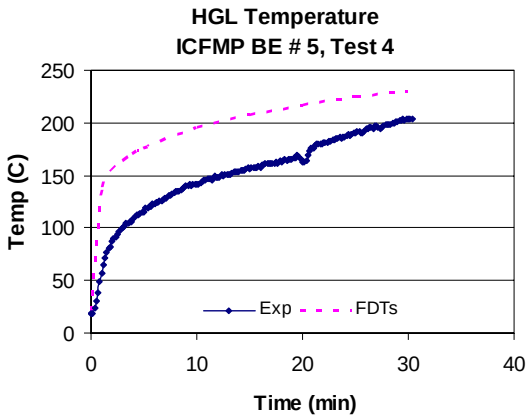

Figure A-7: Hot Gas Layer Temperature, ICFMP BE #5

A.1.5 The FM/SNL Test Series

This test series was conducted in a large closed room with mechanical ventilation. Tests 4 and 21 had a ventilation rate of approximately 0.37 m^3/s (13 ft^3/s), while Test 5 had a ventilation rate of approximately 3.7 m^3/s (131 ft^3/s). The FPA model was used for these tests with forced ventilation (02.2_Temperature_FV.xls). A steady-state HRR of 516 kW based on experimental data was used as input to the spreadsheets. This value represents the steady-state average HRR during the tests. This does introduce some additional error when the experimental HRR is changing with time. No attempt is made to quantify this error other than to lump it in with general uncertainties in the HRR, as described in Volume 2. The input values used for these three tests can be found in Table A-9. Figure A-8 illustrates the experimental and calculated HGL temperature for these tests.

Table A-9: Input Values for FM/SNL Tests

	Test 4	Test 5	Test 21
Air			
Ambient Air Temperature (C)	20	20	20
Ambient Air Density (kg/m^3)	1.2	1.2	1.2
Room Size			
Compartment Width (m)	12.2	12.2	12.2
Compartment Length (m)	18.3	18.3	18.3
Compartment Height (m)	6.1	6.1	6.1
Wall Properties			
Interior Lining Thermal Inertia [(kW/m^2-K)^2-sec]	0.108	0.108	0.108
Interior Lining Thermal Conductivity (kW/m-K)	0.00012	0.00012	0.00012
Interior Lining Specific Heat (kJ/kg-K)	1.25	1.25	1.25
Interior Lining Density (kg/m^3)	720	720	720
Interior Lining Thickness (m)	0.025	0.025	0.025
Ventilation			
Forced Ventilation Flow Rate (cfm)	800	8000	800
Heat Release Rate			
Fire Heat Release Rate (kW)	516	516	516

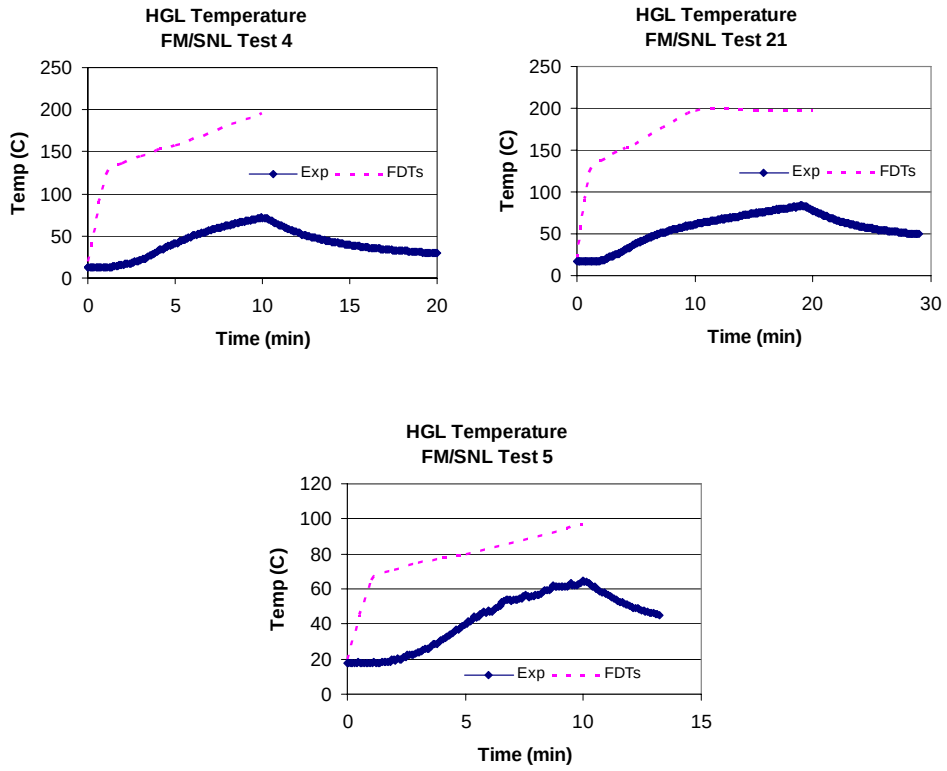

Figure A-8: Hot Gas Layer Temperature, FM/SNL Tests

A.1.6 The NBS Test Series

This test series involved a three compartment configuration with two smaller rooms opening off of a long corridor. One of the smaller rooms contained the fire source. All experimental data used to compare with FDT^S came from the fire room because FDT^S does not have the capability to model conditions in rooms other than the fire room. The three tests considered are labeled 100A, 100O, and 100Z, respectively. The differences between these three tests concerned ventilation conditions in the corridor. Test 100A involved closed doors from the corridor to the outside and from the corridor to the third room. Test 100O involved an open door from the corridor to the outside and a closed door from the corridor to the third room. Test 100Z involved open doors from the corridor to the outside and from the corridor to the third room. Because all tests involved an open door between the fire room and the corridor, the spreadsheet with the MQH model (02.1_Temperature_NV.xls) was used to estimate HGL temperature for the NBS tests. All three tests used a HRR of 110 kW, based on experimental HRR data. This value represents the steady-state average HRR during the tests. This does introduce some additional error when the experimental HRR is changing with time. No attempt is made to quantify this error other than to lump it in with general uncertainties in the HRR, as described in Volume 2. Material properties and other input values can be found in Table A-10. Figure A-9 illustrates the experimental and calculated HGL temperatures for these tests.

Table A-10: Input Values for NBS Tests

Air	
Ambient Air Temperature (C)	22.8
Ambient Air Density (kg/m^3)	1.19
Room Size	
Compartment Width (m)	2.34
Compartment Length (m)	2.34
Compartment Height (m)	2.16
Wall Properties	
Interior Lining Thermal Inertia [(kW/m^2-K)^2-sec]	0.012
Interior Lining Thermal Conductivity (kW/m-K)	0.00009
Interior Lining Specific Heat (kJ/kg-K)	1.04
Interior Lining Density (kg/m^3)	128
Interior Lining Thickness (m)	0.05
Ventilation	
Vent Width (m)	0.8
Vent Height (m)	1.6
Top of Vent from Floor (m)	1.6
Heat Release Rate	
Fire Heat Release Rate (kW)	110

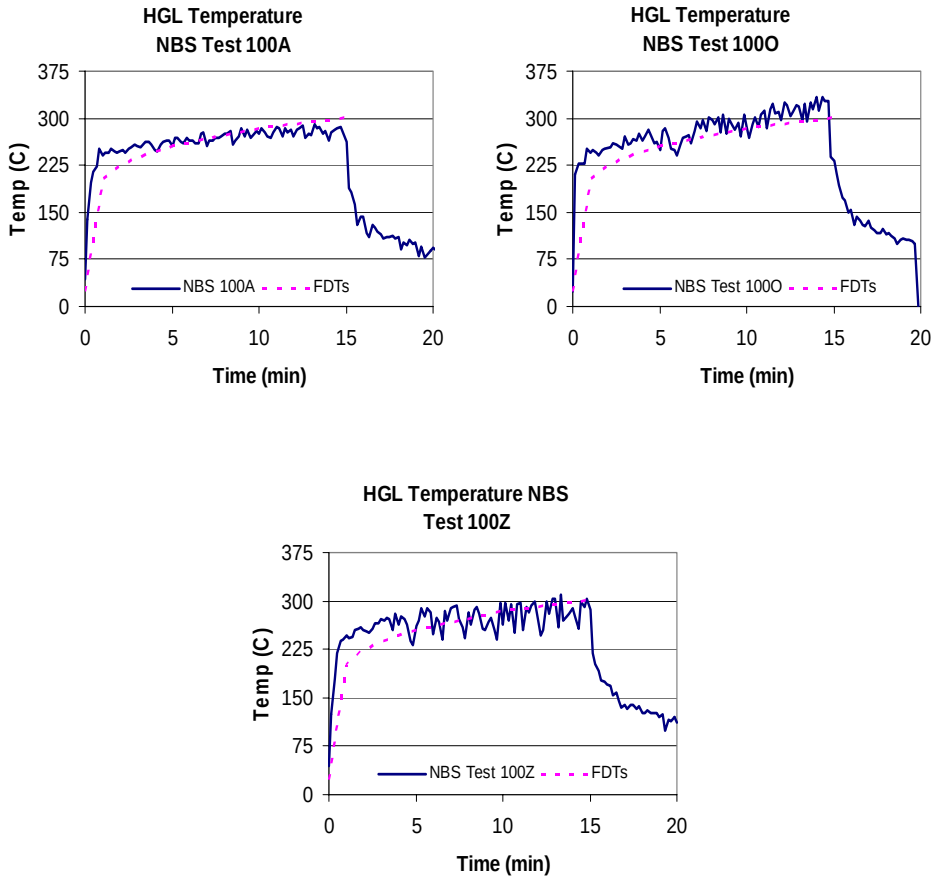

Figure A-9: Hot Gas Layer Temperature, NBS Tests

A.1.7 Summary: Hot Gas Layer Temperature and Height

Table A-11 lists the relative differences between experimental data and model results for HGL temperature. "ΔE" is the difference between the experimental peak and the experimental initial condition. "ΔM" is the difference between model peak and the model initial conditions, which is assumed to be the experimental initial condition. Because FDT^S does not have an appropriate calculation method for layer height for the experimental conditions in these tests, no relative differences are given.

Table A-11: Hot Gas Layer Temperature Relative Differences

		Hot Gas Layer Temperature (°C)		
		Δ E	Δ M	% Difference
ICFMP BE #2	Case 1	55	69	**25%**
	Case 2	86	108	**25%**
	Case 3	83	207	**150%**
ICFMP BE #3	Test 1	123	189	**61%**
	Test 2	229	333	**47%**
	Test 3	207	259	**54%**
	Test 4	204	260	**27%**
	Test 5	175	283	**61%**
	Test 7	117	181	**65%**
	Test 8	218	341	**53%**
	Test 9	204	255	**55%**
	Test 10	198	260	**31%**
	Test 13	290	475	**61%**
	Test 14	208	256	**52%**
	Test 15	211	257	**51%**
	Test 16	268	356	**33%**
	Test 17	135	194	**45%**
	Test 18	194	256	**64%**
BE #4	Test 1	701	734	**-29%**
BE #5	Test 4	186	211	**14%**
FM/SNL	Test 4	60	162	**209%**
	Test 5	47	75	**69%**
	Test 21	66	148	**170%**
NBS	Test 1	248	260	**5%**
	Test 2	310	278	**-10%**
	Test 4	284	277	**-2%**

A.2 Plume Temperature

Plume temperatures are measured with thermocouple trees above the fire source. The test series that included an arrangement for collecting plume temperature data include ICFMP BE #2, #4, and #5, and FM/SNL. During BE #4 and BE #5, the fire and the plume tilted away from the plume thermocouples; therefore, those data will not be used. The following figures present the experimental observations as well as FDT^S predictions for plume temperature using Heskestad's plume temperature correlation (FDT^S spreadsheet: 09_Plume_Temperature_Calculations.xls).

A.2.1 ICFMP BE #2

In the experiment, the two thermocouples in the fire plume were located 6 m (23 ft) and 12 m (43 ft) above the fire source, respectively. HRRs were calculated from fuel mass loss rates during the experiments, modified by an efficiency factor of 0.85. The convective heat release fraction used was 0.65. The input values for this experiment can be found in Table A-12 while the heat release rates can be found in Table A-3. Figure A-10 illustrates the experimental and calculated plume temperatures for these tests. The experimental temperatures are higher at the 12-m (43-ft) level, most likely because of the development of the HGL, and its effect on the thermocouples. The plume correlation does not account for this effect. The HGL would have less of an effect on the 6-m (23-ft) level thermocouples.

Table A-12: Input Values for ICFMP BE #2 Plume Temperature Calculations

	TG1	TG2
Air		
Ambient Air Temperature (C)	20	20
Ambient Air Density (kg/m^3)	1.2	1.2
Fire Characteristics		
Elevation Above the Fire Source (m)	7	13
Area of Combustible Fuel (m^2)	0.5	0.5
Convective Heat Release Rate Fraction (x_c)	0.65	0.65

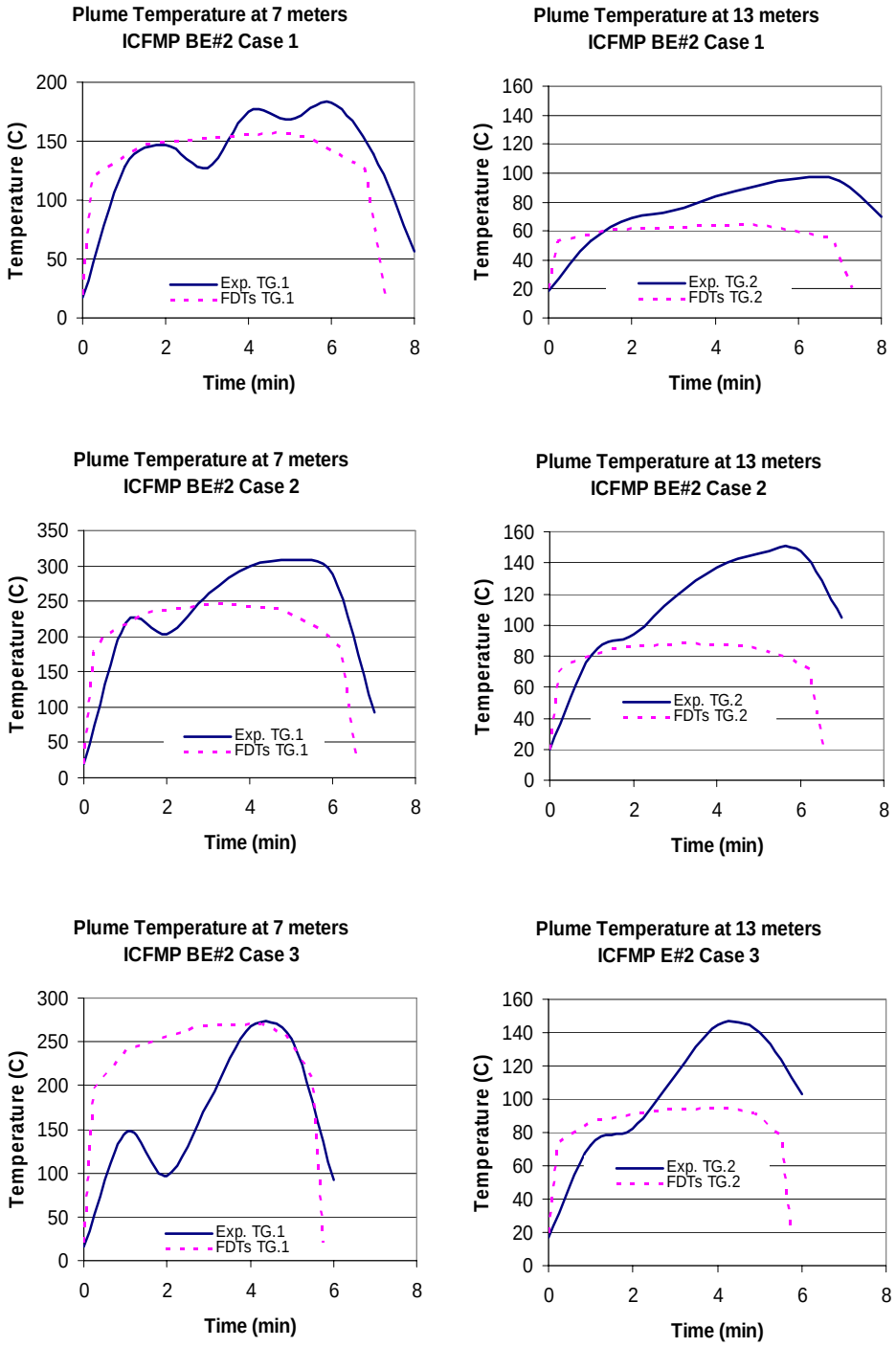

Figure A-10: Plume Temperature, ICFMP BE #2, Cases 1, 2, and 3

A.2.2 The FM/SNL Test Series

The thermocouple for measuring plume temperatures was located 5.66 m (18.6 ft) above the base of the fire, approximately 5.95 m (19.5 ft) above the floor. The HRRs used as inputs were calculated using a t^2 curve with a peak of 516 kW, which matches the experimental data. The convective heat release fraction used was 0.65. Additional input values can be found in Table A-13. Figure A-11 illustrates the experimental and calculated plume temperatures for these tests.

Table A-13: Input Values for FM/SNL Tests Plume Temperature Calculations

Air	
Ambient Air Temperature (C)	20
Ambient Air Density (kg/m^3)	1.2
Fire Characteristics	
Elevation Above the Fire Source (m)	5.66
Area of Combustible Fuel (m^2)	0.17
Convective Heat Release Rate Fraction (x_c)	0.65

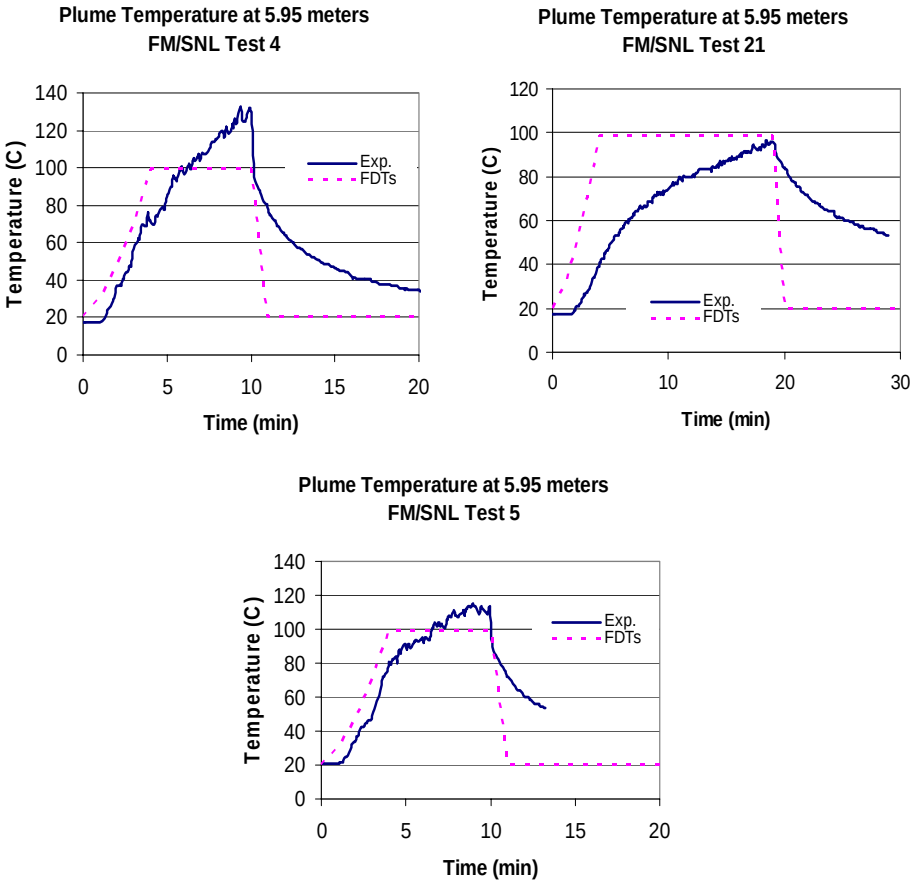

Figure A-11: Plume Temperature, FM/SNL Tests

A.2.3 Summary: Plume Temperature

Table A-14 lists the relative differences between experimental data and model results for plume temperature. "ΔE" is the difference between the experimental peak and the experimental initial condition. "ΔM" is the difference between model peak and the model initial conditions, which is assumed to be the experimental initial condition.

Table A-14: Plume Temperature Relative Differences

			Plume Temperature (°C)		
		Sensor	Δ E	Δ M	% Difference
ICFMP BE #2	Case 1	TG1	166	168	**1%**
		TG2	77	49	**-36%**
	Case 2	TG1	288	239	**-17%**
		TG2	128	70	**-45%**
	Case 3	TG1	252	268	**6%**
		TG2	128	79	**-38%**
FM/SNL	Test 4	5.66 m above fire	116	71	**-39%**
	Test 5	5.66 m above fire	94	64	**-32%**
	Test 21	5.66 m above fire	79	44	**-45%**

A.3 Flame Height

Flame height is recorded by visual observations, photographs or video footage. Photographs from the ICFMP BE #2 test series and video from BE #3 test series are available. It is difficult to precisely measure the flame height, but the photos and videos allow one to make estimates accurate to within a pan diameter. Such observations can be compared with outputs from Heskestad's flame height correlation. Although no accuracy can be calculated, this comparison may provide insights about the capabilities and limitations of the model. The FDT^S spreadsheet used to calculate the flame height was 03_HRR_Flame_Height_Burning_Duration_Calculations.xls.

A.3.1 ICFMP BE #2

Figure A-12 contains photographs of the actual fire. The height of the visible flame in the photographs has been estimated to be between 2.4 and 3 pan diameters [3.8 to 4.8 m (12.5 to 15.7 ft)]. Using Heskestad's method for estimating the height of a pool fire flame, FDT^S estimated flame height to be 4.3 m (14.1 ft).

Figure A-12: Photographs of Heptane Pan Fires, ICFMP BE #2, Case 2
(Courtesy of Simo Hostikka, VTT Building and Transport, Espoo, Finland)

A.3.2 ICFMP BE #3

No measurements were made of the flame height during BE #3, but numerous photographs were taken through the doorway, which measured 2 m x 2 m (6.6 ft x 6.6 ft). Figure A-13 is one such photograph. During BE #3, Test 3, the peak flame height is estimated to be 2.8 m (9.2 ft), roughly consistent with the view through the doorway in the figure below. FDT^S results in a flame height of 3.0 m (9.8 ft) using Heskestad's flame height prediction.

Figure A-13: Photograph and Simulation of ICFMP BE #3, Test 3, as Seen Through the 2 m x 2 m Doorway (Photo courtesy of Francisco Joglar, SAIC)

A.4 Target Heat Flux

A.4.1 ICFMP BE #3

The experimental results for radiant heat flux were obtained from Benchmark Exercise #3. The FDT^S spreadsheet used to calculate the radiant heat flux is 05.1_Heat_Flux_Calculations_Wind_Free.xls. The Point Source Radiation and Solid Flame Radiation model were used. The heat flux measurements were taken using 10 different gauges located at varying distances from the fire. Five gauges measured total heat flux, and five measured radiant heat flux. Because FDT^S calculates radiant heat flux, only those data were compared. Also, one of the five radiant heat flux gauges was oriented in the horizontal direction and not with the proposed targets, so those data were not compared.

Point Source Radiation Model: The HRRs used as inputs are listed in Table A-4, Table A-5, and Table A-6 and are consistent with the experimental measurements of HRR. For all tests, we assumed a constant HRR that represented the steady-state average HRR of the test data. This does introduce some additional error when the experimental HRR is changing with time. No attempt is made to quantify this error other than to lump it in with general HRR uncertainties as described in Volume 2. The radiation fraction for all tests except Test 17 was 0.44.

The radiation fraction used for Test 17 was 0.40. Table A-15 lists the radial distances from fire to target for each test. This number also represents the ratio of distance to the diameter of the fire (L/D) because the diameter of the fire was 1.00 m (3.3 ft). The position of the fire was different for three of the 15 tests in BE #3, so the distances to targets are different for those tests. The point source representing the fire is taken to be 1.00 m above the ground. It is interesting to note that despite the limitation of the point source radiation model as applicable only for L/D > 2.5, this trend is not seen in the data from BE #3. In some cases, for the same fire and gauges at L/D < 2.5, relative differences are smaller than gauges at L/D > 2.5. Two reasons for this result may be either HGL effects or compartment effects. However, there is no clear trend, and therefore, caution should be taken anytime the point source model is used in compartments. Figures A-14 through A-21 illustrates the experimental and calculated radiant heat fluxes for these tests.

Table A-15: Radial Distance and L/D from Fire to Radiant Heat Flux Gauges (meters)

Gauge	Test 14	Test 15	Test 18	All Others
1	4.88	1.33	2.16	3.25
3	4.24	1.52	2.17	2.73
7	3.80	2.17	2.58	2.54
10	1.81	5.65	5.55	3.42

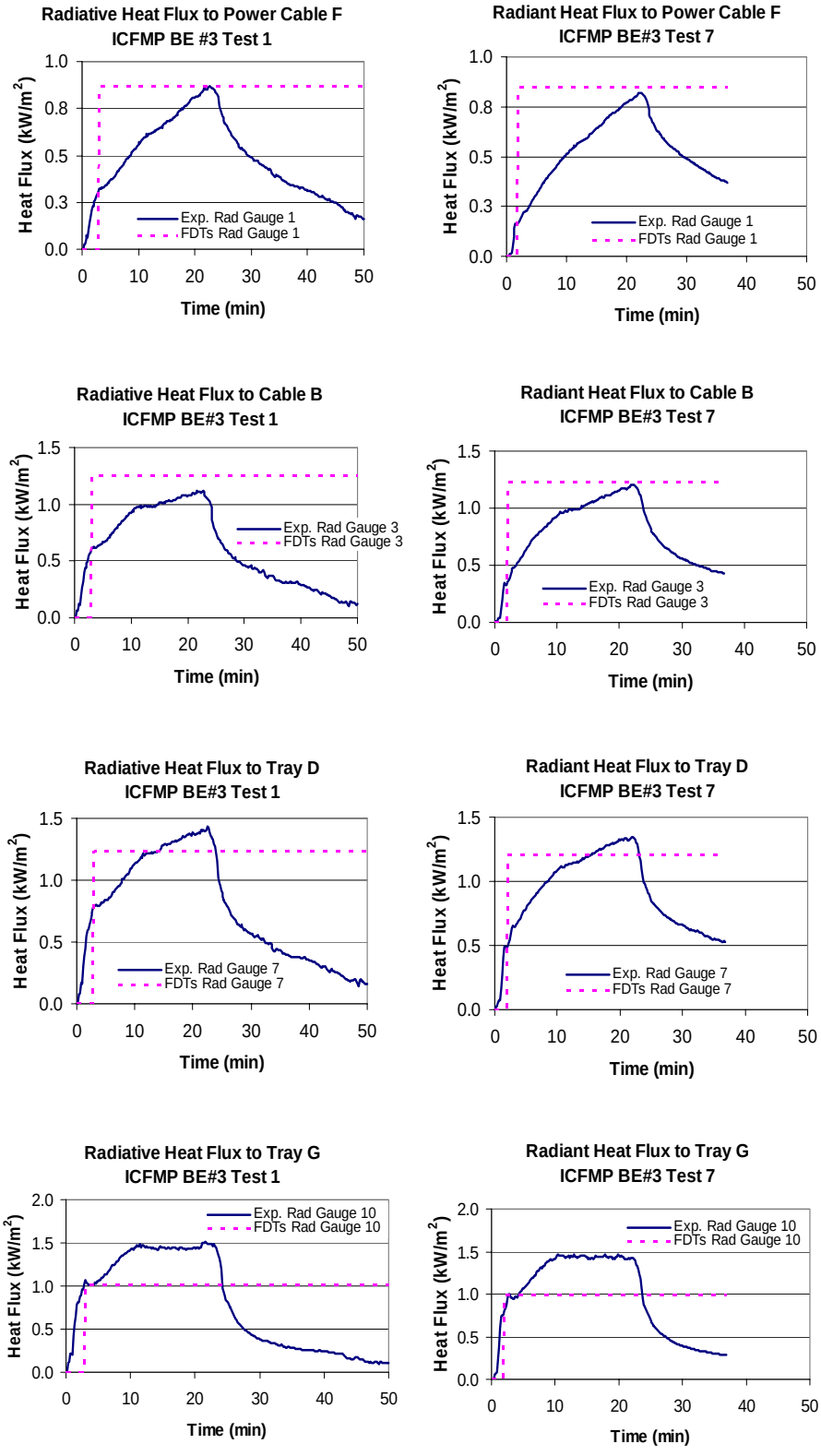

Figure A-14: Radiant Heat Flux, ICFMP BE #3, Tests 1 and 7

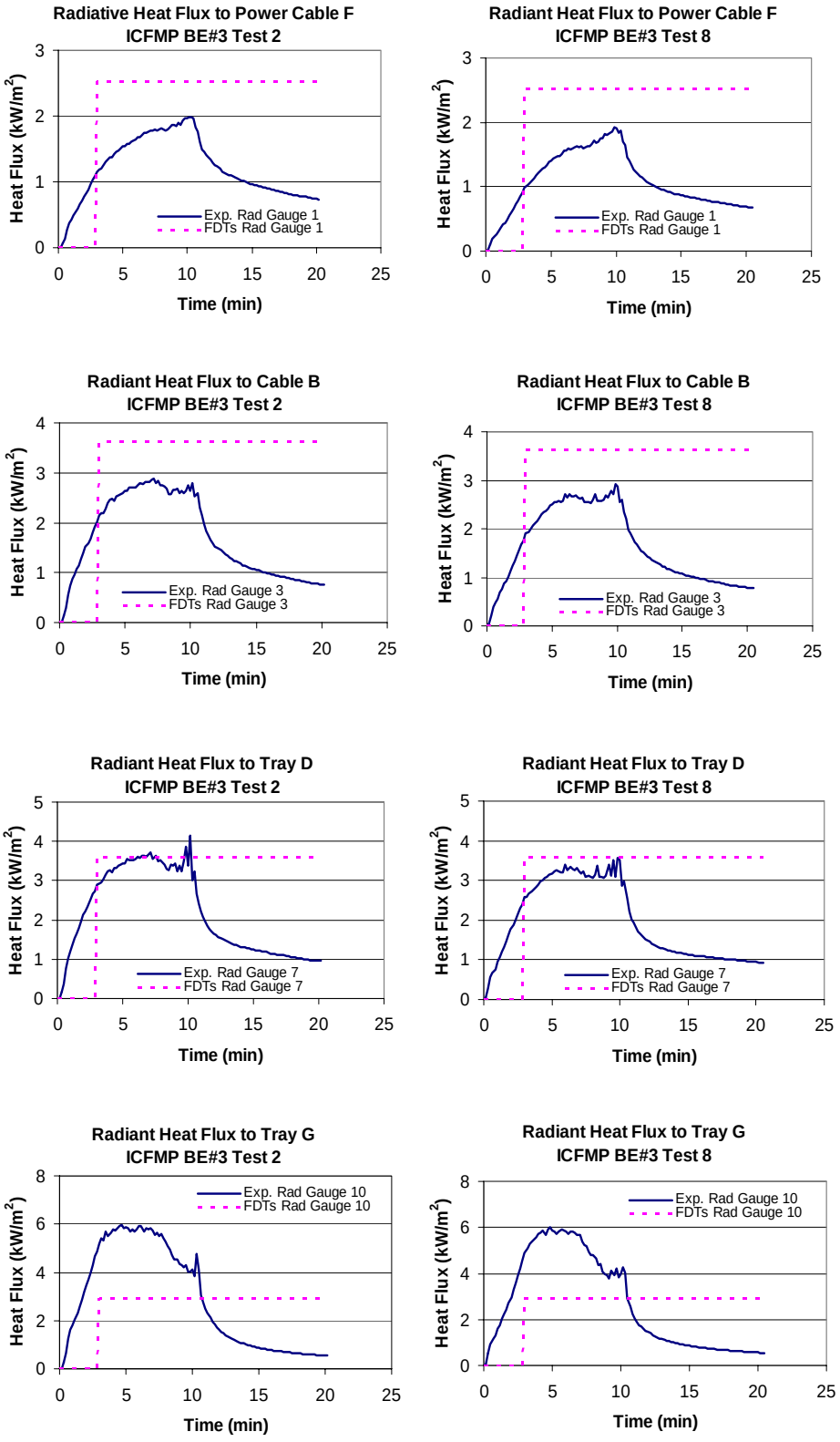

Figure A-15: Radiant Heat Flux, ICFMP BE #3, Tests 2 and 8

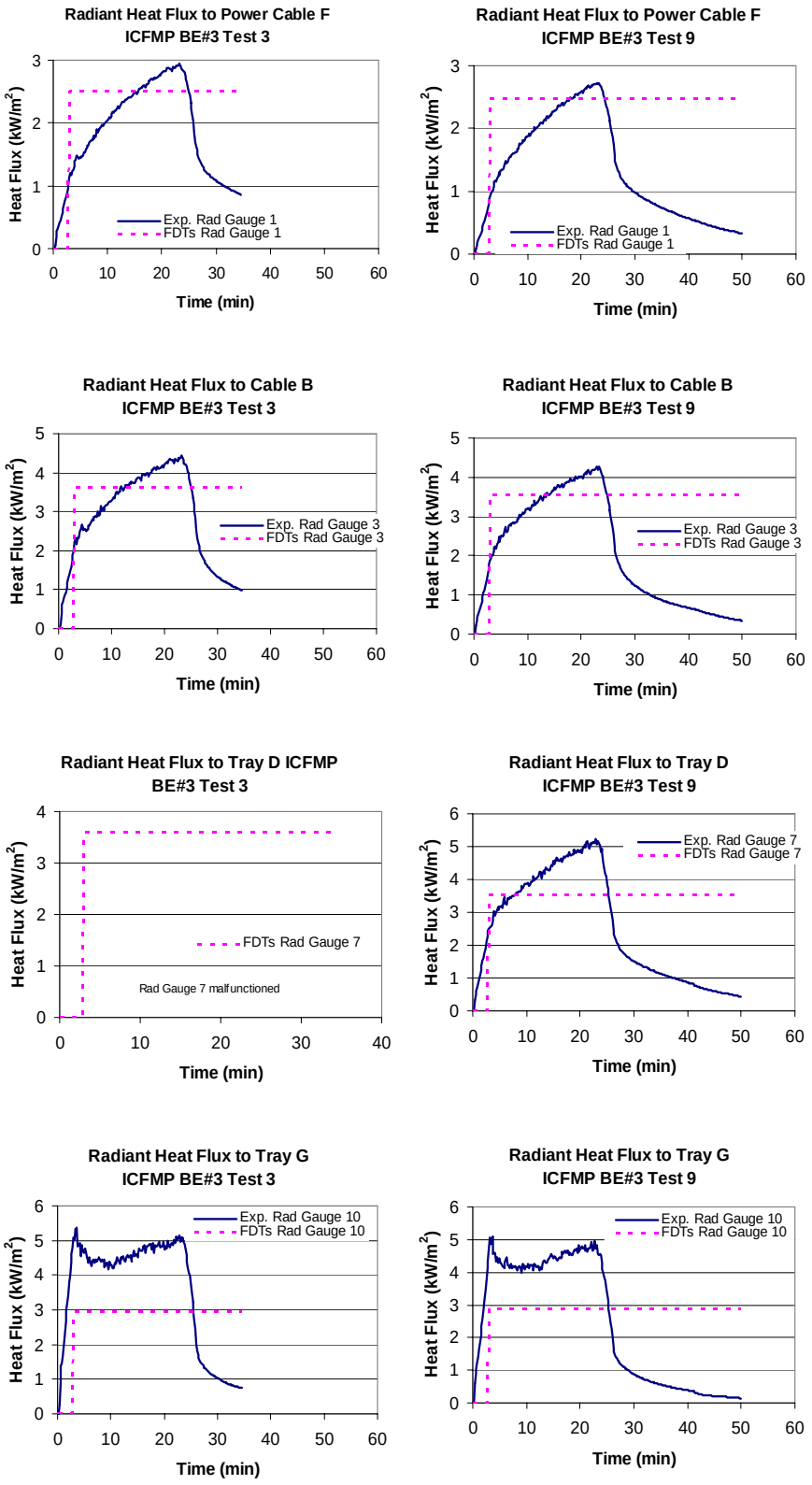

Figure A-16: Radiant Heat Flux, ICFMP BE #3, Tests 3 and 9

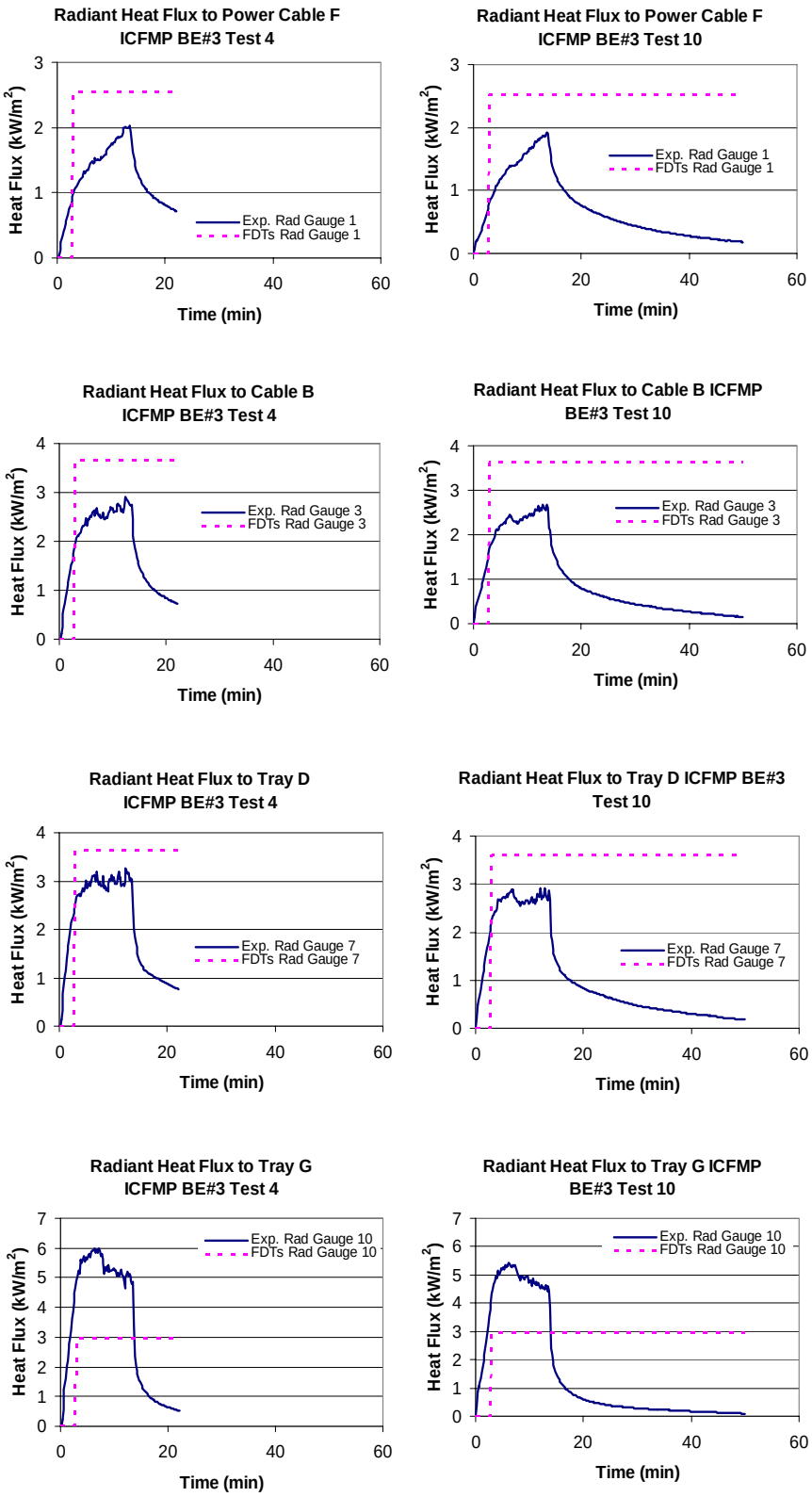

Figure A-17: Radiant Heat Flux, ICFMP BE #3, Tests 4 and 10

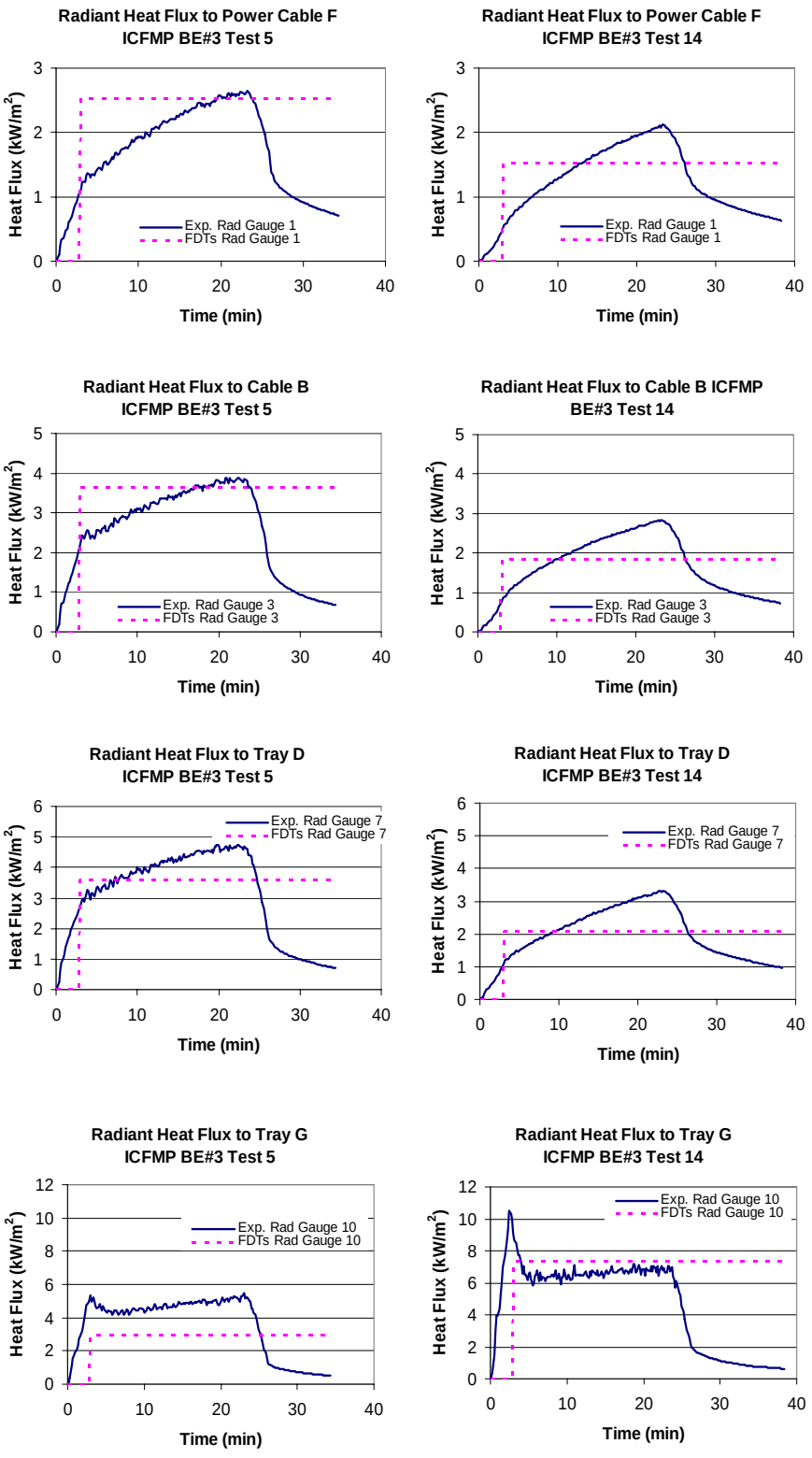

Figure A-18: Radiant Heat Flux, ICFMP BE #3, Tests 5 and 14

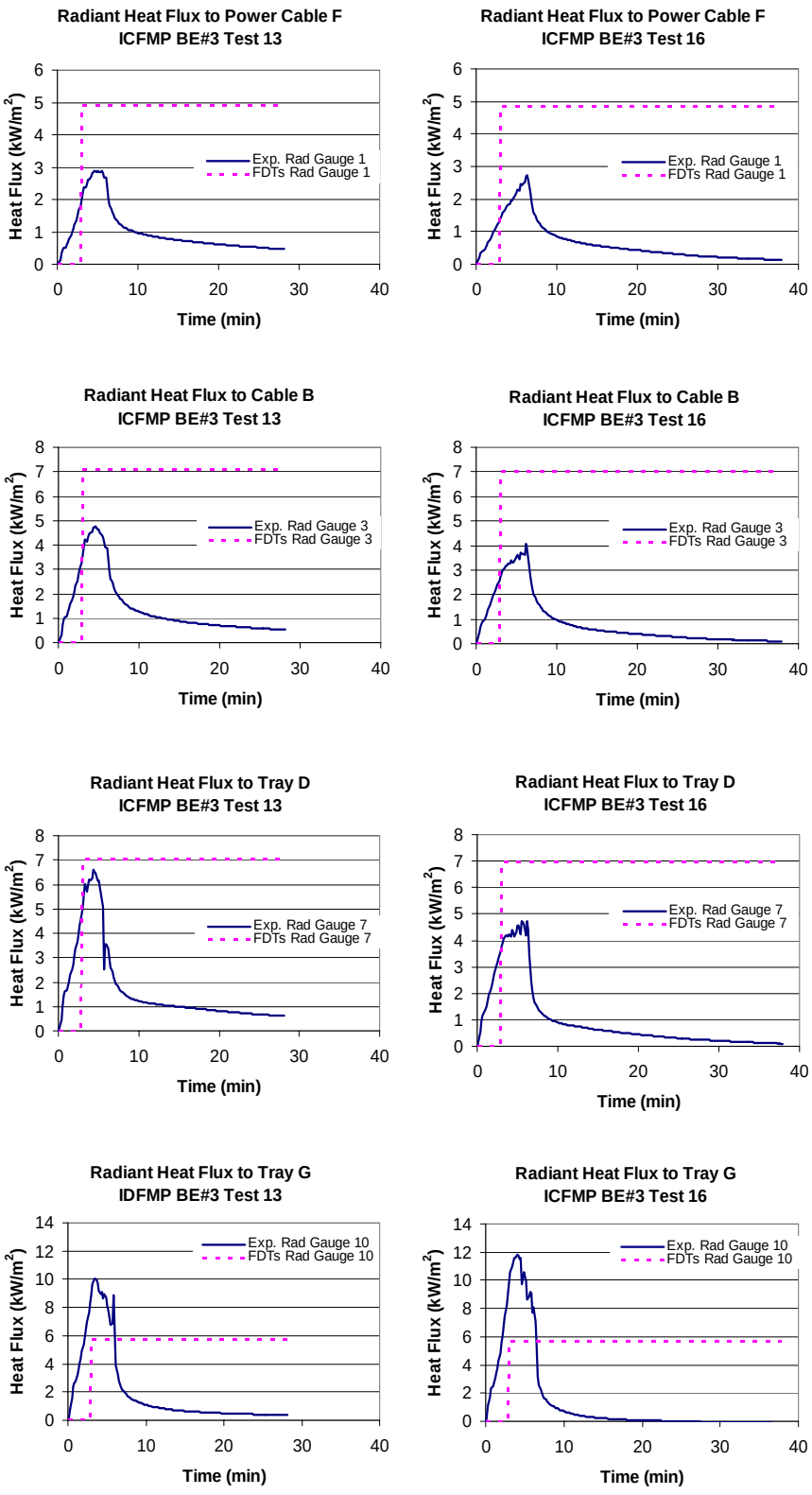

Figure A-19: Radiant Heat Flux, ICFMP BE #3, Tests 13 and 16

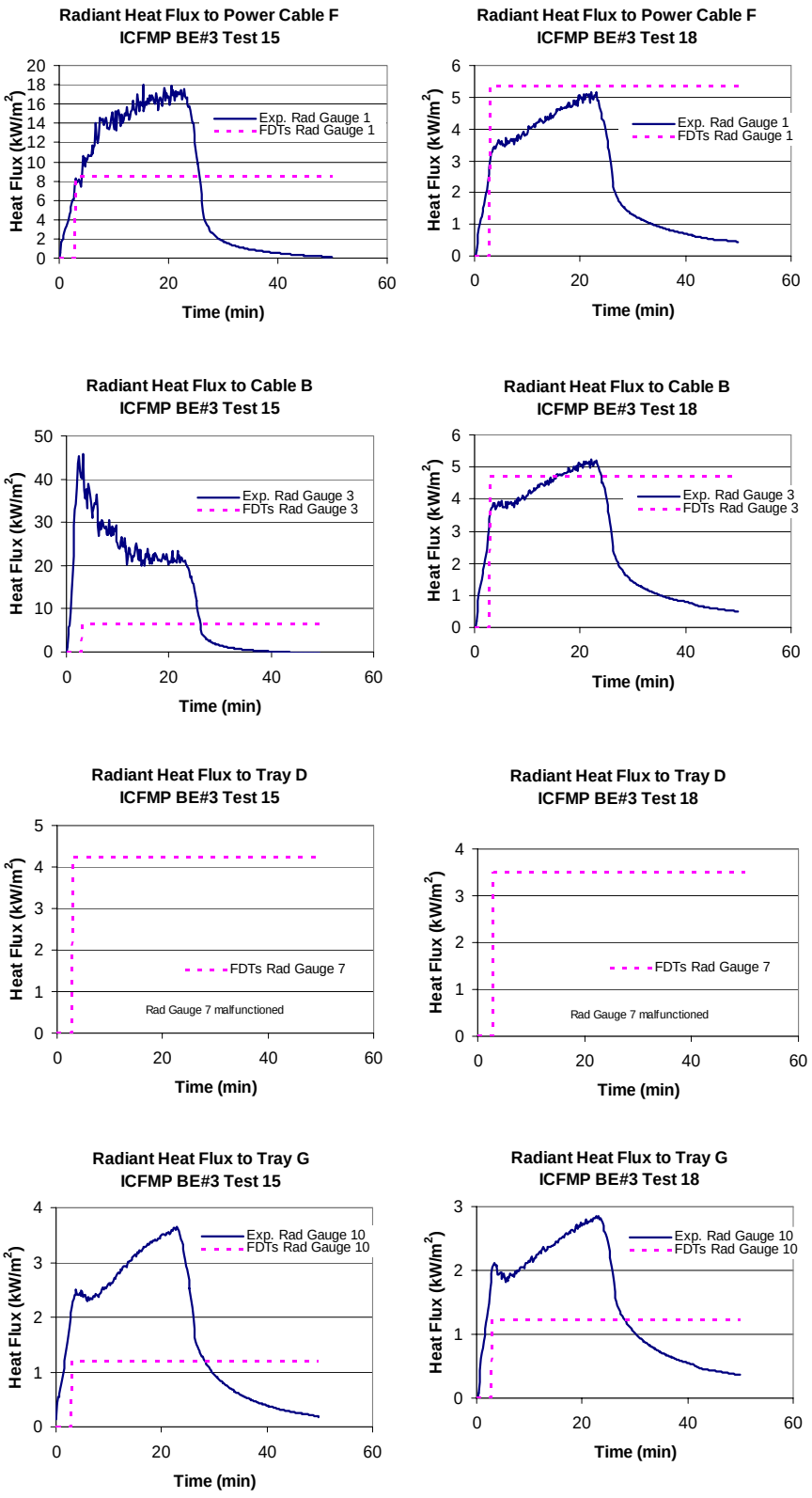

Figure A-20: Radiant Heat Flux, ICFMP BE #3, Tests 15 and 18

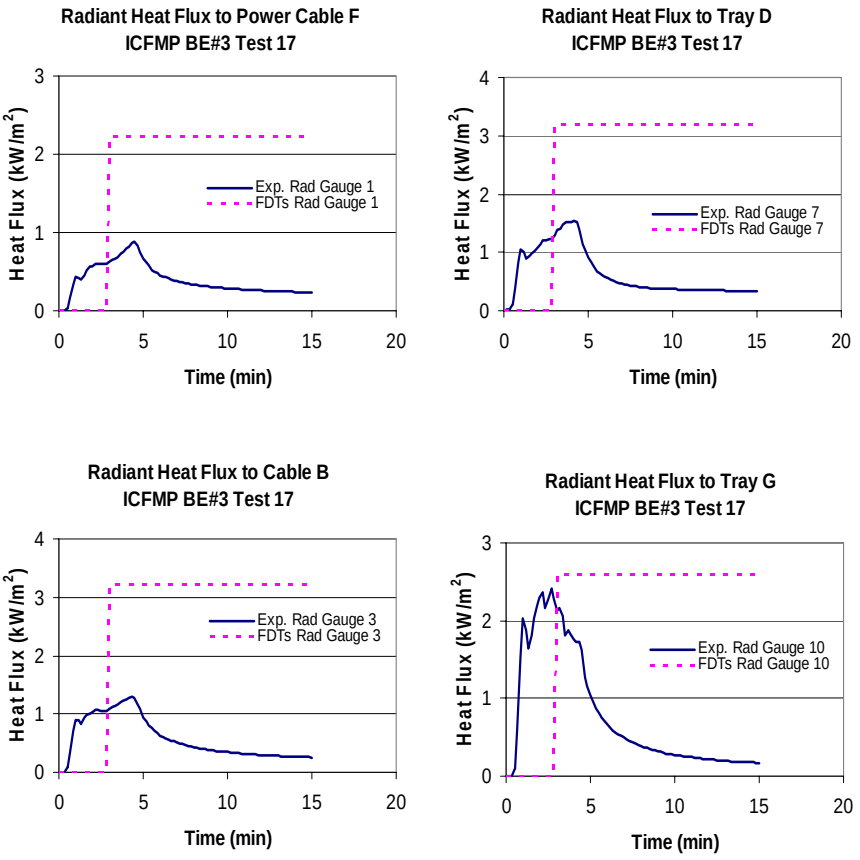

Figure A-21: Radiant Heat Flux, ICFMP BE #3, Test 17

Solid Flame Radiation Model: The HRRs used as inputs are listed in Table A-4, Table A-5, and Table A-6 and are consistent with the experimental measurements of HRR. For all tests, we assumed a constant HRR that represented the steady-state average HRR of the test data. This does introduce some additional error when the experimental HRR is changing with time. No attempt is made to quantify this error other than to lump it in with general HRR uncertainties as described in Volume 2. Table A-16 lists the horizontal distance to each target from the center of the flame. The heights of the targets above the ground are listed in Volume 2**.** The position of the fire was different for three of the 15 tests in BE #3, so the distances to targets are different for those tests. The "effective" emissive power of the flame (Equation 3-20) was determined from a wide range of experimental measurements of diameter from 1 to 50 m (3.3 to 164 ft) for radiant flux from pool fires to targets. All measurements were made with vertical targets at the ground. The radiation fraction is inherently taken into account by the emissive power, which includes the effects of smoke obscuration of the flame. A least squares fit of the "effective" emissive power data shows a reduction from about 60 kW/m^2 at 1 meter diameter to 20 kW/m^2 at about 60 m (197 ft). The least squares fit is adequate for the scatter of data for the overall trend. However, for smaller diameter pool fires on the order of 1 m (3.3 ft), the data are sparse for differing fuel types. Because the BE#3 test series used a fire with a diameter of 1 m (3.3 ft), it is reasonable for the relative differences to be outside the experimental uncertainty of 20%. Other reasons for this result may be either HGL effects or compartment effects. However, there is no clear trend

and, therefore, caution should be taken anytime the solid flame model is used in compartments. Figures A-22 through A-29 illustrate the experimental and calculated radiant heat fluxes for these tests.

Table A-16: Horizontal Distance from Fire to Radiant Heat Flux Gauges (meters)

Gauge	Test 14	Test 15	Test 18	All Others
1	4.77	0.81	1.88	3.08
3	3.96	0.02	1.55	2.27
7	3.21	0.75	1.59	1.52
10	1.64	5.60	5.50	3.33

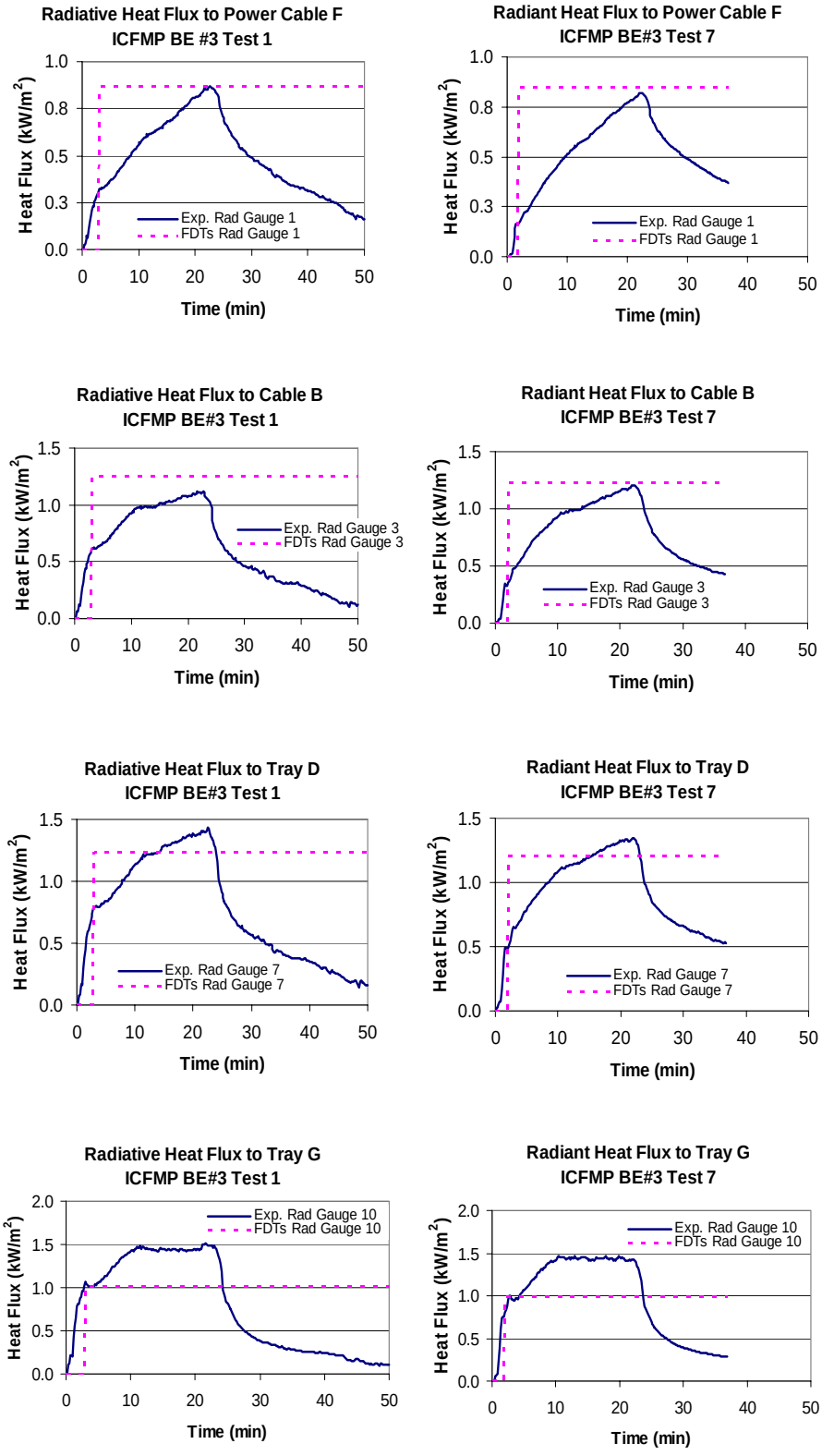

Figure A-22: Radiant Heat Flux, ICFMP BE #3, Tests 1 and 7

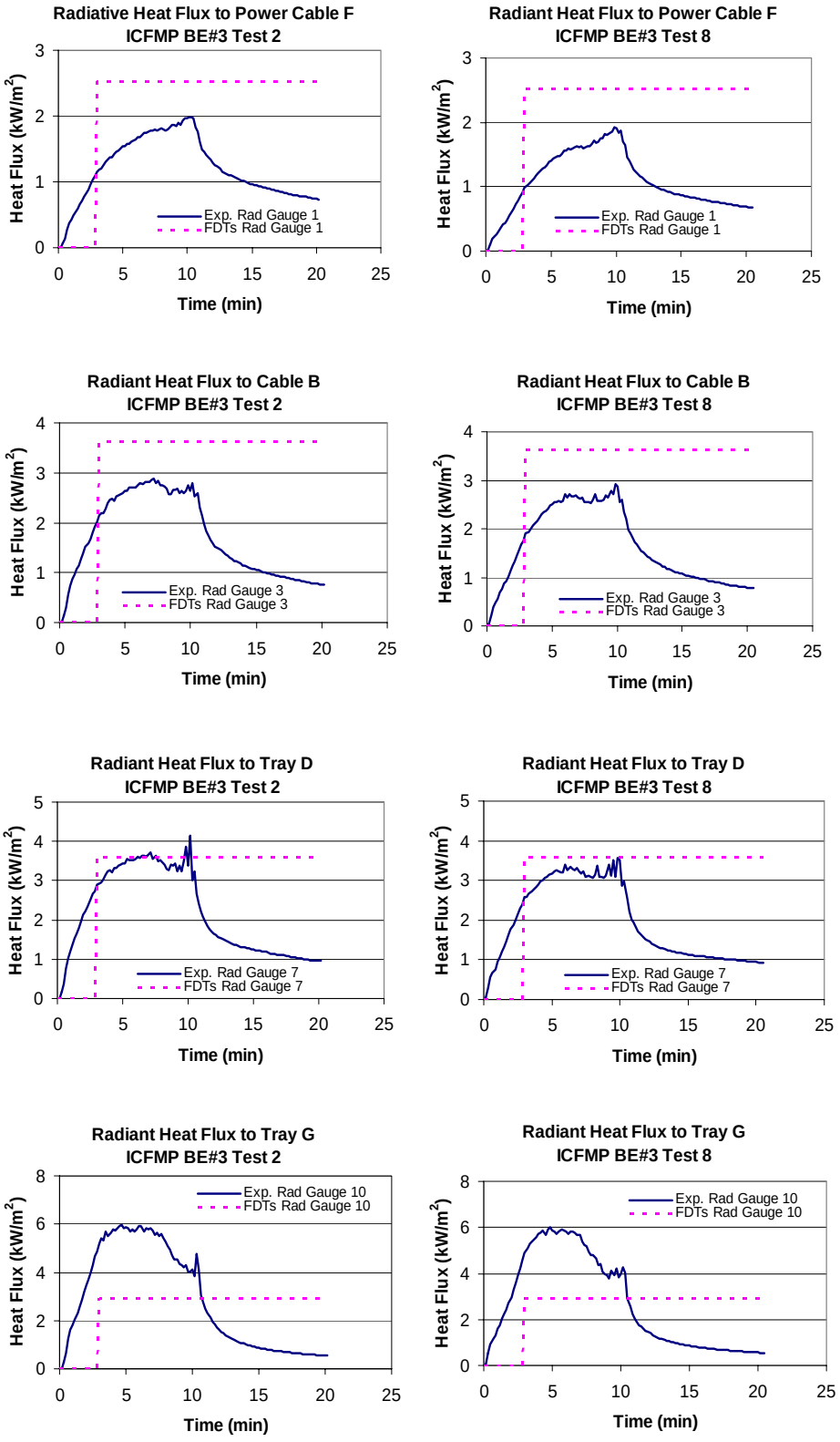

Figure A-23: Radiant Heat Flux, ICFMP BE #3, Tests 2 and 8

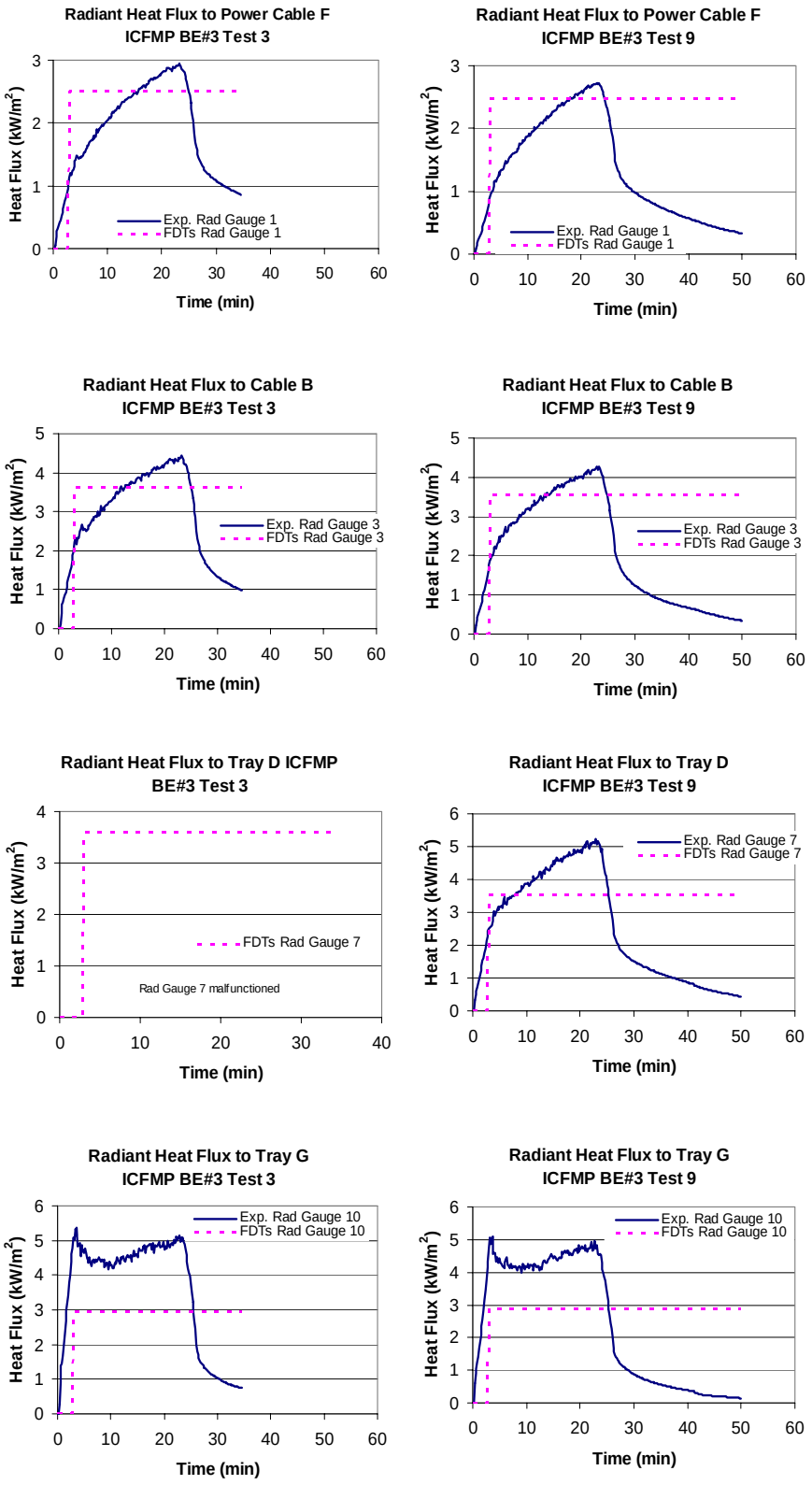

Figure A-24: Radiant Heat Flux, ICFMP BE #3, Tests 3 and 9

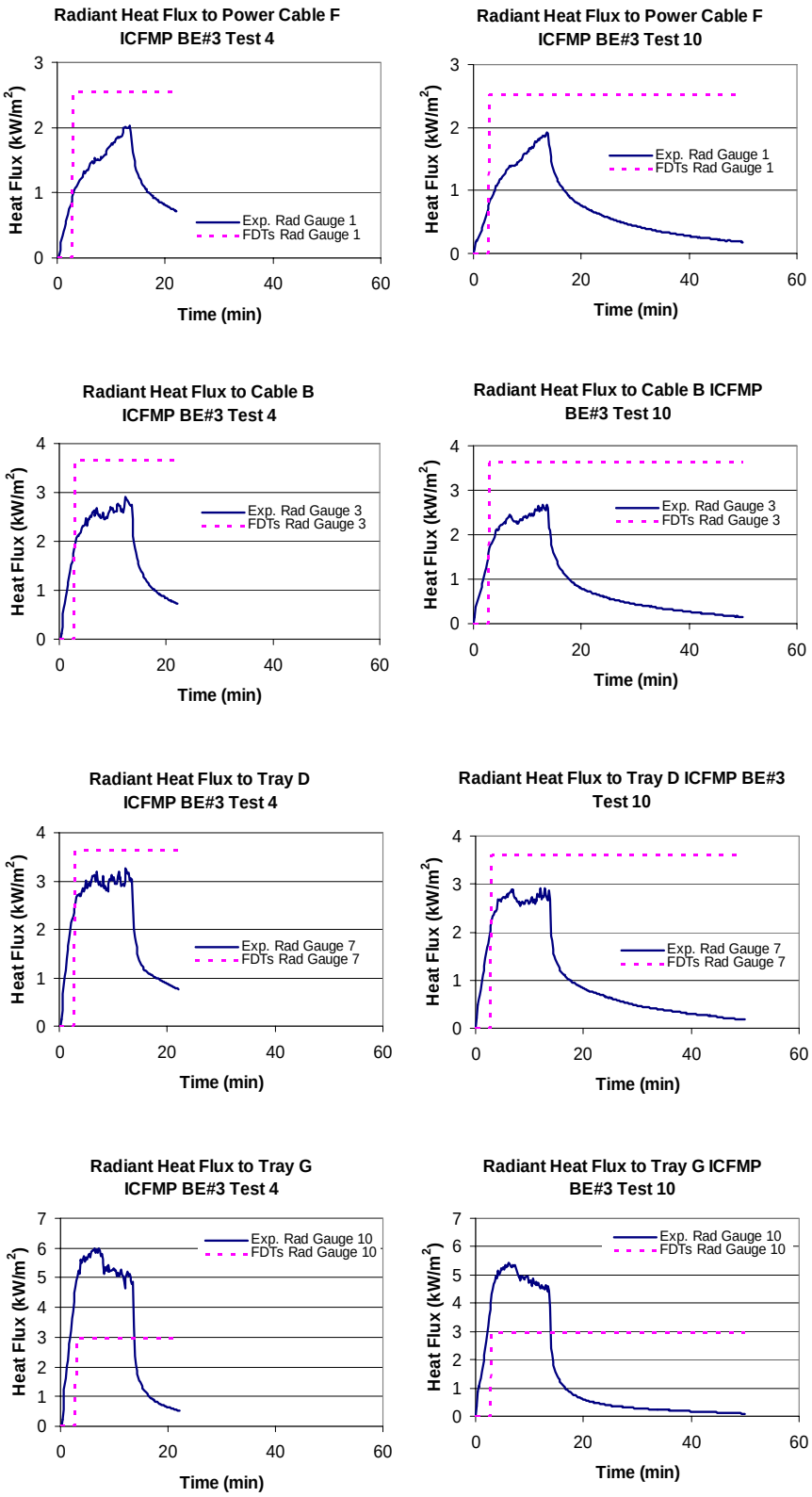

Figure A-25: Radiant Heat Flux, ICFMP BE #3, Tests 4 and 10

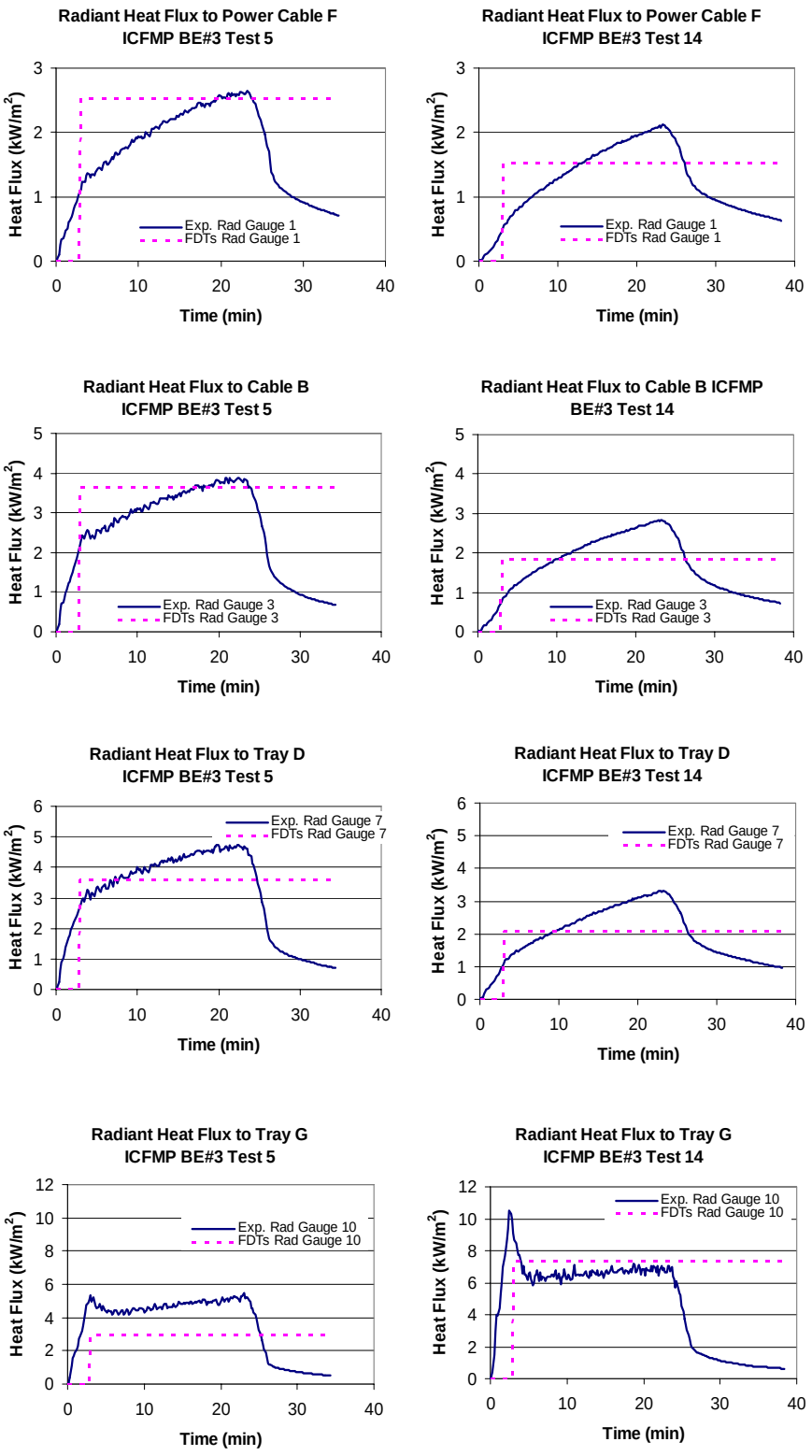

Figure A-26: Radiant Heat Flux, ICFMP BE #3, Tests 5 and 14

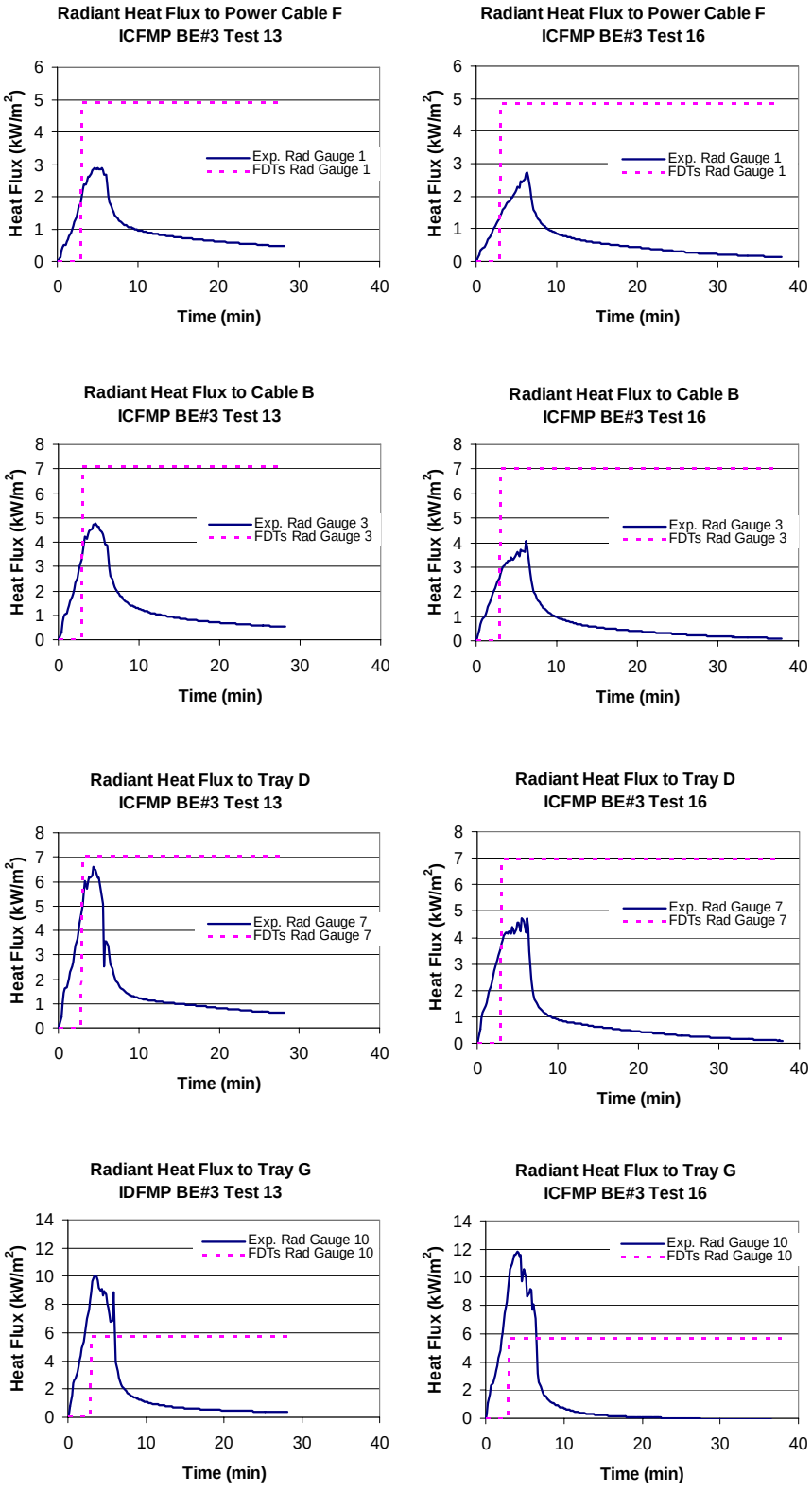

Figure A-27: Radiant Heat Flux, ICFMP BE #3, Tests 13 and 16

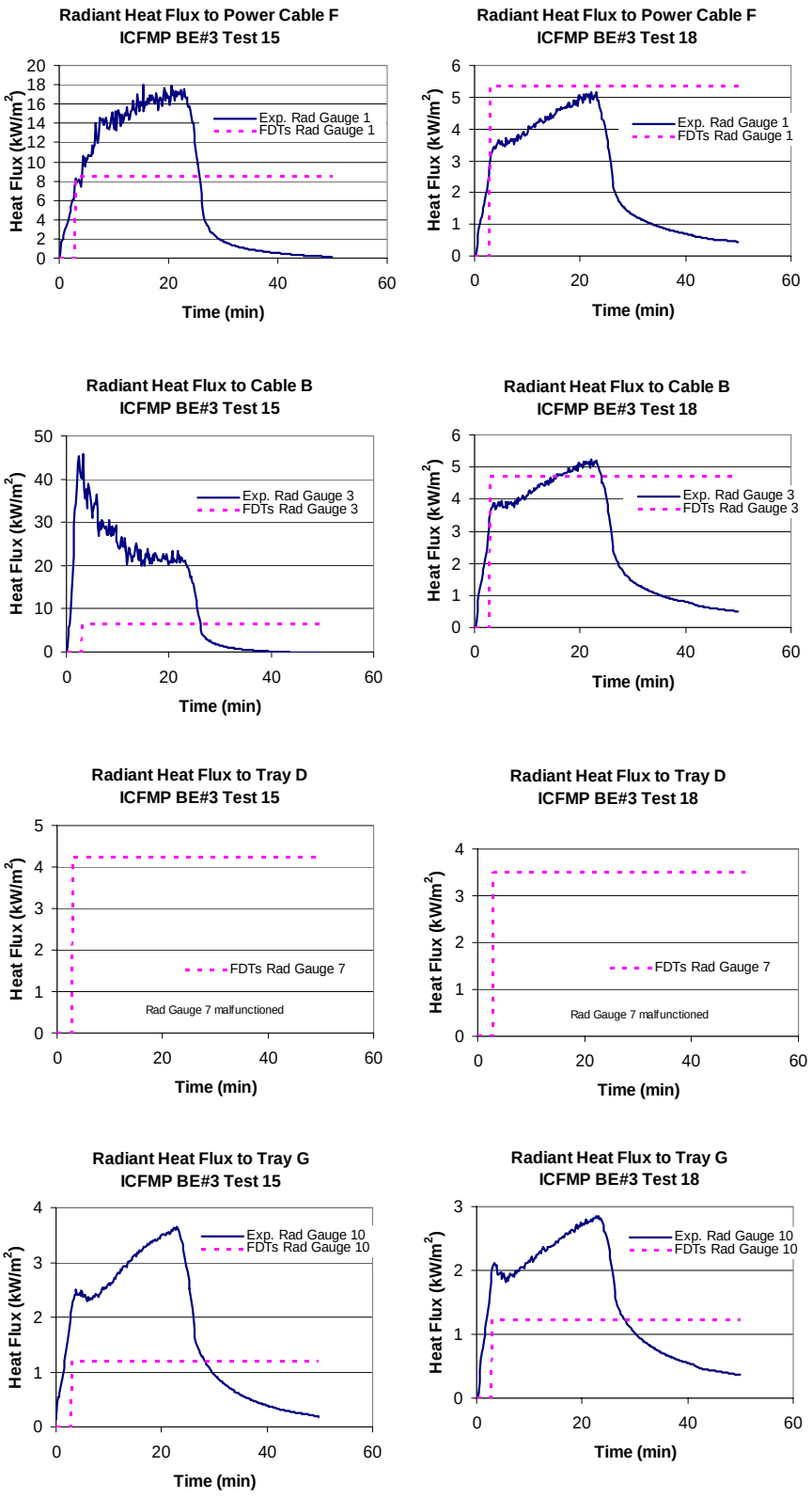

Figure A-28: Radiant Heat Flux, ICFMP BE #3, Tests 15 and 18

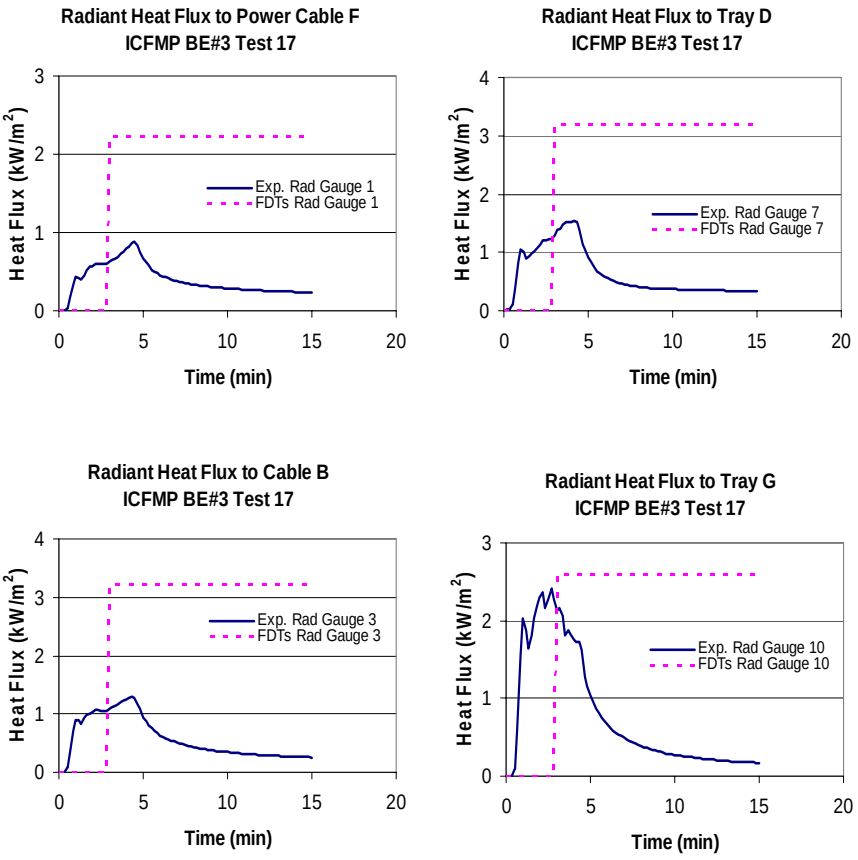

Figure A-29: Radiant Heat Flux, ICFMP BE #3, Test 17

A.4.2 Summary: Radiant Heat Flux

Table A-17 lists the relative differences between experimental data and the point source model results for radiant heat flux. "ΔE" is the difference between the experimental peak and the experimental initial condition. "ΔM" is the difference between model peak and the model initial conditions, which is assumed to be the experimental initial condition.

Table A-17: Relative Differences, Radiant Heat Flux — Point Source

BE #3	Sensor	Radiant Heat Flux (kW/m^2)		
		Δ E	Δ M	% Difference
Test 1	Gauge 1	0.87	1.36	**57%**
	Gauge 3	1.12	1.93	**72%**
	Gauge 7	1.43	2.23	**56%**
	Gauge 10	1.51	1.23	**-19%**
Test 2	Gauge 1	1.99	3.95	**98%**
	Gauge 3	2.88	5.59	**94%**
	Gauge 7	4.16	6.46	**55%**
	Gauge 10	5.97	3.56	**-40%**
Test 3	Gauge 1	2.95	3.95	**34%**
	Gauge 3	4.45	5.59	**26%**
	Gauge 7			
	Gauge 10	5.36	3.56	**-34%**
Test 4	Gauge 1	2.02	3.98	**97%**
	Gauge 3	2.92	5.64	**93%**
	Gauge 7	3.26	6.52	**100%**
	Gauge 10	6.00	3.59	**-40%**
Test 5	Gauge 1	2.65	3.95	**49%**
	Gauge 3	3.88	5.59	**44%**
	Gauge 7	4.78	6.46	**35%**
	Gauge 10	5.45	3.56	**-35%**
Test 7	Gauge 1	0.82	1.33	**62%**
	Gauge 3	1.21	1.88	**56%**
	Gauge 7	1.35	2.17	**61%**
	Gauge 10	1.47	1.20	**-19%**
Test 8	Gauge 1	1.93	3.95	**104%**
	Gauge 3	2.92	5.59	**92%**
	Gauge 7	3.56	6.46	**82%**
	Gauge 10	6.02	3.56	**-41%**
Test 9	Gauge 1	2.72	3.88	**43%**
	Gauge 3	4.27	5.50	**29%**
	Gauge 7	5.23	6.35	**22%**
	Gauge 10	5.10	3.50	**-31%**
Test 10	Gauge 1	1.92	3.95	**105%**
	Gauge 3	2.68	5.59	**109%**
	Gauge 7	2.91	6.46	**122%**
	Gauge 10	5.42	3.56	**-34%**
Test 13	Gauge 1	2.90	7.73	**167%**
	Gauge 3	4.77	10.95	**129%**
	Gauge 7	6.58	12.66	**92%**
	Gauge 10	10.06	6.98	**-31%**
Test 14	Gauge 1	2.12	1.73	**-18%**
	Gauge 3	2.84	2.30	**-19%**
	Gauge 7	3.32	2.86	**-14%**
	Gauge 10	10.50	12.61	**20%**
Test 15	Gauge 1	18.02	23.36	**30%**

BE #3	Sensor	Radiant Heat Flux (kW/m^2)		
		Δ E	Δ M	% Difference
	Gauge 3	45.88	17.88	**-61%**
	Gauge 7			
	Gauge 10	3.65	1.29	**-64%**
	Gauge 1	2.73	7.63	**180%**
	Gauge 3	4.05	10.81	**167%**
	Gauge 7	4.74	12.49	**164%**
Test 16	Gauge 10	11.79	6.89	**-42%**
	Gauge 1	0.88	3.50	**297%**
	Gauge 3	1.30	4.96	**282%**
	Gauge 7	1.53	5.73	**274%**
Test 17	Gauge 10	2.42	3.16	**31%**
	Gauge 1	5.18	8.86	**71%**
	Gauge 3	5.24	8.77	**68%**
	Gauge 7			
Test 18	Gauge 10	2.84	1.34	**-53%**

Table A-18 lists the relative differences between experimental data and the solid flame model results for radiant heat flux. "ΔE" is the difference between the experimental peak and the experimental initial condition. "ΔM" is the difference between model peak and the model initial conditions, which is assumed to be the experimental initial condition.

Table A-18: Relative Differences, Radiant Heat Flux — Solid Flame

BE #3	Sensor	Radiant Heat Flux (kW/m^2)		
		Δ E	Δ M	% Difference
	Gauge 1	0.87	2.35	**170%**
	Gauge 3	1.12	2.18	**95%**
	Gauge 7	1.43	0.83	**-42%**
Test 1	Gauge 10	1.51	2.36	**56%**
	Gauge 1	1.99	5.22	**162%**
	Gauge 3	2.88	7.51	**161%**
	Gauge 7	4.16	8.49	**104%**
Test 2	Gauge 10	5.97	4.70	**-21%**
	Gauge 1	2.95	5.22	**77%**
	Gauge 3	4.45	7.51	**69%**
	Gauge 7			
Test 3	Gauge 10	5.36	4.70	**-12%**
	Gauge 1	2.02	5.25	**159%**
	Gauge 3	2.92	7.56	**159%**
	Gauge 7	3.26	8.63	**165%**
Test 4	Gauge 10	6.00	4.72	**-21%**
	Gauge 1	2.65	5.22	**97%**
	Gauge 3	3.88	7.51	**93%**
	Gauge 7	4.78	8.49	**78%**
Test 5	Gauge 10	5.45	4.70	**-14%**
Test 7	Gauge 1	0.82	2.29	**180%**

BE #3	Sensor	Radiant Heat Flux (kW/m^2)		
		Δ E	Δ M	% Difference
	Gauge 3	1.21	2.11	**75%**
	Gauge 7	1.35	0.80	**-41%**
	Gauge 10	1.47	2.31	**57%**
	Gauge 1	1.93	5.22	**170%**
	Gauge 3	2.92	7.51	**157%**
	Gauge 7	3.56	8.49	**139%**
Test 8	Gauge 10	6.02	4.70	**-22%**
	Gauge 1	2.72	5.17	**90%**
	Gauge 3	4.27	7.40	**73%**
	Gauge 7	5.23	8.19	**57%**
Test 9	Gauge 10	5.10	4.66	**-9%**
	Gauge 1	1.92	5.22	**171%**
	Gauge 3	2.68	7.51	**180%**
	Gauge 7	2.91	8.49	**192%**
Test 10	Gauge 10	5.42	4.70	**-13%**
	Gauge 1	2.90	6.76	**133%**
	Gauge 3	4.77	10.54	**121%**
	Gauge 7	6.58	16.99	**158%**
Test 13	Gauge 10	10.06	5.89	**-41%**
	Gauge 1	2.12	2.33	**10%**
	Gauge 3	2.84	3.04	**7%**
	Gauge 7	3.32	3.57	**8%**
Test 14	Gauge 10	10.50	14.93	**42%**
	Gauge 1	18.02	34.63	**92%**
	Gauge 3	45.88	56.80	**24%**
	Gauge 7			
Test 15	Gauge 10	3.65	1.74	**-52%**
	Gauge 1	2.73	6.74	**147%**
	Gauge 3	4.05	10.50	**159%**
	Gauge 7	4.74	16.93	**257%**
Test 16	Gauge 10	11.79	5.88	**-50%**
	Gauge 1	0.88	5.15	**484%**
	Gauge 3	1.30	7.35	**467%**
	Gauge 7	1.53	8.05	**425%**
Test 17	Gauge 10	2.42	4.65	**92%**
	Gauge 1	5.18	11.68	**126%**
	Gauge 3	5.24	13.05	**149%**
	Gauge 7			
Test 18	Gauge 10	2.84	1.80	**-37%**